NOAA Technical Memorandum ERL ETL-295

REFRACTION AND SCATTERING INTERFEROMETRIC ERRORS IN THE LOWER ATMOSPHERE

J.H. Churnside
I.M. Fuks

Environment Technology Laboratory
Boulder, Colorado
December 1998

noaa NATIONAL OCEANIC AND ATMOSPHERIC ADMINISTRATION / Environmental Research Laboratories

NOAA Technical Memorandum ERL ETL-295

REFRACTION AND SCATTERING INTERFEROMETRIC ERRORS IN THE LOWER ATMOSPHERE

J.H. Churnside
I.M. Fuks

Environment Technology Laboratory
Boulder, Colorado
December 1998

UNITED STATES DEPARTMENT OF COMMERCE

William M. Daley
Secretary

NATIONAL OCEANIC AND ATMOSPHERIC ADMINISTRATION

D. JAMES BAKER
Under Secretary for Oceans and Atmosphere/Administrator

Environmental Research Laboratories

James L. Rasmussen
Director

NOTICE

Mention of a commercial company or product does not constitute an endorsement by the NOAA Environmental Research Laboratories. Use of information from this publication concerning proprietary products or the test of such products for publicity or advertising purposes is not authorized.

For sale by the National Technical Information Service, 5285 Port Royal Road
Springfield, VA 22061

Contents

ABSTRACT. When two targets are simultaneously tracked by a single radar, the atmosphere can introduce errors in the observed relative positions of the targets. These errors arise because of average gradients and turbulent fluctuations in the index of refraction. When the observations are made with a radar interferometer, the important quantity is the difference between the signals from the two targets of the phase differences across the interferometer. If the profiles of the average refraction index and of turbulence are known, the performance of such a system can be estimated. In this case, performance is expressed as the root-mean-square (rms) of the error in the angular difference of the two targets. If these profiles are known, the angles can be corrected for the average refraction effect, which leads to improved performance. In this report a geometrical optics approach was developed for calculating phase and interferometric bearing angle variations of radio waves propagating in an inhomogeneous vertically stratified atmosphere with plane homogeneous layers. Effects of the atmospheric refraction on the angular difference errors of two simultaneously interferometric tracking target's were investigated analytically for two different scenarios of that targets rapprochement:

a. horizontal missile approaches to the target at the same altitude as the target, and

b. inclined missile approaches to the target along the line connecting the interferometer and the target.

Numerical calculations of refraction angle errors were carried out for the following:

a. standard exponential radio atmosphere profile,

b. exponential radio atmosphere profile with the near-earth refractive-index value adjusted to the real measured (balloon) data,

c. real refractive-index profiles retrieved from the standard balloon meteorological data for specific climate conditions at Denver, Colorado, for two daytime and nighttime measurements for two seasons, summer and winter.

Effects of atmosphere turbulence on the angular difference errors of two simultaneously interferometric tracking targets were investigated analytically in framework of geometrical optics for isotropic locally homogeneous turbulence with an infinite turbulence outer scale: it was shown that the correlation between bearing angle fluctuations of two simultaneously tracking targets leads to a considerable reduction in the angular difference error compared to the bearing angle errors for each of the targets. The program and the computer code for retrieving the turbulence structure parameter C_n^2 altitude profile from the routine meteorological balloon data were created and tested on the eight samples of data (two daytime and nighttime balloon launchings for winter and summer seasons). It is shown that although the errors due to the average refractive-index profile exceed essentially those due to the turbulent fluctuations of the refractive index, they can be corrected if the average refractive-index profile is known.

1 Phase Variations - Geometrical Optics Approach

We will consider propagation of centimeter-decimeter radio waves in the inhomogeneous atmosphere for a distance of $R \simeq 10$ km or less. Since the dielectric constant of air $\varepsilon(\mathbf{r})$ varies slowly on the scale of the radio wavelength λ, and the following inequality is usually fulfilled:

$$\lambda \left| \nabla_{\mathbf{r}} \varepsilon \right| \ll \varepsilon, \tag{1}$$

we can represent the spatial dependence of the electric field $E(\mathbf{r})$ as:

$$E(\mathbf{r}) = A \exp[i\Phi] = A \exp[ikS], \tag{2}$$

where $k = 2\pi/\lambda = 2\pi f/c$ is the wave number, f is the radio signal frequency, c is the velocity of light, and the amplitude A, phase gradient $\nabla\Phi$, and eikonal S are slowly varying (on the scale of λ) functions of the coordinate $\mathbf{r}$. For the distances R under consideration, the Fresnel zone size $\sqrt{\lambda R}$ is much smaller than the outer scale size L; i.e. the following inequality is fulfilled:

$$\sqrt{\lambda R} \ll L_0. \tag{3}$$

Conditions (1) and (3) allow us to use the geometrical optics approach for solving the propagation problem and to represent the phase Φ as an integral over the ray trajectory $\mathbf{r}(s)$ (see, for example, [1] and [2]):

$$\Phi = k \int_0^s \sqrt{\varepsilon[\mathbf{r}(s)]} ds, \tag{4}$$

where s is the distance along the ray. In the worst case, this approximation will overestimate the error by no more than a factor of 2. For the radio wave band considered here, the deviation of the dielectric constant $\varepsilon(\mathbf{r})$ from unity is small and can be represented as:

$$\varepsilon(\mathbf{r}) = 1 + \Delta\varepsilon(z) + \delta\varepsilon(\mathbf{r}), \tag{5}$$

where $\Delta\varepsilon(z)$ corresponds to the "regular refraction" (large-scale variation of ε with height z above the earth's surface), and $\delta\varepsilon(\mathbf{r})$ is the small-scale random turbulent fluctuation of ε with a mean value equal to zero: $\langle \delta\varepsilon(\mathbf{r}) \rangle =$

0; here and below $\langle ... \rangle$ denotes the statistical average over the ensemble of random function $\delta\varepsilon(\mathbf{r})$ realizations. Assuming that

$$\Delta\,\varepsilon(z)\,,\delta\varepsilon(\mathbf{r}) \ll 1, \tag{6}$$

we can use the small perturbation method for solving the equation for the ray trajectory $\mathbf{r}(s)$ as well as for the integral (4) expansion of the series for small $\Delta\,\varepsilon(z)$ and $\delta\varepsilon(\mathbf{r})$:

$$\Phi = kR + \frac{k}{2}\int_0^R [\Delta\,\varepsilon(z) + \delta\varepsilon(\mathbf{r})]\,ds, \tag{7}$$

where the integral is along the straight ray path connecting the initial and the final points ($s = 0$ and $s = R$, respectively). Instead of the dielectric constant $\varepsilon(\mathbf{r})$, the refractive index $n(\mathbf{r}) = \sqrt{\varepsilon(\mathbf{r})}$ is often used, and it can be represented in a form similar to (5) :

$$n(\mathbf{r}) = 1 + \Delta n(z) + \delta n(\mathbf{r}), \tag{8}$$

where $\Delta n(z) = \Delta\,\varepsilon(z)/2$ and $\delta n(\mathbf{r}) = \delta\varepsilon(\mathbf{r})/2$. From (7) and (8) we obtain the following expression for the eikonal S :

$$S = R + \int_0^R [\Delta n(z) + \delta n(\mathbf{r})]\,ds. \tag{9}$$

2 Interferometric Angle Measurement Errors

Unlike optical propagation, where the arrival direction is defined as normal to the phase wave front (see, for example, [3]), for radio waves, an interferometric system that measures the phase difference is usually used. The simplest interferometric system consists of two receivers located at points a and b (Fig. 1) with distance (base) L between them. The zenith angle ζ between the normal to the base (axis Oz) and the direction to the point source M can be found if we measure the signal phases Φ_a and Φ_b at points a and b, respectively:

$$\sin\zeta = \frac{\Phi_a - \Phi_b}{kL} = \frac{S_a - S_b}{L} = \sin\zeta_0 + \frac{1}{L}\left[\int_0^{R_a} \Delta n(z)\,ds_a - \int_0^{R_b} \Delta n(z)\,ds_b\right]$$

$$+\frac{1}{L}\left[\int_0^{R_a} \delta n(\mathbf{r})\,ds_a - \int_0^{R_b} \delta n(\mathbf{r})\,ds_b\right], \tag{10}$$

where R_a and R_b are the distances from the source M to the points a and b, respectively, ds_a and ds_b are the differentials of length along the corresponding rays, and ζ_0 is the unperturbed zenith angle, defined by the equation:

$$\sin\zeta_0 = \frac{R_a - R_b}{L}. \tag{11}$$

Because of the random fluctuations of $\delta n(\mathbf{r})$, the zenith angle ζ defined by (10) is a random value that consists of three components:

$$\zeta = \zeta_0 + \Delta\zeta + \delta\zeta, \tag{12}$$

where $\Delta\zeta$ is the regular error due to refraction by the $\Delta n(z)$ profile:

$$\Delta\zeta = \frac{1}{L\cos\zeta_0}\left[\int_0^{R_a} \Delta n(z)\, ds_a - \int_0^{R_b} \Delta n(z)\, ds_b,\right], \tag{13}$$

and $\delta\zeta$ is the random error due to scattering by the turbulent refractive-index fluctuations $\delta n(\mathbf{r})$:

$$\delta\zeta = \frac{1}{L\cos\zeta_0}\left[\int_0^{R_a} \delta n(\mathbf{r})\, ds_a - \int_0^{R_b} \delta n(\mathbf{r})\, ds_b\right]. \tag{14}$$

It is evident from the last equation that $\langle\delta\zeta\rangle = 0$, i.e. $\delta\zeta$ is a fluctuating error on zenith angle measurements. Equation (13) for a regular refraction error can be simplified if we replace the integrals along the rays by an integral along the axis Oz (see Fig. 1):

$$\Delta\zeta = \frac{1}{L\cos\zeta_0}\left[\frac{1}{\cos\zeta_a} - \frac{1}{\cos\zeta_b}\right]\int_0^{z_M} \Delta n(z)\, dz, \tag{15}$$

where z_M is the altitude of the source M, and the angles ζ_a and ζ_b are defined by the following equations:

$$\cos\zeta_a = \frac{z_M}{R_a}, \quad \cos\zeta_b = \frac{z_M}{R_b}. \tag{16}$$

Substituting (16) into (15) and using definition (11), we obtain the following expression for the "regular" (or "systematic") error:

$$\Delta\zeta = \frac{\tan\zeta_0}{z_M}\int_0^{z_M} \Delta n(z)\, dz. \tag{17}$$

3 Atmospheric Refraction Errors for Two Targets

Let us consider now two targets, 1 (M) and 2 (T) (see Fig. 2), with corresponding zenith angles ζ_1 and ζ_2, and an angular distance $\theta = \zeta_2 - \zeta_1$ between them in the vertical plane. According to (17), the refractive (nonfluctuating) error $\Delta\theta$ of the angular distance θ, is equal to the following difference:

$$\Delta\theta = \Delta\zeta_2 - \Delta\zeta_1 = \frac{\tan\zeta_2}{z_2}\int_0^{z_2} \Delta n\,(z)\,dz - \frac{\tan\zeta_1}{z_1}\int_0^{z_1} \Delta n\,(z)\,dz. \qquad (18)$$

Introducing the "mean" zenith angle $\zeta = (\zeta_1 + \zeta_2)/2$, we can express ζ_1 and ζ_2 through ζ and θ:

$$\zeta_1 = \zeta - \theta/2 \text{ and } \zeta_2 = \zeta + \theta/2.$$

For small angular distances between targets ($\theta \ll 1$) we may expand (18) in θ and confine it only to the linear term:

$$\Delta\theta = [q\,(z_2) - q\,(z_1)]\tan\zeta + \frac{\theta}{2\cos^2\zeta}[q\,(z_2) + q\,(z_1)]\,, \qquad (19)$$

where we introduce the function:

$$q\,(z) = \frac{1}{z}\int_0^z \Delta n\left(z'\right) dz'. \qquad (20)$$

It is worthwhile to draw attention to two limiting cases:

1. If the altitudes of the sources are equal ($z_1 = z_2 = z$), then the relative error $\Delta\,\theta/\theta$ can be estimated by the simple formula:

$$\frac{\Delta\theta}{\theta} = \frac{q\,(z)}{\cos^2\zeta}. \qquad (21)$$

2. If the two sources are along the same ray so that the angular distance $\theta = \zeta_2 - \zeta_1$ between them is equal to zero, a measurement of θ will differ from zero by the value:

$$\Delta\theta = [q\,(z_2) - q\,(z_1)]\tan\zeta. \qquad (22)$$

It should be noted that, because $\Delta n\left(z'\right) \to 0$ when $z \to \infty$, the function $q\,(z)$ decreases at the rate of $1/z$ for high altitudes, and, according to (19), $\Delta\theta \to 0$ for distant targets. This result is valid only for a planar layered atmosphere. For spherical layers $\Delta\theta \to const.$ when $z \to \infty$.

3.1 Refraction Angle Errors in the Standard Atmosphere

The atmosphere refractive index for super-high frequency (SHF) radio waves ("μ" waves) can be represented as:

$$n = 1 + N \cdot 10^{-6}, \tag{23}$$

where N is the reduced refractive index that depends on air temperature T (in K), pressure P, and humidity e (both in millibars mB) according to the formula (see, for example, [1]):

$$N = \frac{77.6}{T}\left(P + \frac{4810e}{T}\right). \tag{24}$$

Because of the exponential average dependence of pressure P and humidity e on altitude z, the large-scale behavior of the reduced refractive index N with z is also exponential, and therefore can be written as:

$$n(z) = 1 + N_0 \cdot 10^{-6} e^{-\beta z}, \tag{25}$$

where $\beta \simeq 0.13\ (km)^{-1}$, and N_0 is the value of the reduced refractive index at the surface that can be estimated by Eq.(24). For standard atmospheric conditions ($P = 1013.2\ mB, \quad T = 288.2K$), it follows that $N_0 = 335.3$. For this "standard radio atmosphere," function $q(z)$, introduced by (20), takes the simple form:

$$q(z) = \frac{N_0 \cdot 10^{-6}}{\beta z}\left(1 - e^{-\beta z}\right). \tag{26}$$

The dependence of the angular error $\Delta\theta\,(rad)$ on the source M altitude z_1 is exemplified in Fig. 3 (a,b,c) for the case $\theta = 0$ ($\zeta_1 = \zeta_2$) and $z_1 \leq z_2$ [calculations by Eq.(22)]. The plots of the relative angular error $\Delta\theta/\theta$ for the special case $z_1 = z_2$ and for four zenith angles ζ are shown in Fig. 4 [calculations by Eq.(21)].

3.2 Refraction Angle Errors in the Real Atmosphere

Generally, the vertical profile of refractive index $n(z)$ in the real atmosphere will differ from the standard exponential model (25). The profile $n(z)$ could be obtained, for example, from radiosonde (balloon) data like those in Table 1, where RH is relative humidity in % and z is altitude above sea level in

m. Some examples of altitude profiles of meteorological parameters P(mB), T ^{0}C and RH(%) are shown in Fig. 5a,b,c trough Fig. 8a,b,c for summer and winter seasons and day- and nighttime. To use Eq.(24) for calculating the reduced refractive index $N(z)$, we have to express the vapor pressure e through RH% according to the equation (see, for example, [4]):

$$e(mB) = 6.11 \cdot RH \cdot 10^{\frac{7.63*T^0C}{242+T^0C}-2}. \tag{27}$$

Examples of calculated profile of $N(z)$ are shown in Fig. 5d trough Fig. 8d. For comparison, in the same figures, we plot the adjusted exponential profiles (25) with the near-earth values $N_0 = N(0)$ that correspond to the real experimental data obtained from the balloon measurements (the first line from Table 1).

Refraction error calculations were performed for two different cases:

1.The altitudes of the sources are equal ($z_1 = z_2 = z$). Then the angle difference error $\Delta\,\theta$ is a function (21) of the mean zenith angle $\zeta = (\zeta_1 + \zeta_2)/2$ and the angle difference $\theta = \zeta_2 - \zeta_1$ between these two sources. It follows from (21) that in this case the relative error $\Delta\,\theta/\theta$ depends on the zenith angle ζ only through the factor $1/\cos^2\zeta$. The value $(\Delta\,\theta/\theta)\cos^2\zeta$ is shown as a function of altitude z in Fig. 5e-Fig. 8e as a solid curve, the long-dashed curve corresponds to the "adjusted" (for near-earth refractive index $N(0)$) exponential profile (25), and the short-dashed curve corresponds to the standard radio atmosphere with $N_0 = 335.3$.

2. The two sources have the same zenith angles $\zeta_1 = \zeta_2 = \zeta$. The angular distance error $\Delta\theta$ in this case depends on ζ only through the factor $\tan\zeta$, as in (22). The value of $\Delta\theta\cot\zeta$ is shown as a function of the source M altitude z_1 for three values of the source T altitude z_2 in Fig. 5f,g,h through Fig. 8f,g,h by the solid curves. The dashed curves are, as in Fig. 5e-Fig. 8e , the "adjusted" exponential profile (longed-dashed) and the standard radio atmosphere profile (short-dashed).

In addition to these two general cases, we consider in detail the specific case when the target (T) is located at the range $R_2 = 10$ km. at an altitude $z_2 = 6$ km. ($\zeta_2 = 53^o$). Two different scenarios of a missile (M) approaching the target (T) are investigated (see Fig. 9):

1) Missile (M) approaches the target (T) horizontally at the same altitude z_1 as that of the target ($z_1 = z_2 = 6km$) shown in Fig. 10a,b,c,d.

2) Missile (M) approaches the target (T) along the direction (OT) from the interferometer to the target ($\zeta_1 = \zeta_2 = 53^o$) shown in Fig. 11a,b,c,d.

In both of these scenarios, we denote the distance between the target (T) and the missile (M) as s.

In the **upper** plots of Fig. 10a,b,c,d and Fig. 11a,b,c,d, three different refraction errors $\Delta\theta(\mu rad)$ are shown. The solid curves correspond to the refraction error $\Delta\theta_{\text{real}}$ due to the real refractive-index profile obtained directly from the balloon data. The short-dashed curves correspond to the refraction error $\Delta\theta_{\text{stand}}$ predicted by the exponential (25) standard atmospheric ($N_0 = 335.3$) refractive-index profile. The long-dashed curves correspond to the refraction error $\Delta\theta_{adj}$ predicted by the exponential refractive-ndex profile (25), adjusted to the real value at the surface, i.e. $N_0 = N(0)$.

In the **lower** plots of Fig. 10a,b,c,d and Fig. 11a,b,c,d two residual errors are shown. The long-dashed curves correspond to the residual $\Delta\theta_{\text{stand}} - \Delta\theta_{\text{real}}$, and the solid curves correspond to the residual error $\text{Res}\Delta\theta = \Delta\theta_{adj} - \Delta\theta_{\text{real}}$.

The main results of these calculations for the refraction error $\Delta\theta_{\text{real}}$ obtained by integrating the real refractive-index profile, and for the residual error $\text{Res}\Delta\theta = \Delta\theta_{adj} - \Delta\theta_{\text{real}}$, are represented briefly in Table 2. for target separation distance $s = 5km$ between two simultaneously tracking targets T and M. For smaller or larger separations s, the value of error can be estimated easily because of approximately linear dependence of these errors on target separation s, as it follows from Fig. 10 and Fig.11.

Table 2.

s=2 km.		Scenario 1 ($z_1 = z_2$)		Scenario 2 ($\zeta_1 = \zeta_2$)	
		$\Delta\theta_{\text{real}}$ (μr)	Res$\Delta\theta$ (μr)	$\Delta\theta_{\text{real}}$ (μr)	Res$\Delta\theta$ (μr)
Summer	Night	70	1.5	21	-1
	Day	70	3.5	21	-0.5
Winter	Night	60	0	16	1.5
	Day	60	-1	16	1.2

In summer the refraction error $\Delta\theta_{\text{real}}$ is larger than in winter, and in Scenario 1 it is much more (about four times) then in Scenario 2. These errors can be compensated almost entirely (with the accuracy of several μrad) using the exponential refractive-index profile adjusted to the real near-earth value of refractive index.

4 Tracking Errors in the Turbulent Atmosphere

Let us consider now the fluctuating error $\delta\zeta$ of the zenith bearing angle ζ of point source M in the turbulent atmosphere described by Eq.(14). If we introduce the fluctuations δS_a and δS_b

$$\delta S_{a,b} = \int_0^{R_{a,b}} \delta n\left(\mathbf{r}\right) ds_{a,b}, \tag{28}$$

of the eikonal S over the propagation paths Ma and Mb (see Fig. 1), then the fluctuating error $\delta\zeta$ takes the form:

$$\delta\zeta = \frac{1}{L\cos\zeta}\left(\delta S_a - \delta S_b\right). \tag{29}$$

Statistical averaging of the square of the error $(\delta\zeta)^2$ leads to the following expression for the error variance σ_ζ^2:

$$\sigma_\zeta^2 = \left\langle(\delta\zeta)^2\right\rangle = D_S\left(Ma, Mb\right) / \left(L\cos\zeta\right)^2, \tag{30}$$

where $D_S\left(Ma, Mb\right)$ is the structure function of the eikonal fluctuations at the final points a and b of the paths Ma and Mb, respectively:

$$D_S\left(Ma, Mb\right) = \left\langle\left(\delta S_a - \delta S_b\right)^2\right\rangle. \tag{31}$$

Substituting (28) into (31) we can express $D_S\left(Ma, Mb\right)$ through the spatial structure function D_n of the refractive-index fluctuations :

$$D_n(\mathbf{r}_1, \mathbf{r}_2) = \left\langle\left[\delta n\left(\mathbf{r}_2\right) - \delta n\left(\mathbf{r}_1\right)\right]^2\right\rangle. \tag{32}$$

We confine ourselves to consideration of the special case of a locally homogeneous and isotropic refractive-index random field $n\left(\mathbf{r}\right)$, when $D_n(\mathbf{r}_1, \mathbf{r}_2)$ is a function only of the distance $\rho = |\mathbf{r}_2 - \mathbf{r}_1|$ between points $\mathbf{r}_1$ and $\mathbf{r}_2$ that varies slowly with the "mean" coordinate $\mathbf{R} = \left(\mathbf{r}_2 + \mathbf{r}_1\right)/2$. Spectral expansion of $D_n(\mathbf{r}_1, \mathbf{r}_2) \equiv D_n\left(\rho, \mathbf{R}\right)$ in this case has the form:

$$\begin{aligned} D_n(\rho, \mathbf{R}) &= 2\iiint_{-\infty}^{\infty}\left[1 - \cos\boldsymbol{\kappa}\boldsymbol{\rho}\right]\Phi_n\left(\boldsymbol{\kappa}, \mathbf{R}\right) d^3\kappa = \\ & 8\pi\int_0^{\infty}\left(1 - \frac{\sin\kappa\rho}{\kappa\rho}\right)\Phi_n\left(\kappa, \mathbf{R}\right)\kappa^2 d\kappa, \end{aligned} \tag{33}$$

where the spatial spectral density $\Phi_n(\kappa, \mathbf{R})$ of the refractive-index fluctuations is connected with their structure function $D_n(\rho, \mathbf{R})$ by the formula:

$$\Phi_n(\kappa, \mathbf{R}) = \frac{1}{16\pi^3\kappa^2} \iiint \boldsymbol{\kappa} \nabla_\rho D_n(\rho, \mathbf{R}) \sin \boldsymbol{\kappa}\rho d^3\rho = \frac{1}{16\pi^3\kappa^2} \int_0^\infty (\sin\kappa\rho - \kappa\rho\cos\kappa\rho) \frac{\partial}{\partial\rho} D_n(\rho, \mathbf{R}) d\rho. \tag{34}$$

Using expansion (33) we can represent $D_S(Ma, Mb)$ (31) in a form that generalizes the well-nown result of [1] and [2] for wave propagation in an inhomogeneous medium:

$$D_S(Ma, Mb) = 8\pi^2 \int_0^R ds \int_0^\infty \Phi_n(\kappa, \mathbf{r}(s)) \{1 - J_0[\kappa\rho(s)]\} \kappa d\kappa, \tag{35}$$

where J_0 is the zero-order Bessel function of the first kind, $\mathbf{r}(s)$ is a radius-vector of points on the ray OM (see Fig. 1), s is the distance along this ray from the origin of coordinates O, R is a distance between the origin of coordinates O and source M, and $\rho(s)$ is a separation between rays aM and bM in a direction orthogonal to the ray OM at every point $\mathbf{r}(s)$:

$$\rho(s) = L\cos\zeta\left(1 - \frac{s}{R}\right). \tag{36}$$

Denoting spacial spectral density $\Phi_n(\kappa, \mathbf{r}(s))$ as a $\Phi_n(\kappa, s)$ we will represent it for further derivations as follows:

$$\Phi_n(\kappa, s) = \frac{0.033 C_n^2(s)}{[\kappa^2 + \kappa_0^2(s)]^{11/6}}, \tag{37}$$

where C_n is a so-called "structure constant," $\kappa_0 = 2\pi/\Lambda_0$, and Λ_0 is the outer turbulence scale - the dimension of the largest turbulence vortex in the atmosphere. Generally speaking, these parameters are slowly varying functions in space, so we can consider here not only a statistically homogeneous but a "locally homogeneous" turbulent atmosphere as well. Substituting (37) into (35), we can rewrite (35) after the variable changing $\kappa\rho = x$ in the following general form:

$$D_S(Ma, Mb) = 2.6 \int_0^R C_n^2(s) \rho^{5/3}(s) ds \times \int_0^\infty \frac{[1 - J_0(x)] x dx}{[x^2 + \kappa_0^2(s)\rho^2(s)]^{11/6}}. \tag{38}$$

Using (30) and (38) for estimating the zenith angle dispersion error σ_ζ^2, we can calculate this value for very different states of atmospheric turbulence. If the outer turbulence scale Λ_0 exceeds essentially the interferometer base projection in a direction orthogonal to the mean ray direction $\mathbf{r}(s)$, i.e. the inequality $\Lambda_0 \gg L\cos\zeta$ is fulfilled, then we can neglect the term $\kappa_0^2(s)\rho^2(s) \ll 1$ in (38), and after calculating the integral over dx we obtain:

$$D_S(Ma, Mb) = 2.9\int_0^R C_n^2(s)\rho^{5/3}(s)\,ds. \tag{39}$$

In most atmospheric turbulence models C_n^2 is considered as a function of altitude z above the earth's surface. Therefore, it can be more convenient to change (39) from integrating over ray length s to integrating over the altitude z using the obvious relation $s = s(z) = z/\cos\zeta$:

$$D_S(Ma, Mb) = \frac{2.9}{\cos\zeta}\int_0^{z_M} C_n^2(z)\rho^{5/3}[s(z)]\,dz, \tag{40}$$

where z_M is the point M altitude. For a rough estimation of the $D_S(Ma, Mb)$ we can replace the value of $C_n^2(s)$ in (39) by its mean value C_n^2 on the path OM, and then fulfill integration on ds taking into account (36):

$$\begin{aligned} D_S(Ma, Mb) &= 2.9C_n^2\int_{\rho(0)}^{\rho(R)}\frac{\rho^{5/3}d\rho}{|d\rho/ds|} = \\ &1.08C_n^2R\frac{\rho^{8/3}(R) - \rho^{8/3}(0)}{\rho(R) - \rho(0)}, \end{aligned} \tag{41}$$

where $\rho(0) = L\cos\zeta$ and $\rho(R) = 0$ according to (36). Substituting (41) into (30) we obtain the following simple formula for the error dispersion:

$$\sigma_\zeta^2 = 1.08\frac{C_n^2R}{l^{1/3}}, \tag{42}$$

where $l = L\cos\zeta$ is the projection of the interferometric base L on a plane that is orthogonal to the direction OM. It follows from this formula that for $C_n^2 = 10^{-14}\ \mathrm{m}^{-2/3}$, range $R = 10$ km and $l = 5$ m, the rms error of the zenith angle measurement is $\sigma_\zeta \simeq 8\cdot 10^{-6}$rad. It should be noted that σ_ζ^2 decreases very slowly with the interferometric base increasing as $\sim l^{1/3}$. This means that even increasing l ten times results in reduction of σ_ζ of less than 1.5 times.

5 Atmospheric Turbulence Errors for Two Targets

Let us consider again two point sources $1(M)$ and $2(T)$ (Fig. 2) that are simultaneously tracked by a single radar interferometer consisting of two receivers at points a and b separated by a distance L, interferometric base. Fluctuations $\delta\zeta_1$and $\delta\zeta_2$ of each of zenith angles ζ_1 and ζ_2 are given by (29):

$$\delta\zeta_1 = \frac{1}{L\cos\zeta_1}\left(\delta S_{a1} - \delta S_{b1}\right), \quad \delta\zeta_2 = \frac{1}{L\cos\zeta_2}\left(\delta S_{a2} - \delta S_{b2}\right), \tag{43}$$

where $\delta S_{\alpha i}$ is a fluctuation that eikonal acquires on the way from the source $i = (1,2)$ to the receiver $\alpha = (a,b)$. The fluctuations $\delta\theta$ of the angular difference $\theta = \zeta_2 - \zeta_1$ between that two sources is equal to the following :

$$\delta\theta = \delta\zeta_2 - \delta\zeta_1 \simeq \frac{1}{l}\left(\delta S_{a2} - \delta S_{b2} - \delta S_{a1} + \delta S_{b1}\right). \tag{44}$$

Here, we confine ourselves only to the linear terms of $\delta S_{\alpha i}$ and introduce the mean interferometric base projection $l = L\cos\zeta$, where $\zeta = (\zeta_1 + \zeta_2)/2$, assuming that the angular distance between the points M and T is small enough ($\theta \ll 1$). To simplify the subsequent formulae we number the rays connecting receivers a, b and points M, T as shown in Fig. 12. After squaring (44) and statistical averaging, we obtain with these notations:

$$\begin{aligned}\sigma_\theta^2 &= \left\langle(\delta\theta)^2\right\rangle = \frac{1}{l^2}\left\langle(\delta S_3 - \delta S_4 - \delta S_1 + \delta S_2)^2\right\rangle = \\ &\frac{1}{l^2}\left(D_{12} + D_{34} + D_{13} + D_{24} - D_{23} - D_{14}\right),\end{aligned} \tag{45}$$

where the eikonal structure functions D_{ik} were introduced according to (31):

$$D_{ik} = \left\langle(\delta S_i - \delta S_k)^2\right\rangle. \tag{46}$$

Without loss of generality we can assume that $R_2 \geq R_1$ and then each of these structure functions can be calculated by the formula (38) with the following parameter R value: $R = R_2$ for D_{34}, and $R = R_1$ for the all other D_{ik}. As to function $\rho(s)$ it can be written in a general form (for straight rays):

$$\rho(s) = \rho(0) + \frac{s}{R}\left[\rho(R) - \rho(0)\right] \tag{47}$$

with the following values of parameters $\rho(0)$ and $\rho(R)$ for each D_{ik}:

$$\begin{aligned} D_{12} \text{ and } D_{34} &: \quad \rho(0) = l, \quad \rho(R) = 0; \\ D_{13} \text{ and } D_{24} &: \quad \rho(0) = 0, \quad \rho(R) = \Delta; \\ D_{23} &: \quad \rho(0) = l, \quad \rho(R) = -\Delta; \\ D_{14} &: \quad \rho(0) = l, \quad \rho(R) = \Delta. \end{aligned} \tag{48}$$

where $\Delta = R_1\theta$ is the spatial separation between rays OM and OT at a distance R_1 from the radar position. For a large enough turbulence outer scale $\Lambda_0 \gg l, \Delta$ we can use the simpler formula (39) for D_{ik} calculations if we know the C_n^2 as a function of the coordinates. For a plane layered atmospheric model when C_n^2 depends only on the altitude z, we can use (40) instead of (39). In the simplest case $C_n^2 = const$ we have the explicit form (41) for the eikonal structure function D_{ik}, substituting of which in (45) and taking into account (48) we obtain:

$$\sigma_\theta^2 = \sigma_{\zeta 1}^2 + \sigma_{\zeta 2}^2 - 2\sigma_{\zeta 1}^2 B(x), \tag{49}$$

where the error dispersions $\sigma_{\zeta 1}^2, \sigma_{\zeta 2}^2$ of zenith angles ζ_1 and ζ_2 are given by (42) :

$$\sigma_{\zeta 1}^2 = 1.08\frac{C_n^2 R_1}{l^{1/3}}, \quad \sigma_{\zeta 2}^2 = 1.08\frac{C_n^2 R_2}{l^{1/3}}, \tag{50}$$

and the correlation coefficient $B(x)$ of their fluctuations as a function of $x = \Delta/l$ has the form:

$$B(x) = \frac{1 - x^{5/3}}{1 - x^2}. \tag{51}$$

In the limiting case of a very small angular difference between two sources, i.e. when $x \ll 1$, the value of correlation coefficient $B(x)$ is very close to the unit:

$$B(x) \approx 1 - x^{5/3} + x^2 ... \qquad (x \ll 1), \tag{52}$$

and from (49) it follows:

$$\sigma_\theta^2 = \sigma_{\zeta 2}^2 - \sigma_{\zeta 1}^2. \tag{53}$$

It should be noted that $\sigma_\theta^2 \neq 0$ even for the case $\Delta = 0$ when both sources are on the same ray but at different distances $R_1 \neq R_2$. Taking into account

(50) and the fact that in the real atmosphere C_n^2 decreases with altitude we can give a rough upper estimate of σ_θ^2 in this case:

$$\sigma_\theta^2 < 1.08\,(R_2 - R_1)\,\frac{C_n^2}{l^{1/3}}. \tag{54}$$

From Fig. 13a,b it is easy to see that with x increasing the correlation coefficient $B\,(x)$ decreases very slowly according to (52), so that formula (53) remains valid with a great accuracy even for $x \simeq 1$. For $x \gg 1$ the correlation coefficient $B\,(x)$ tends to zero very slowly:

$$B\,(x) \approx \frac{1}{x^{1/3}} \qquad (x \gg 1), \tag{55}$$

and it follows from (49) that in this limiting case, when we can neglect the correlation of signal phase fluctuations of the two sources, the error dispersion on interferometric measurement of angular difference θ is equal to the sum of error dispersions for measurement of each angle ζ_1 and ζ_2 :

$$\sigma_\theta^2 = \sigma_{\zeta 2}^2 + \sigma_{\zeta 1}^2. \tag{56}$$

It might be worth emphasizing that such slow decreasing of $B\,(x)$ as shown by (55) with the increase of value of x takes place until the distance between rays remains less than the outer turbulence scale:

$$\max\{l, \Delta\} \ll \Lambda_0.$$

In the opposite case, i.e. for large space separation between rays, the correlation coefficient $B\,(x)$ decreases much more rapidly than (55), and formula (56) becomes valid for lesser values of x.

For small enough angular difference when $x \ll 1$ it is more convenient to use the following formula instead of (49) :

$$\sigma_\theta^2 = \sigma_{\zeta 2}^2 - \sigma_{\zeta 1}^2 + 2\sigma_{\zeta 1}^2 F\,(x), \tag{57}$$

where

$$F\,(x) = 1 - B\,(x) = \frac{x^{5/3}\left(1 - x^{1/3}\right)}{1 - x^2}. \tag{58}$$

The $F\,(x)$ plots are shown in Fig. 14a,b,c. For targets that are close enough it may be assumed that $\sigma_{\zeta 2}^2 = \sigma_{\zeta 1}^2 \equiv \sigma_\zeta^2$, $x \ll 1$ and from (57) it follows:

$$\sigma_\theta^2 = 2\sigma_\zeta^2 F\,(x) \approx 2\sigma_\zeta^2 x^{5/3}. \tag{59}$$

Numerical estimation of σ_θ by this formula and (42) for the following parameter values: $C_n^2 = 10^{-14}$ m$^{-2/3}$, range $R_1 \simeq R_2 \simeq 5$ km, interferometer base $l = 5$ m and $\Delta \simeq 0.1l$, leads to the result: $\sigma_\theta \simeq 0.9 \cdot 10^{-7}$ rad. Even for twice the ranges $R_1 \simeq R_2 \simeq 10$ km and ten times more target separation $\Delta = l$, which corresponds to $x = 1$ and $F(x) = 1/6$), we obtain all the same extremely small rms errors: $\sigma_\theta \simeq 4.6 \cdot 10^{-6}$ rad.

6 Retrieval of C_n^2 from Meteorological Balloon Data

The structure function $D_n(\rho)$ of atmospheric refractive-index fluctuations $\delta n(\mathbf{r})$ in the frame of the theory of local homogeneous and isotropic turbulence can be represented in a simple form (Obukhov-Kolmogorov "2/3 law"):

$$D_n(\rho) = \left\langle [\delta n(\mathbf{r}+\boldsymbol{\rho}) - \delta n(\mathbf{r})]^2 \right\rangle = C_n^2(z)\,\rho^{2/3}. \tag{60}$$

It is easy to prove that the spatial spectral density $\Phi_n(\kappa, s)$ of this structure function $D_n(\rho)$ coincides with the (37) if $\kappa_0 = 0$, which corresponds to the infinite outer scale Λ_0 of turbulence. The structure parameter C_n^2 is a slowly varying function of height and for **optical** waves depends on atmospheric parameters such as (see, for example, [1]):

$$C_{n0}^2 = \left(7.9 * 10^{-5} \frac{P}{T^2}\right)^2 C_T^2, \tag{61}$$

where P is air pressure in millibars, T is air temperature in Kelvins (K^o), C_T^2 is structure parameter of temperature fluctuations in $\left(K^o/m^{1/3}\right)^2$.

The structure parameter C_n^2 for the **radio** waves depends not only on air pressure and temperature but on humidity as well (see [5]):

$$\begin{aligned} C_n^2 &= \left(6.1 * 10^{-4} \frac{P}{T^2}\right)^2 \left[C_q^2 - 2a_r C_{Tq} + a_r^2 C_T^2\right], \\ a_r &= 0.13\left(1 + 15.4\frac{q}{T}\right), \end{aligned} \tag{62}$$

where q is the moisture content in grams of water per kilogram of air, C_q^2 is the structure parameter of the moisture content q fluctuations. Assuming that

$$C_{Tq} = -(C_T^2 C_q^2)^{1/2}, \tag{63}$$

we obtain from (62)(see [6] and [7]):

$$C_n^2 = \left(7.9 * 10^{-5} \frac{P}{T^2}\right)^2 \left[7.7 C_q + \left(1 + 15.4 \frac{q}{T}\right) C_T\right]^2. \tag{64}$$

The structure parameters C_q and C_T of moisture q and temperature T fluctuations can be retrieved from the meteorological balloon data using the existing theories of turbulence in stratified media.

6.1 Free Atmosphere Turbulence

At high enough altitudes it is possible to neglect the earth's influence on the turbulent processes in the atmosphere. This assumption leads to the so-called "free atmosphere model." The free atmosphere stratification is characterized by the Brunt-Vaisala frequency ω_b :

$$\omega_b^2 = \frac{g}{\theta} \frac{\partial \theta}{\partial z}, \tag{65}$$

where g =9.8 $[m/s^2]$ is the gravity acceleration, and θ is the so-called "potential temperature":

$$\theta = T \left(\frac{P_0}{P}\right)^{0.286}, \tag{66}$$

where P_0 is a reference pressure, usually taken as a pressure at the level of the earth's surface. The greater the Brunt-Vaisala frequency ω_b is, the more hydrostatically stable is the condition of the atmosphere. Turbulence in the free atmosphere appears in regions where temperature and wind gradients create conditions favorable for generating internal gravity waves, propagation and breakdown. The greater the wind vertical gradient (so-called "wind shear")

$$S = \sqrt{\left(\frac{\partial u}{\partial z}\right)^2 + \left(\frac{\partial v}{\partial z}\right)^2} \tag{67}$$

(u and v are the projections of wind speed on the horizontal plane), the more unstable the atmosphere becomes (often referred to as Kelvin-Helmholz instability). The Richardson number **Ri** is the ratio of the stabilizing factor ω_b^2 to this destabilizing factor S^2 :

$$\mathbf{Ri} = \frac{\omega_b^2}{S^2}. \tag{68}$$

From experimental investigation it follows that if **Ri** <0.25, then the atmosphere is dynamically unstable so that small disturbances (like the internal gravity waves, for example) grow until they break down into turbulence. After turbulence breakdown occurs, the turbulence mixes the atmospheric layers and the wind gradients S are reduced until **Ri** becomes greater than 0.25 and the turbulence in this particular layer begins to decay. These actively turbulent regions are on the order of a few meters to hundreds of meters thick, with 30 m being typical.

The structure parameter C_x^2 of any **passive (or conservative)** variable fluctuations x relates to the local vertical gradients $\partial \langle x \rangle / \partial z$ of average value $\langle x \rangle$ by an approximate equation [1]:

$$C_x^2 = 2.8 \left(\frac{\partial \langle x \rangle}{\partial z} \right)^2 \Lambda_0^{4/3}, \tag{69}$$

where Λ_0 is the outer scale of turbulence. Using this formula for estimation of C_q^2 and C_T^2 we have to take into account that the temperature T is not a passive addition, but the potential temperature θ is.

It is follows from (69) that

$$\frac{C_q^2}{C_T^2} = \left[\frac{\partial \langle q \rangle / \partial z}{\partial \langle \theta \rangle / \partial z} \right]^2. \tag{70}$$

Compare (64) with (61), and using (70) we obtain:

$$Y_n \equiv \frac{C_n^2}{C_{n0}^2} = \left[-7.7 \frac{\partial \langle q \rangle / \partial z}{\partial \langle \theta \rangle / \partial z} + \left(1 + 15.4 \frac{\langle q \rangle}{\langle T \rangle} \right) \right]^2. \tag{71}$$

For free-atmosphere conditions we can use (69) for calculating the temperature fluctuation structure parameter C_T^2 and obtain from (61), (71):

$$C_{n0}^2 = 2.8 \left(7.9 * 10^{-5} \frac{P}{T^2} \right)^2 \left(\frac{\partial \langle \theta \rangle}{\partial z} \right)^2 \Lambda_0^{4/3}, \tag{72}$$

$$C_n^2 = \left[-7.7 \frac{\partial \langle q \rangle / \partial z}{\partial \langle \theta \rangle / \partial z} + \left(1 + 15.4 \frac{\langle q \rangle}{\langle T \rangle} \right) \right]^2 C_{n0}^2. \tag{73}$$

6.2 Planetary Boundary-Layer Turbulence

For the near-earth atmospheric turbulence description [in the planetary boundary layer (PBL)] it is necessary to distinguish two different limiting cases: stable (nighttime) conditions and unstable (daytime) conditions. In contrast to the free atmosphere the main reason for turbulent processes in the PBL is not Kelvin-Helmholz instability (produced by the large values of wind shear S) but the convection processes due to near earth-heating fluxes.

6.2.1 Nighttime PBL turbulent parameters

During night -time (mostly stable conditions with small turbulence) the depth of the PBL, denoted below as z_i, is typically about 100 m, and surface-layer parameterization for C_T^2 valid at altitudes $z < z_i$ can be written in a form [7]:

$$C_T^2 = T_*^2 z^{-2/3} \left[1 + 2.7 \left(\frac{z}{L}\right)^{2/3}\right], \tag{74}$$

where L is the Monin-Obukhov similarity (MOS) stability length:

$$L = \frac{T}{kg} \frac{u_*^2}{T_*}, \tag{75}$$

k =0.4 is the von Karman constant, u_* is friction wind speed

$$u_* = \frac{k}{\ln\left(z_r/z_0\right)} u\left(z_r\right), \tag{76}$$

$u\left(z_r\right)$ is the horizontal wind speed at the reference height z_r above the earth's surface, z_0 is the roughness length, and the MOS surface-layer parameter T_* is connected with the surface turbulent heat flux H_{s0} :

$$T_* = -\frac{H_{s0}}{\rho c_p u_*}, \tag{77}$$

where $\rho = 1.29\,[kg/m^3]$ is the air specific density and $c_p = 10^3 \left[\frac{joul}{kg \cdot \deg}\right]$ is the specific heat of air. In its turn the turbulent heat flux H_{s0} can be expressed through the land net radiation R_{net}, Bowen ratio β_0 and the soil flux partition ratio α:

$$H_{s0} = \frac{(1-\alpha) R_{net}}{1 + 1/\beta_0}. \tag{78}$$

The structure parameter C_q^2 of humidity fluctuations is given by the equation similar to (74):

$$C_q^2 = q_*^2 z^{-2/3} \left[1 + 2.7 \left(\frac{z}{L}\right)^{2/3}\right], \tag{79}$$

where q_* is the humidity MOS surface-layer scaling parameter:

$$q_* = T_* \frac{c_p}{L_e \beta_0}, \tag{80}$$

and L_e is the latent heat of water vaporization. Substituting (74) and (80) in the general equation (64) we can obtain the C_n^2 profile in the PBL for nighttime conditions.

As an example of the typical values of all PBL parameters introduced above for Colorado in the Denver/Boulder area are given in Table 3.

Table 3.

	Winter		Summer	
	Day	Night	Day	Night
β_0	1	10	2	10
α	0.4	0.9	0.2	0.9
$u_* \, (m/s)$	0.5	0.1	0.35	0.1
$R_{net} \, (W/m^2)$	300	-100	600	-100
$z_i \, (m)$	1200	100	2000	100

6.2.2 Daytime PBL turbulent parameters

During day-time (usually unstable conditions) and cloud-free skies the depth z_i of the PBL is typically between 1 km and 2 km, and the profile of C_T^2 is given by the following equation (see [8]):

$$C_n^2 = Q_*^2 z_i^{-2/3} \left(6 \cdot 10^{-4} \frac{P}{T^2}\right)^2 f_q(\xi) \, \alpha_\tau^2, \tag{81}$$

where Q_* is the standard moisture convective scaling parameter (connected with the moisture turbulent scalar surface flux):

$$Q_* = \theta_* \frac{\beta_0 c_p}{L_e} \tag{82}$$

and the value of standard temperature convective scaling parameter θ_* is connected with the vertical turbulent heat flux H_{tb}

$$H_{tb} = -u_* T_* = \frac{H_{s0}}{\rho c_p} \tag{83}$$

by the following relation:

$$\theta_* = \left(\frac{H_{tb}^2 T}{g z_i} \right)^{1/3}. \tag{84}$$

In (81) the following functions of the dimensionless height variable $\xi = z/z_i$, surface Bowen ratio β_0 and inversion Bowen ratio β_i are introduced :

$$\alpha_r^2 = 1 - 5 a_r \beta_0 \frac{f_{Tq}(\xi)}{f_q(\xi)} + (2.5 a_r \beta_0)^2 \frac{f_T(\xi)}{f_q(\xi)} \tag{85}$$

$$f_T(\xi) = h_b(\xi) + R_T h_{tb}(\xi) + R_T^2 h_t(\xi) \tag{86}$$

$$f_q(\xi) = h_b(\xi) + \frac{\beta_0}{\beta_i} R_T h_{tb}(\xi) + \left(\frac{\beta_0}{\beta_i} \right)^2 R_T^2 h_t(\xi) \tag{87}$$

$$f_{Tq}(\xi) = h_b(\xi) + 0.5 \left(1 + \frac{\beta_0}{\beta_i} \right) R_T h_{tb}(\xi) + \frac{\beta_0}{\beta_i} R_T^2 h_t(\xi) \tag{88}$$

$$R_t = -0.2 \left(1 - 3.2 \frac{L}{z_i} \right), \tag{89}$$

$$h_b(\xi) = 10 \left(-\frac{z_i}{L} \right)^{2/3} \left[\xi \left(1 - \frac{7z}{L} \right) \right]^{-2/3}, \tag{90}$$

$$h_{tb}(\xi) = 8 (1 - 0.8\xi), \tag{91}$$

$$h_t(\xi) = 10 (1 - \xi)^{-2/3} (2 - \xi)^{-1}. \tag{92}$$

In Fig. 15 through Fig. 18 the potential temperature θ and the specific humidity q profiles, obtained from the balloon data of the Denver Meteorological Observatory (longitude 104.87, latitude 39.75; altitude above the sea level 1611 m), are represented for two winter and summer days at daytime

and nighttime conditions. To calculate the average temperature and humidity gradients, the balloon data (given with the $6s$ interval that corresponds to a 20-30 m difference in altitude) were averaged by three consecutive indicators. The altitude z_i of the PBL for daytime conditions was found as the altitude of the characteristic "step" in the $\theta(z)$ and $q(z)$ plots (see the dashed lines in Fig. 16a,b winter daytime and Fig. 18a,b summer daytime). For nighttime conditions the altitude z_i of the PBL was chosen as equal to 100 m for winter as well as for summer.

According to the [7] and [6] we choose $\Lambda_0 = 35m$ as a mean value of the turbulence vertical outer scale, and $z_0 = 0.1$ as an intermediate roughness length value between farmland ($z_0 = 0.05$) and woodlend ($z_0 = 0.3$). The inversion Bowen ratio β_i was chosen as equal to (- 0.4) as a mean value for the Central Plains according to [8]. The other parameters were chosen from Table 3. The structure C_n^2 profiles obtained as a result of balloon data processing according to the above described theoretical approach are presented in Fig. 19 through Fig. 22 for the same four days as the meteorological data presented in Fig. 15 through Fig. 18. Above the PBL ($z > z_i$) the results of C_n^2 calculations by equations (72) and (73) were rejected to the zero value (for logarithmic scale in these graphs we choose this value as 10^{-19}) in the stable condition layers where the Richardson number **Ri** exceeded the 0.25 value.

7 Conclusions

We will summarize separately the main results obtained for the regular refraction error $\Delta\theta$, for the rms error σ_θ due to the scattering by turbulent inhomogeneities, and for C_n^2 profiles retrieved from the balloon data.

7.1 Regular refraction error

1. According to (19) the value of the regular refraction error $\Delta\theta$ on measuring the angular difference θ between two targets in the planar stratified atmosphere depends only on the integral (20) of the average refractive-index deviation $\Delta n(z) = \langle n(z_T) \rangle - 1$. It means that this kind of "regular" error does not depend on the details of altitude behavior of $\Delta n(z)$, but mainly only on a difference $\langle n(0) \rangle - \langle n(z_T) \rangle$ between the near-earth value $\langle n(0) \rangle$ and its value $\langle n(z_T) \rangle$ at the target altitude z_T.

2. The value of $\Delta\theta$ increases drastically (see Fig. 3a,b,c and Fig. 4) for low-grazing angles (when the zenith angle ζ tends to 90^0) .

3. The value of $\Delta\theta$ increases when the range separation $\Delta R = R_2 - R_1$ between targets increases, but it decreases with the "mean" distance $R = (R_2 + R_1)/2$ increasing.

4. It follows from the real balloon data processing that in summer the regular refraction error $\Delta\theta$ is larger than in winter. The diurnal difference of errors $\Delta\theta$ is much smaller than the seasonal one.

5. The value of the refraction error $\Delta\theta$ for the fixed separation distance s between two simultaneously tracked targets depends on the scenario of their approach: for a horizontal trajectory it is several times more than for an inclined trajectory (when the interferometer and these two targets are in the same line).

6.The refracting errors $\Delta\theta$ can be compensated for almost entirely (with the accuracy of several μrad for distances s about 2 km) using the exponential refractive-index profile adjusted to the real near-earth value of the refractive index.

7.2 Error due to scattering by turbulent inhomogeneities

1. The dispersion σ_θ^2 of the random fluctuations $\delta\theta$ of the angle difference θ between two targets due to scattering by turbulent refractive-index variations δn is determined by the altitude dependence of structure constant C_n^2 and the outer scale of turbulence Λ_0.

2. If the projections of the interferometric base l and the spatial separation Δ between targets on the plane perpendicular to the mean direction to the targets, are small enough $(l, \Delta \ll \Lambda_0)$, the value of σ_θ^2 depends only on integrals of $C_n^2(z)$ over the height z of Eq.(40) .

3. Although the rms value σ_ζ of the zenith angle ζ (missile and target) fluctuations according to (42) can run into enough large values ($\sigma_\zeta \simeq 10^{-4} rad$ for the mean value $C_n^2 \simeq 10^{-12} m^{-2/3}$) the rms angular difference error σ_θ is much smaller as it follows from (57) and (59) because of the high level of these fluctuations correlation for a small angular difference θ between targets and their spatial separation ΔR.

7.3 C_n^2 profile altitude behavior

1. The procedure of C_n^2 profile retrieval from the meteorological balloon data includes information about the near-earth values of temperature, humidity, heat flux and wind speed in addition to the balloon data for heights above several tens of meters.

2. For more precise C_n^2 profile determination it is necessary to use the procedure of turbulence outer scale Λ_0 estimation from the radiosonde data (we used for the above calculations only statistical mean value $\Lambda_0 = 35m$).

3. The C_n^2 profile plots given in Fig. 19 through Fig. 22 show the very fast oscillation of C_n^2 for every realization of balloon data and can be used only for a rough estimation of seasonal or diurnal C_n^2 profiles variations .

4. It follows from Fig. 19 trough Fig. 22 that on average the C_n^2 value in summer is several times larger than in winter.

Acknowledgments

We are grateful to Dr. Vyacheslav V. Tatarskii for making many helpful suggestions on numerical calculations and on graphical representation of the computer results. We wish also to thank Michael J. Falls for supplying the meteorological radiosonde data and Dr. Maya S. Tatarskaya for help in the interpretation of these data . We express our appreciation to Dr. Christopher W. Fairall for his helpful advice in using the theoretical models describing the atmosphere turbulence.

References

[1] V.I. Tatarskii, The Effects of the Turbulent Atmosphere on Wave Propagation, Israel Program for Scientific Translation, Jerusalem, 1971.

[2] S.M. Rytov, Yu.A. Kravtsov and V.I. Tatarskii, Principles of Statistical Radio Physics, Springer-Verlag, Berlin, New York, 1987.

[3] J.W. Strohbehn, editor, Laser Beam Propagation in the Atmosphere, Springer-Verlag, Berlin, Heidelberg, New York, 1978.

[4] D.H. McIntosh and A.S. Thom, Essentials of Meteorology, Springer-Verlag, London, New York, 1972.

[5] M.L. Wesely, The combined effects of temperature and humidity fluctuations on refractive index, J. Appl. Meteor., Vol. 15, No. 1, pp. 43-49, 1976.

[6] C.W. Fairall and A.S. Frish, Diurnal and annual variations in mean profiles of C_n^2, NOAA Technical Memorandum ERL WPL-195, Boulder, Colorado, USA, March 1991.

[7] C.W. Fairall, A.B. White and D.W. Thomson, A stochastic model of gravity-wave-induced clear-air turbulence, J. Atmos. Sci., Vol. 48, No. 15, pp. 1771-1790, 1991.

[8] C.W. Fairall, The humidity and Temperature sensitivity of clear-air radars in the convective boundary layer, J. Appl. Meteor., Vol. 30, No. 8, pp. 1064-1074, 1991.

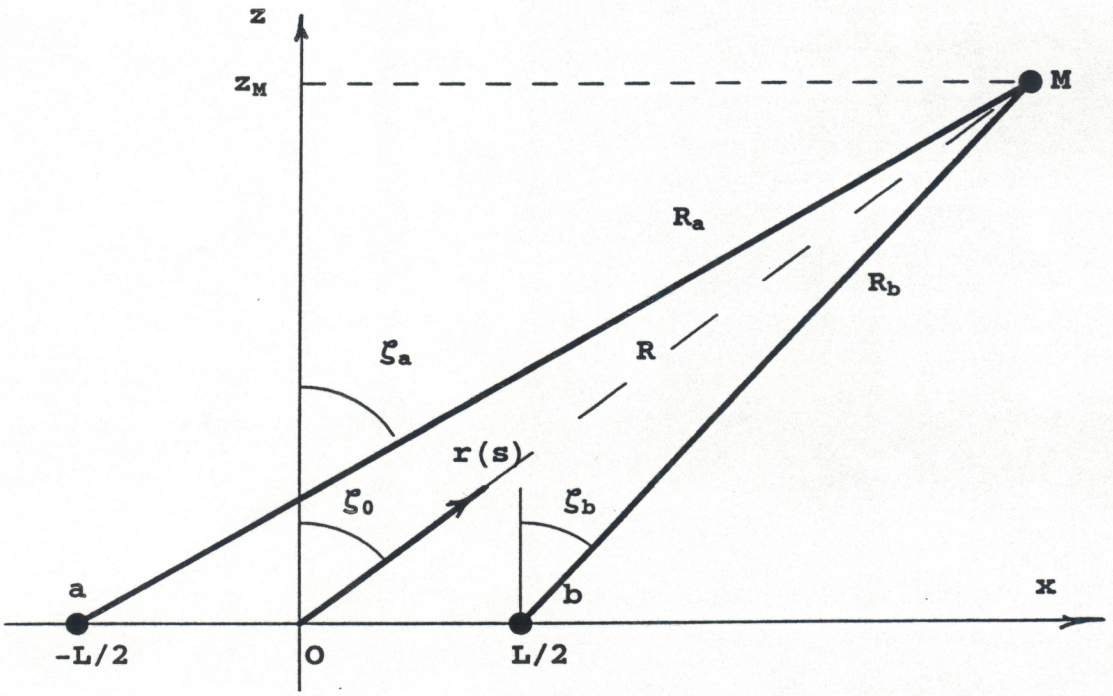

Fig .1
Interferometry
of a point source M (distance - R, zenith angle - ζ_0),
receiver positions - "a" and "b",
interferometric base - L.

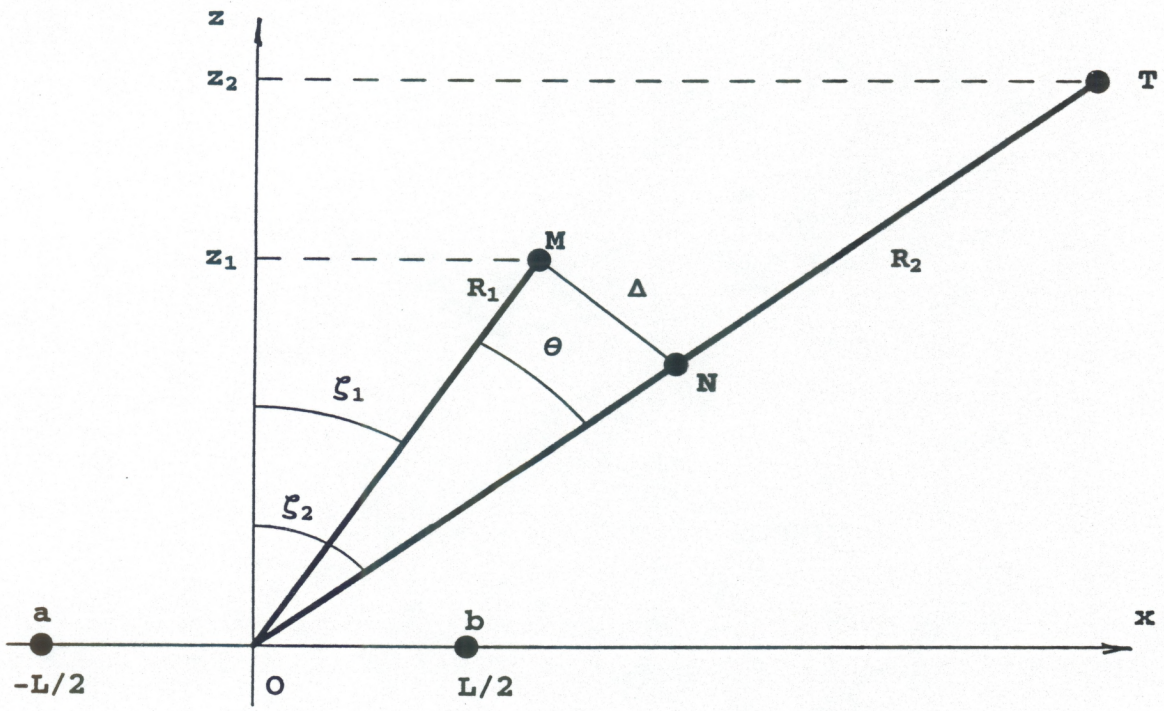

Fig .2

Interferometry of two sources -

M (distance - R_1, zenith angle - ζ_1) and T

(distance - R_2, zenith angle - ζ_2) with the angular

difference θ and the space ray separation - Δ

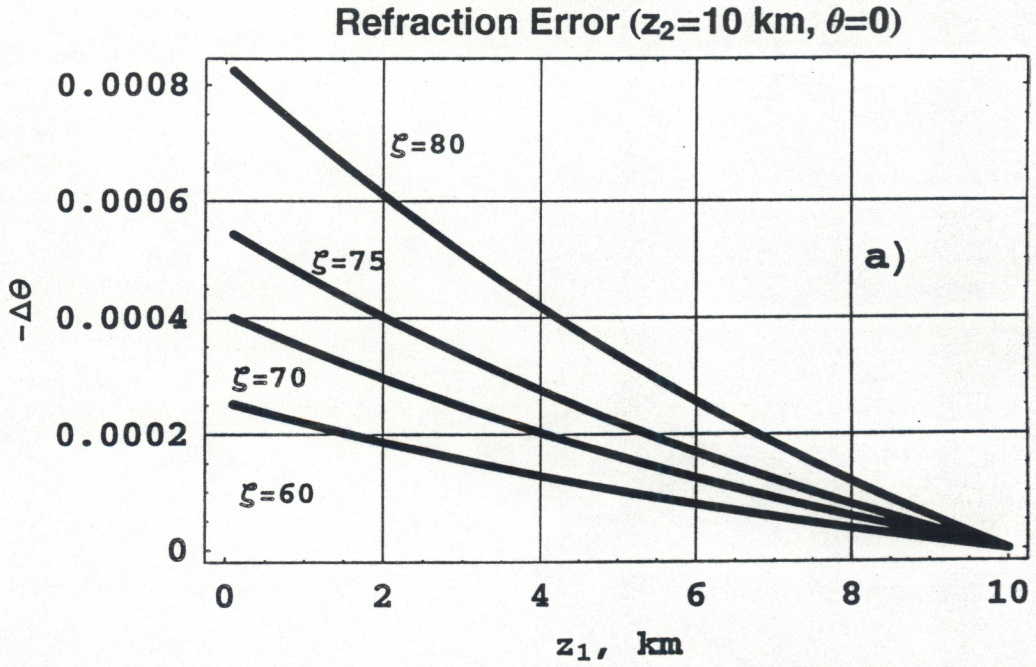
Refraction Error (z_2=10 km, θ=0)
0.0008
0.0006
0.0004
0.0002
0
-Δθ
ζ=80
ζ=75
ζ=70
ζ=60
a)
0
2
4
6
8
10
z_1, km

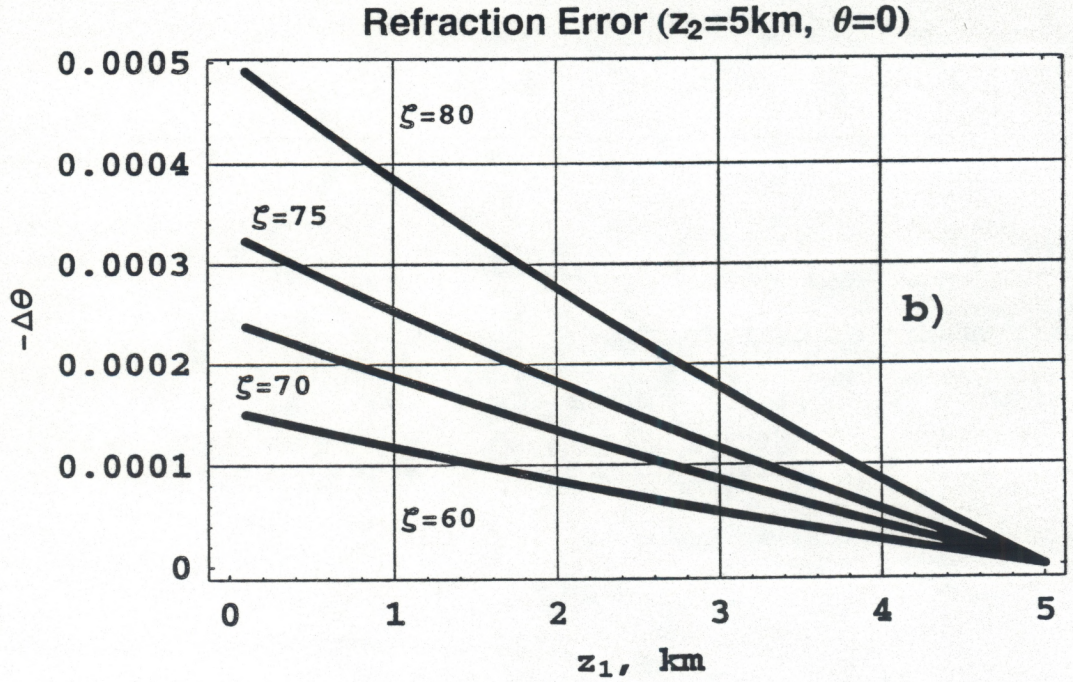
Refraction Error (z_2=5km, θ=0)
0.0005
0.0004
0.0003
0.0002
0.0001
0
-Δθ
ζ=80
ζ=75
ζ=70
ζ=60
b)
0
1
2
3
4
5
z_1, km

Fig .3 a, b

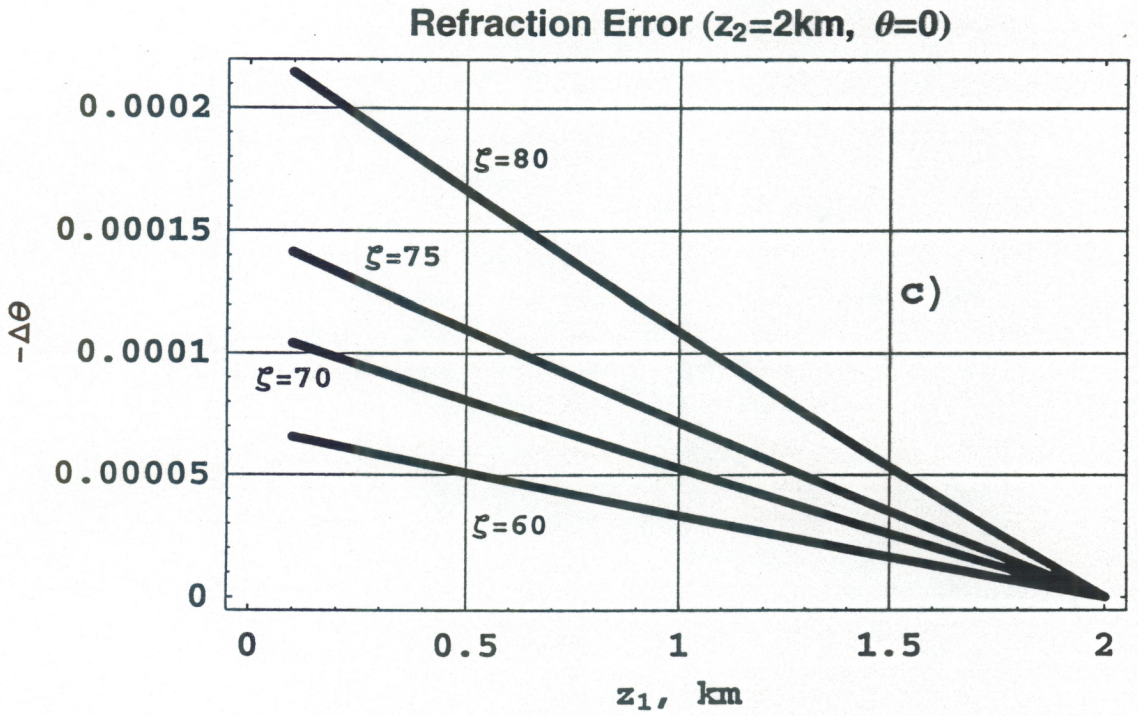
Refraction Error (z_2=2km, θ=0)
0.0002
0.00015
0.0001
0.00005
0
-Δθ
ζ=80
ζ=75
ζ=70
ζ=60
c)
0
0.5
1
1.5
2
z_1, km

Fig .3 c

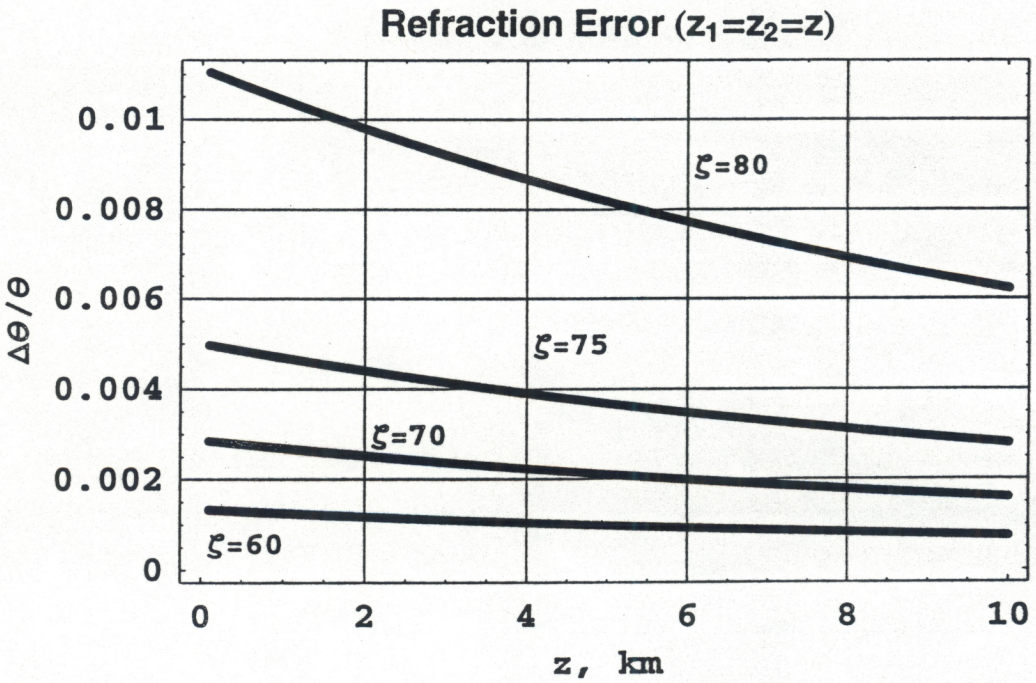
Refraction Error ($z_1=z_2=z$)
0.01
0.008
0.006
0.004
0.002
0
Δθ/θ
ζ=80
ζ=75
ζ=70
ζ=60
0
2
4
6
8
10
z, km

Fig .4

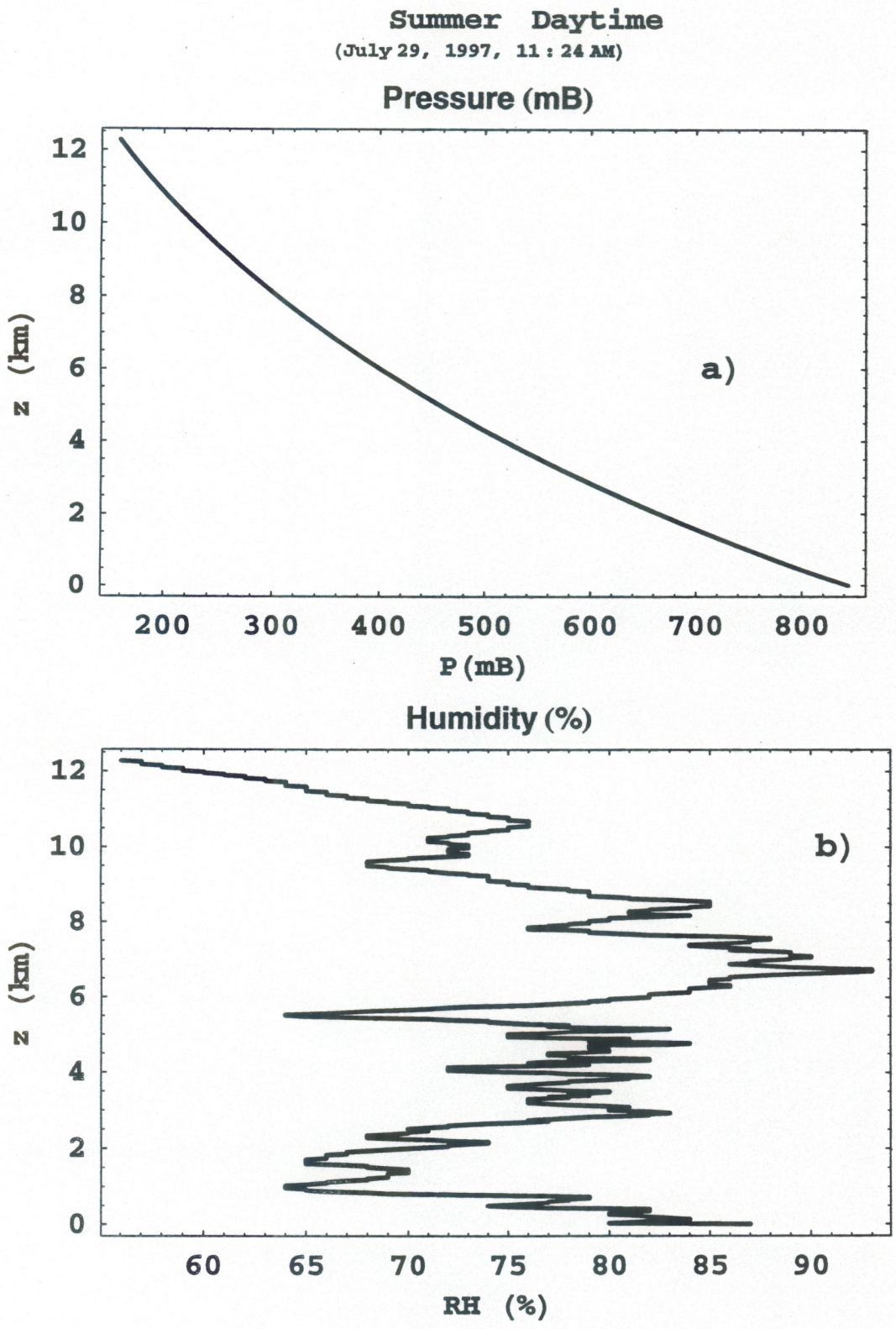
Summer Daytime
(July 29, 1997, 11 : 24 AM)
Pressure (mB)
z (km)
a)
P (mB)
Humidity (%)
z (km)
b)
RH (%)

Fig .5 a, b

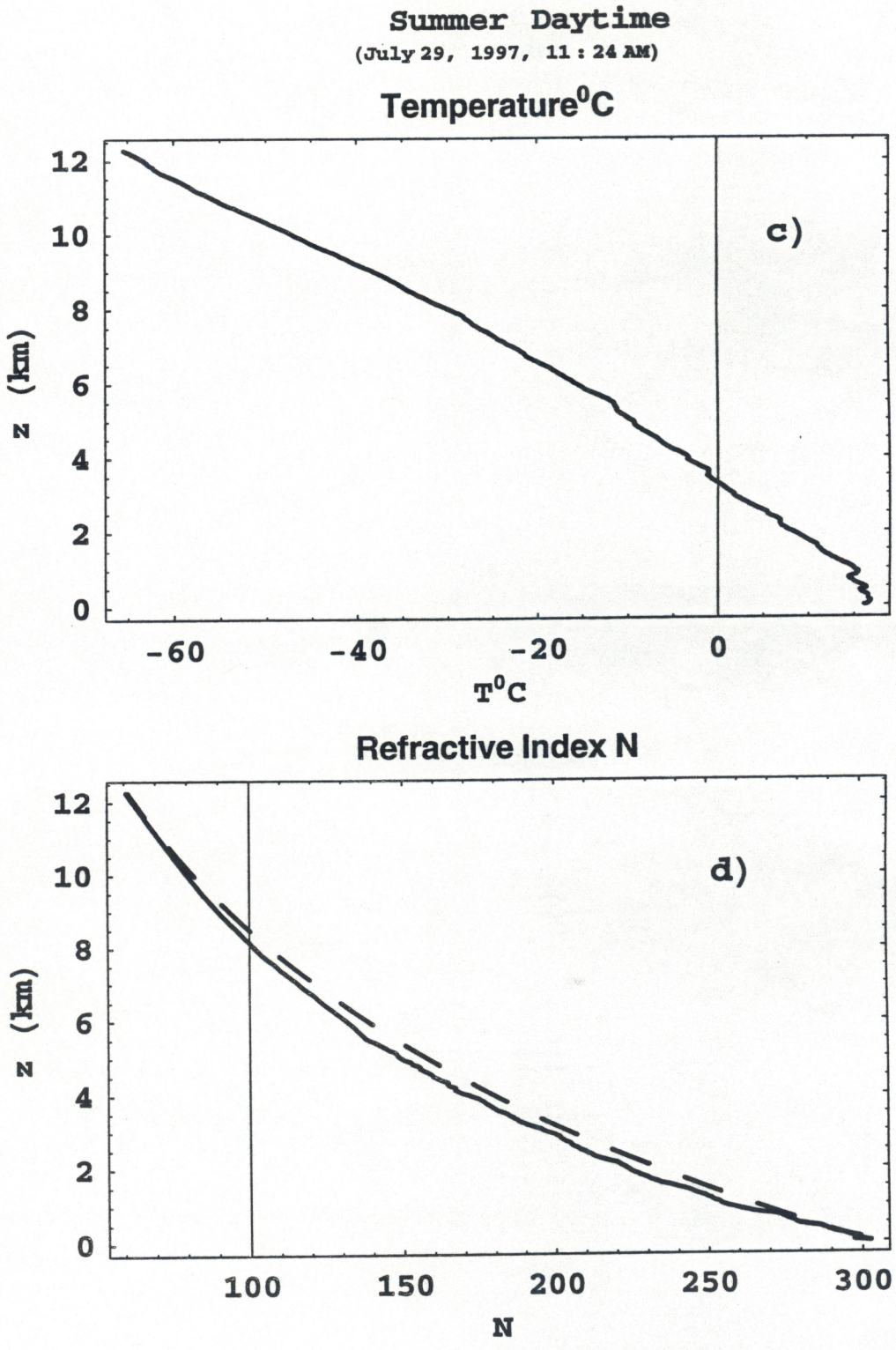
Summer Daytime
(July 29, 1997, 11 : 24 AM)
Temperature^{0}C
c)
z (km)
T^{0}C
Refractive Index N
d)
z (km)
N

Fig .5 c, d

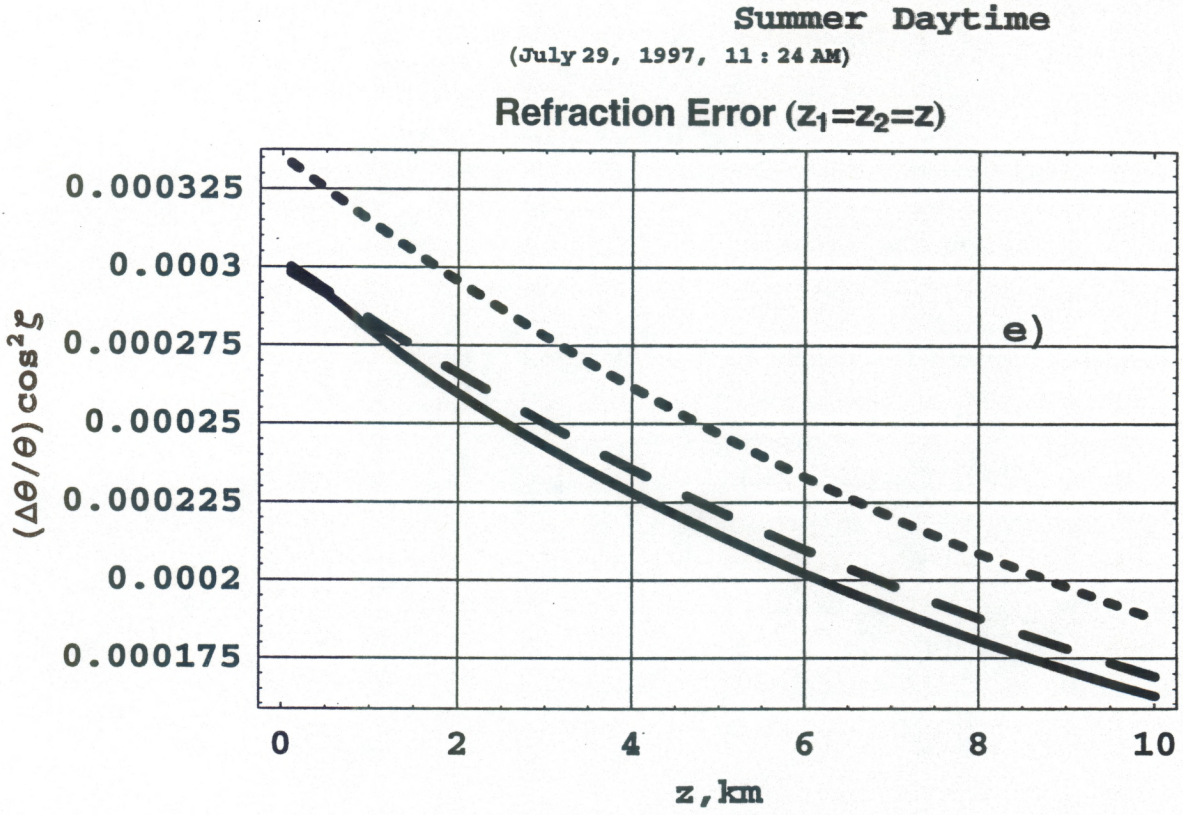
Summer Daytime
(July 29, 1997, 11 : 24 AM)
Refraction Error ($z_1=z_2=z$)
$(\Delta\theta/\theta)\cos^2\zeta$
0.000325
0.0003
0.000275
0.00025
0.000225
0.0002
0.000175
e)
0
2
4
6
8
10
z, km

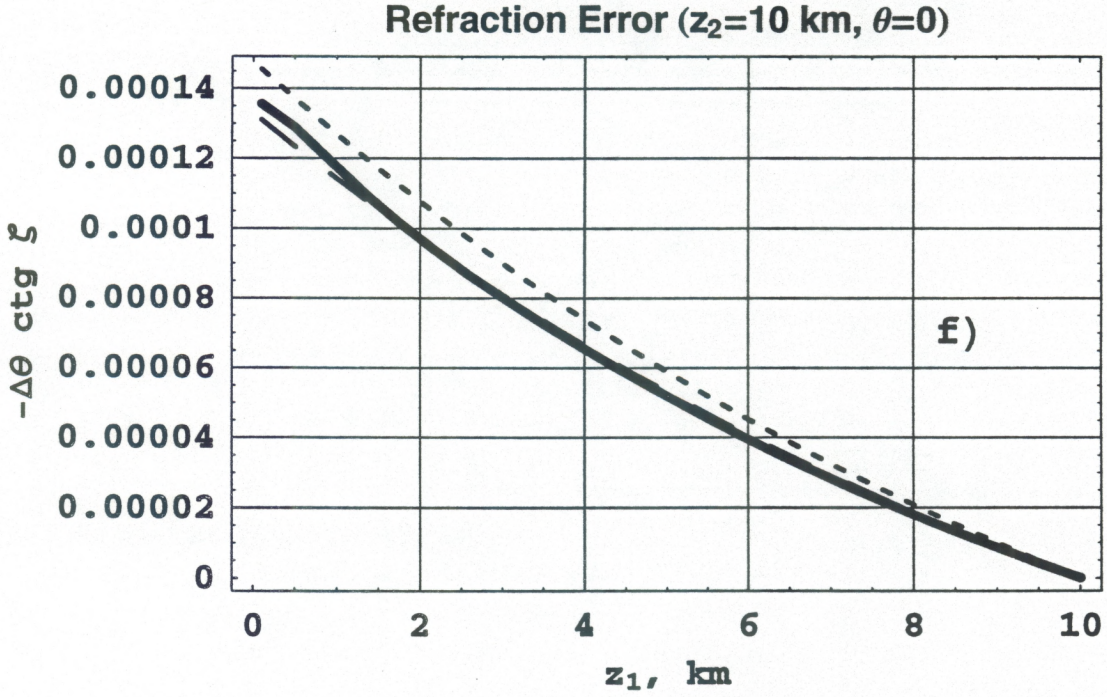
Refraction Error (z_2=10 km, θ=0)
$-\Delta\theta$ ctg ζ
0.00014
0.00012
0.0001
0.00008
0.00006
0.00004
0.00002
0
f)
0
2
4
6
8
10
z_1, km

Fig .5 e, f

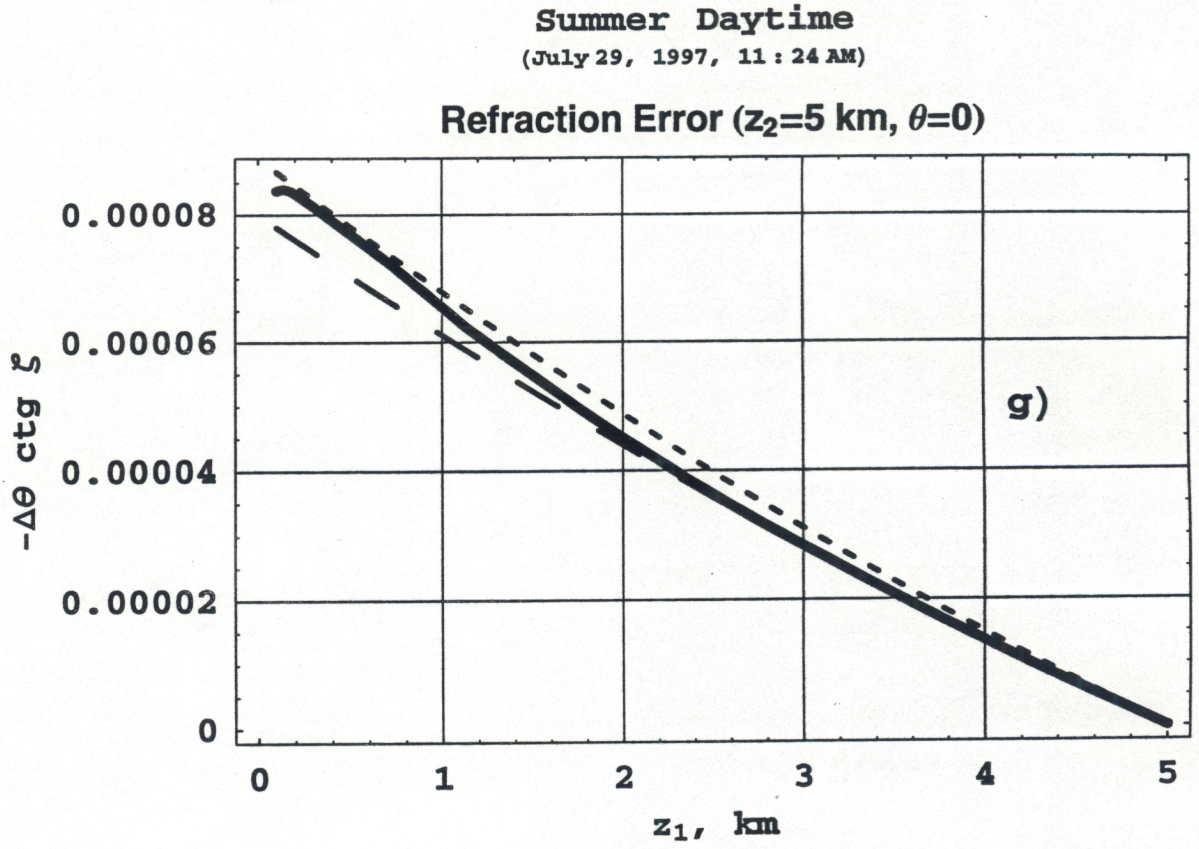
Summer Daytime
(July 29, 1997, 11 : 24 AM)
Refraction Error (z_2=5 km, θ=0)
0.00008
0.00006
0.00004
0.00002
0
-Δθ ctg ζ
g)
0
1
2
3
4
5
z_1, km

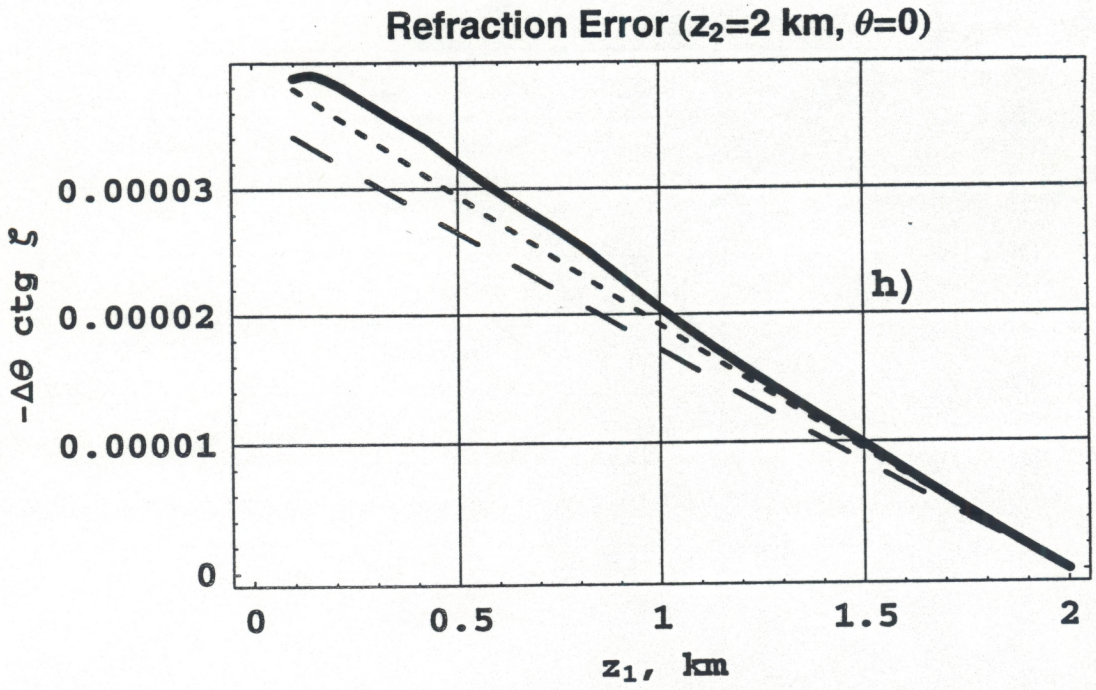
Refraction Error (z_2=2 km, θ=0)
0.00003
0.00002
0.00001
0
-Δθ ctg ζ
h)
0
0.5
1
1.5
2
z_1, km

Fig. 5 g, h

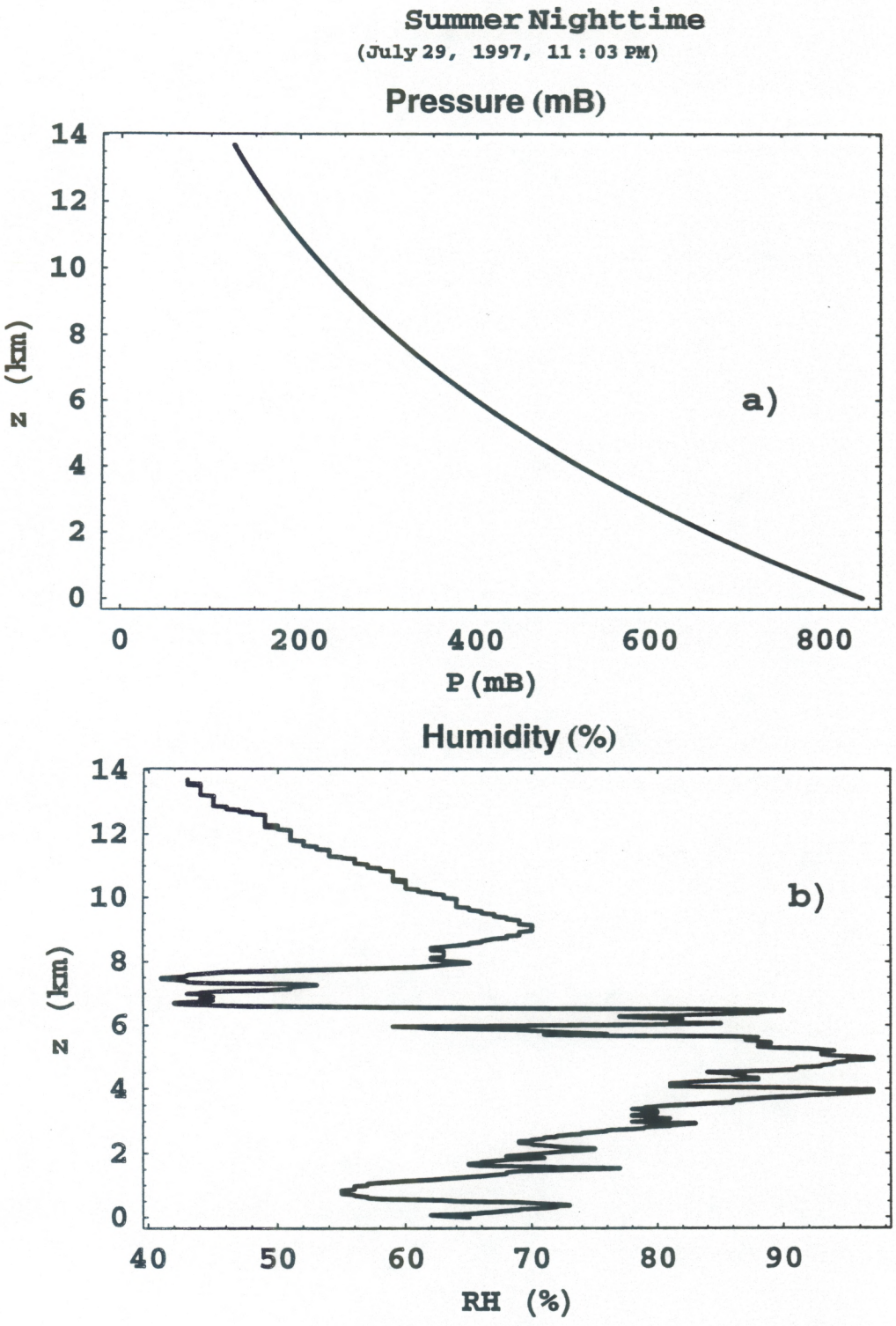
Summer Nighttime
(July 29, 1997, 11 : 03 PM)
Pressure (mB)
z (km)
P (mB)
a)
Humidity (%)
z (km)
RH (%)
b)

Fig. 6 a, b

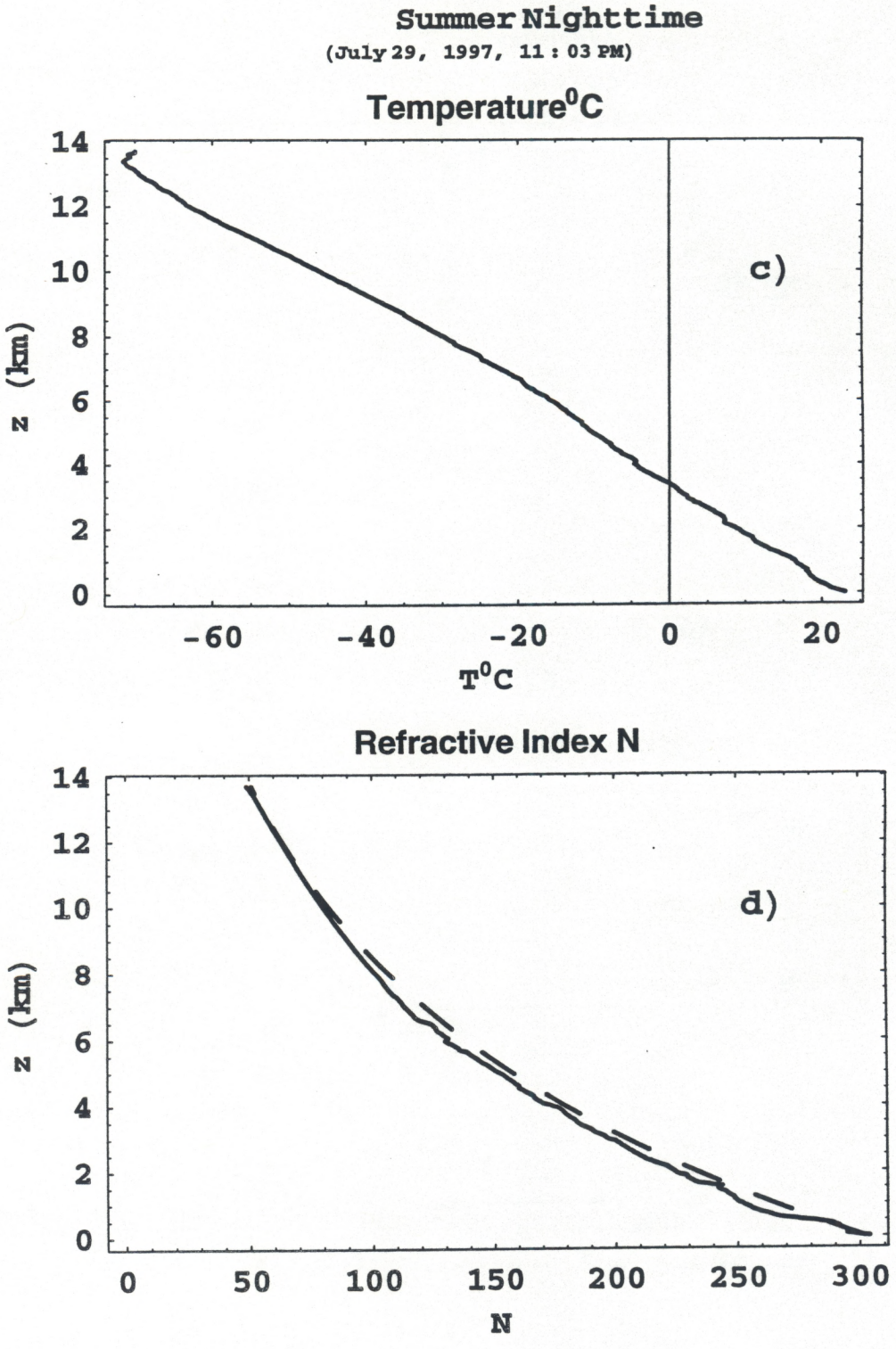
Summer Nighttime
(July 29, 1997, 11 : 03 PM)
Temperature^{0}C
c)
z (km)
T^{0}C
Refractive Index N
d)
z (km)
N

Fig .6 c, d

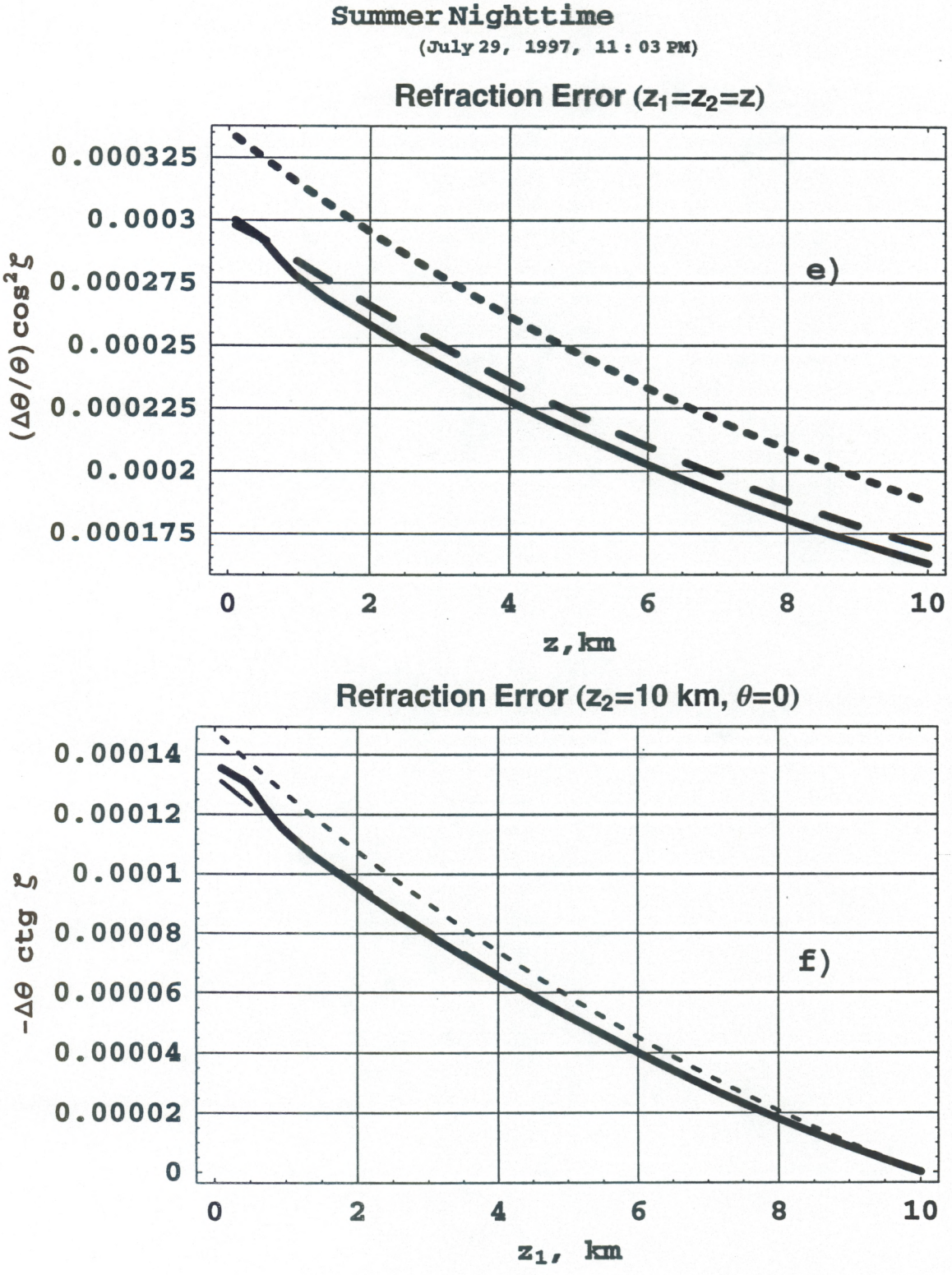
Summer Nighttime
(July 29, 1997, 11 : 03 PM)
Refraction Error ($z_1=z_2=z$)
$(\Delta\theta/\theta)\cos^2\zeta$
0.000325
0.0003
0.000275
0.00025
0.000225
0.0002
0.000175
e)
0
2
4
6
8
10
z, km
Refraction Error (z_2=10 km, θ=0)
$-\Delta\theta$ ctg ζ
0.00014
0.00012
0.0001
0.00008
0.00006
0.00004
0.00002
0
f)
0
2
4
6
8
10
z_1, km

Fig .6 e, f

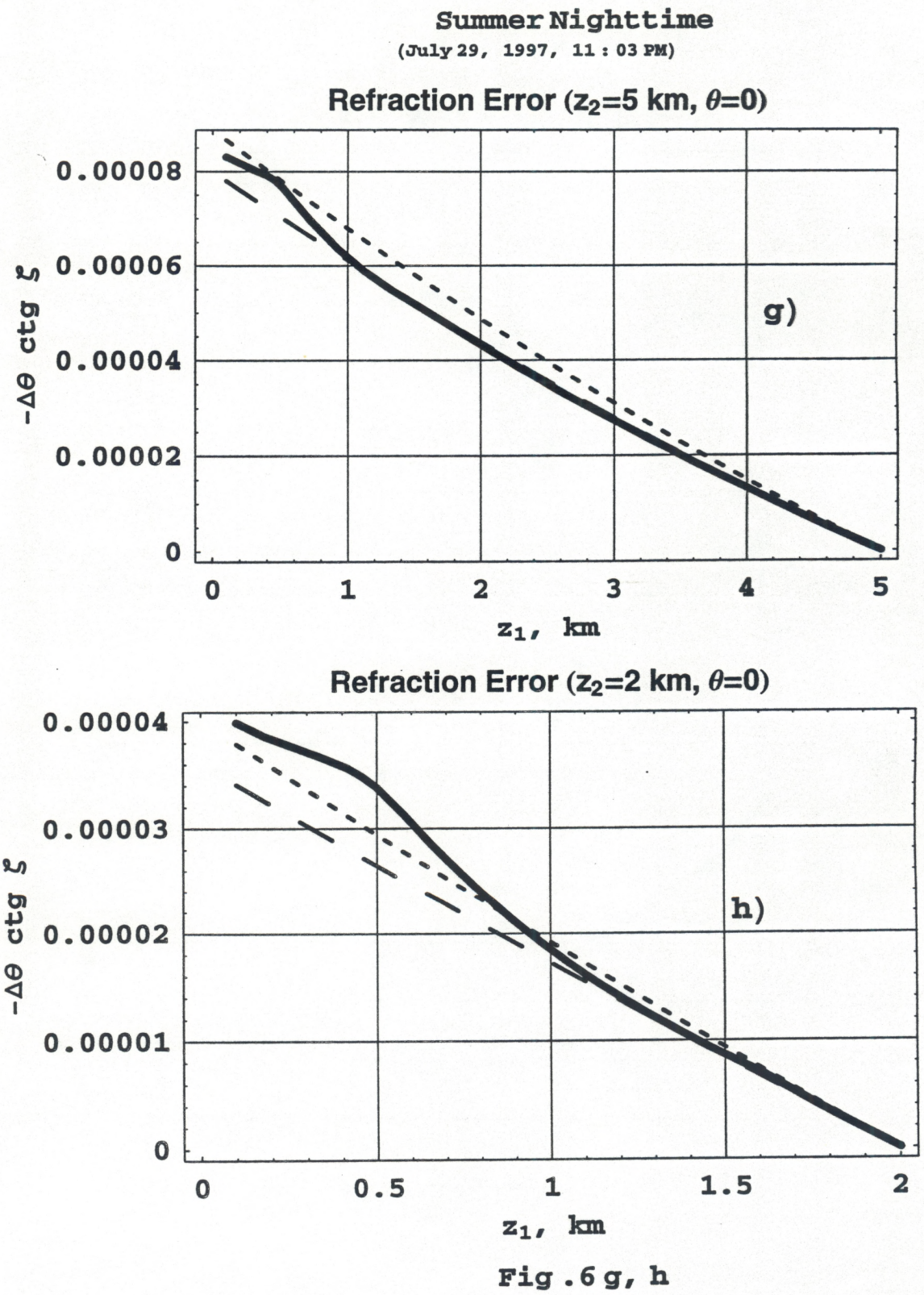
Summer Nighttime
(July 29, 1997, 11 : 03 PM)
Refraction Error (z_2=5 km, θ=0)
0.00008
0.00006
0.00004
0.00002
0
$-\Delta\theta$ ctg ζ
g)
0
1
2
3
4
5
z_1, km
Refraction Error (z_2=2 km, θ=0)
0.00004
0.00003
0.00002
0.00001
0
$-\Delta\theta$ ctg ζ
h)
0
0.5
1
1.5
2
z_1, km

Fig .6 g, h

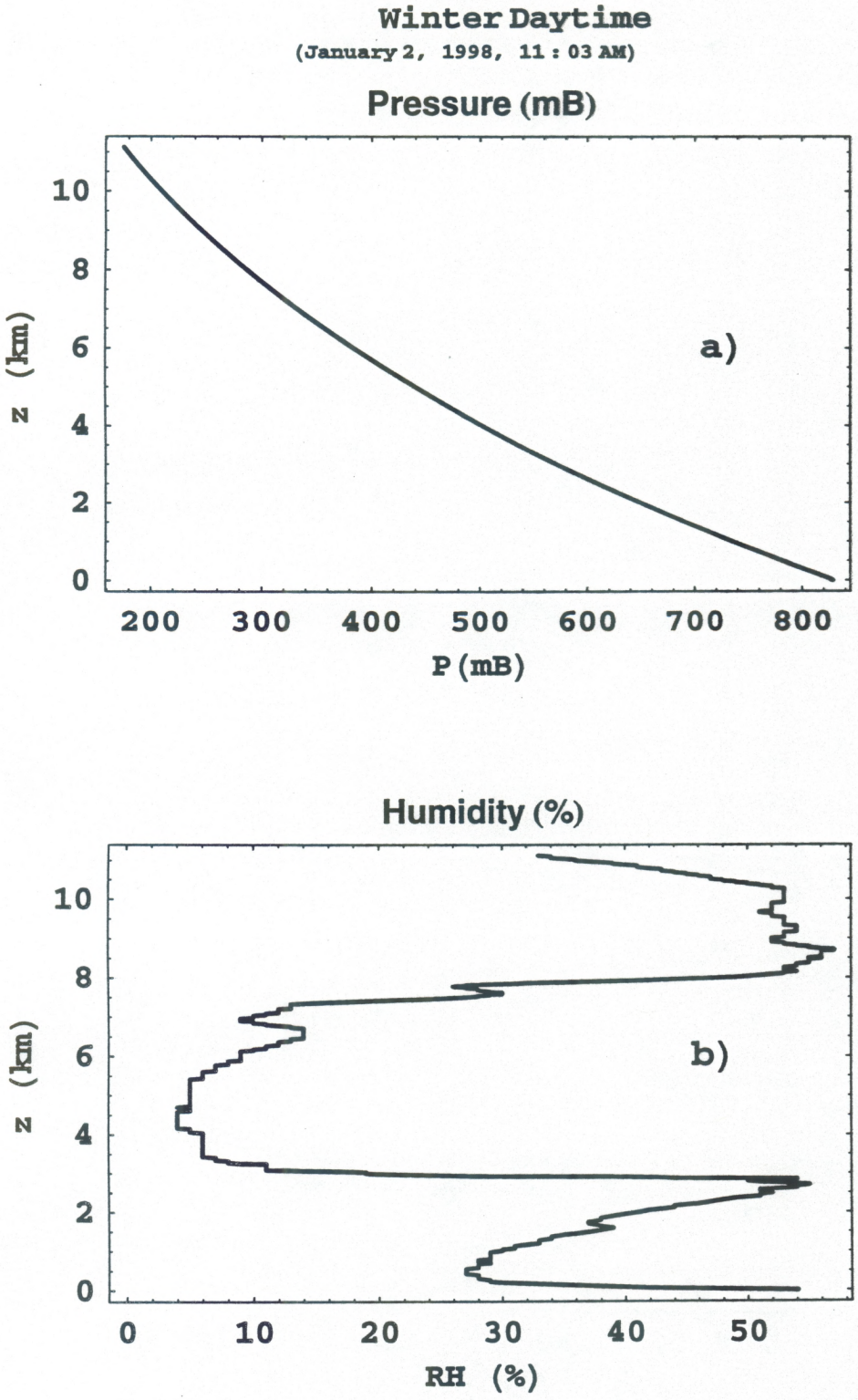
Winter Daytime
(January 2, 1998, 11 : 03 AM)
Pressure (mB)
z (km)
10
8
6
4
2
0
200
300
400
500
600
700
800
P (mB)
a)
Humidity (%)
z (km)
10
8
6
4
2
0
0
10
20
30
40
50
RH (%)
b)

Fig .7 a, b

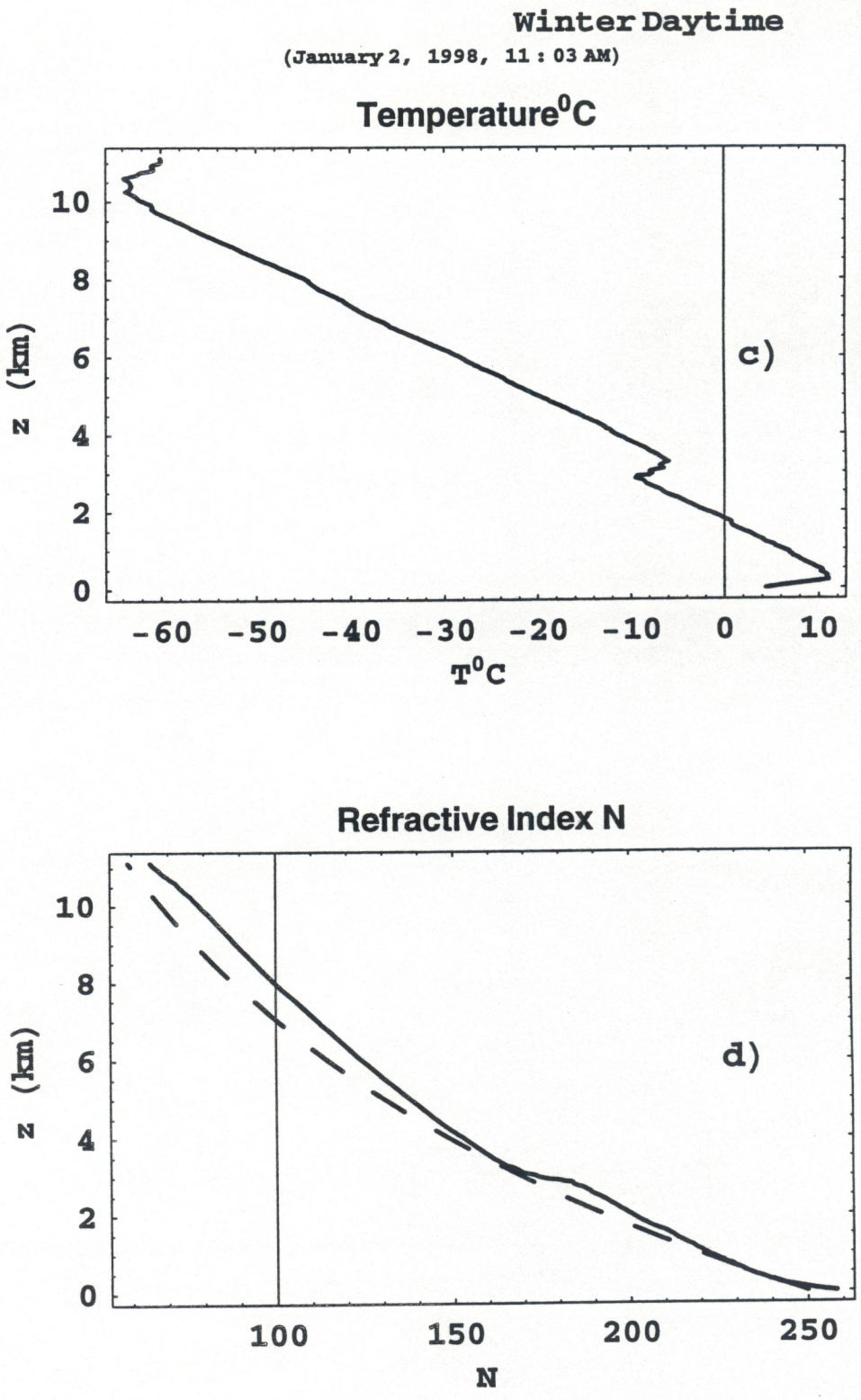
Winter Daytime
(January 2, 1998, 11 : 03 AM)
Temperature^{0}C
z (km)
10
8
6
4
2
0
-60 -50 -40 -30 -20 -10 0 10
T^{0}C
c)
Refractive Index N
z (km)
10
8
6
4
2
0
100 150 200 250
N
d)

Fig .7 c, d

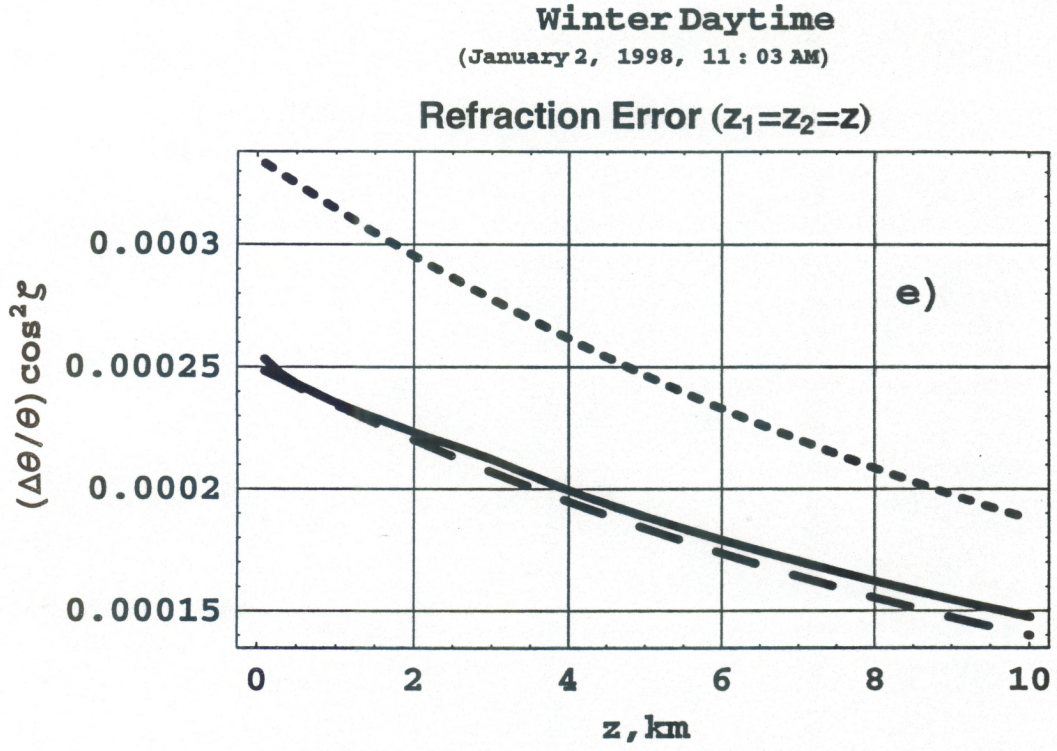
Winter Daytime
(January 2, 1998, 11 : 03 AM)
Refraction Error ($z_1=z_2=z$)
$(\Delta\theta/\theta)\cos^2\zeta$
0.0003
0.00025
0.0002
0.00015
e)
0
2
4
6
8
10
z, km

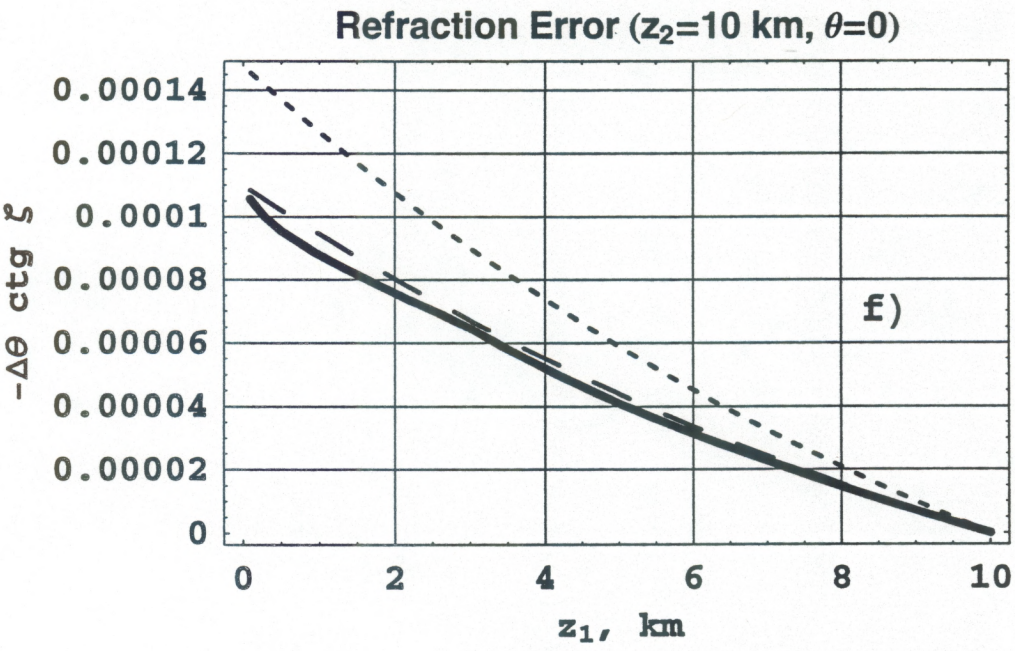
Refraction Error (z_2=10 km, θ=0)
$-\Delta\theta$ ctg ζ
0.00014
0.00012
0.0001
0.00008
0.00006
0.00004
0.00002
0
f)
0
2
4
6
8
10
z_1, km

Fig .7 e, f

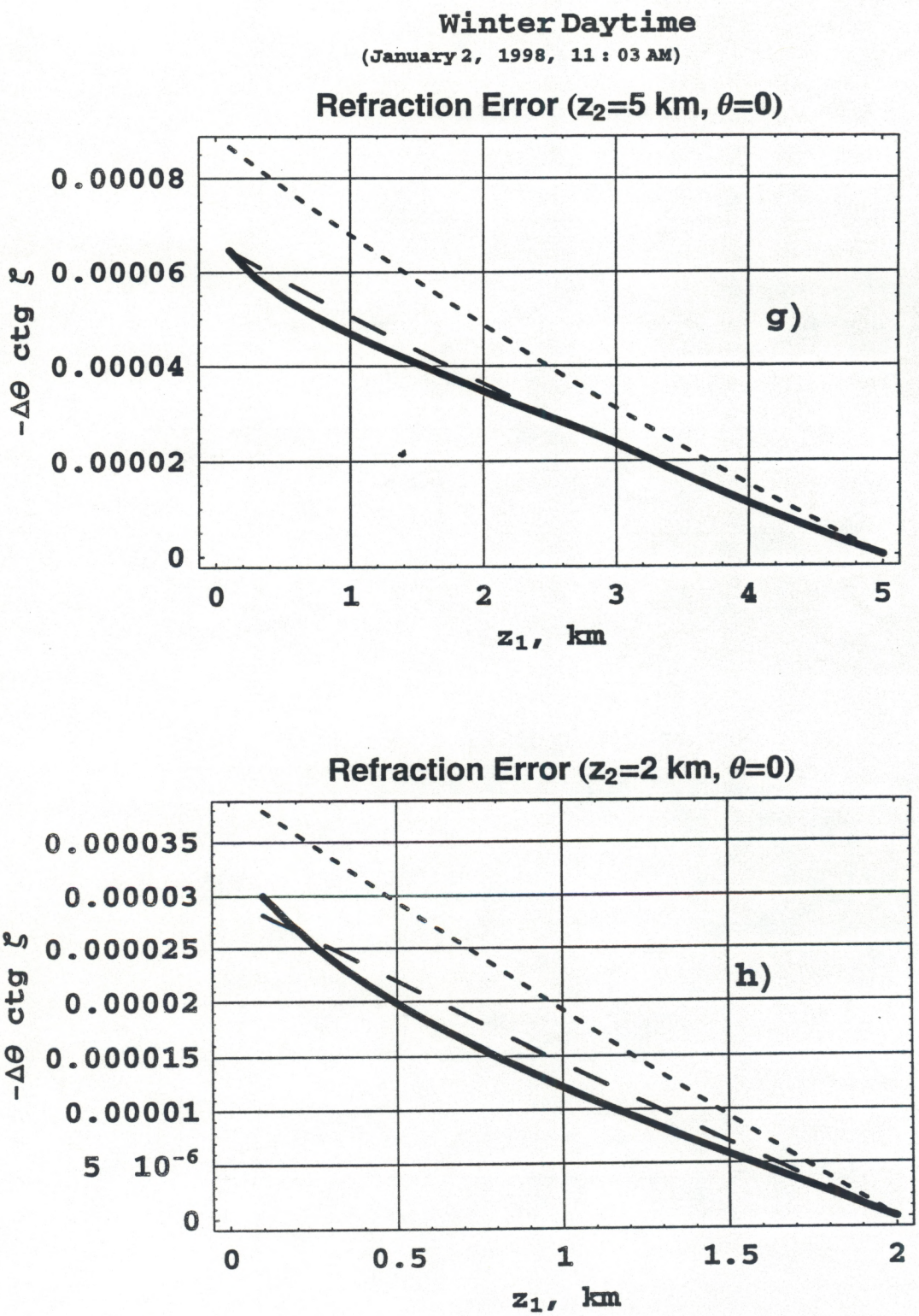
Winter Daytime
(January 2, 1998, 11 : 03 AM)
Refraction Error (z_2=5 km, θ=0)
0.00008
0.00006
0.00004
0.00002
0
$-\Delta\theta$ ctg ζ
g)
0
1
2
3
4
5
z_1, km
Refraction Error (z_2=2 km, θ=0)
0.000035
0.00003
0.000025
0.00002
0.000015
0.00001
5 10^{-6}
0
$-\Delta\theta$ ctg ζ
h)
0
0.5
1
1.5
2
z_1, km

Fig .7 g, h

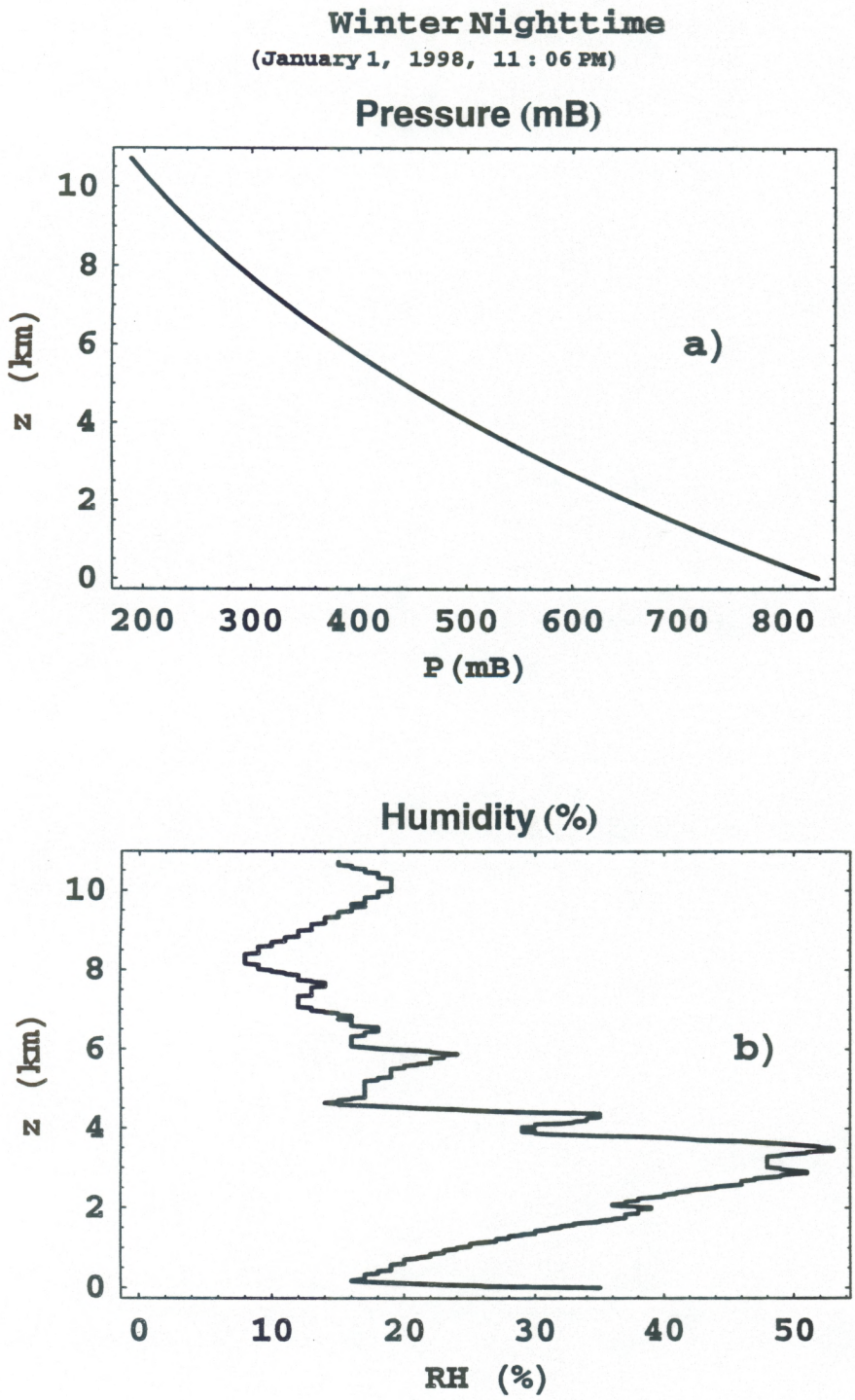
Winter Nighttime
(January 1, 1998, 11 : 06 PM)
Pressure (mB)
z (km)
10
8
6
4
2
0
a)
200 300 400 500 600 700 800
P (mB)
Humidity (%)
z (km)
10
8
6
4
2
0
b)
0 10 20 30 40 50
RH (%)

Fig .8 a, b

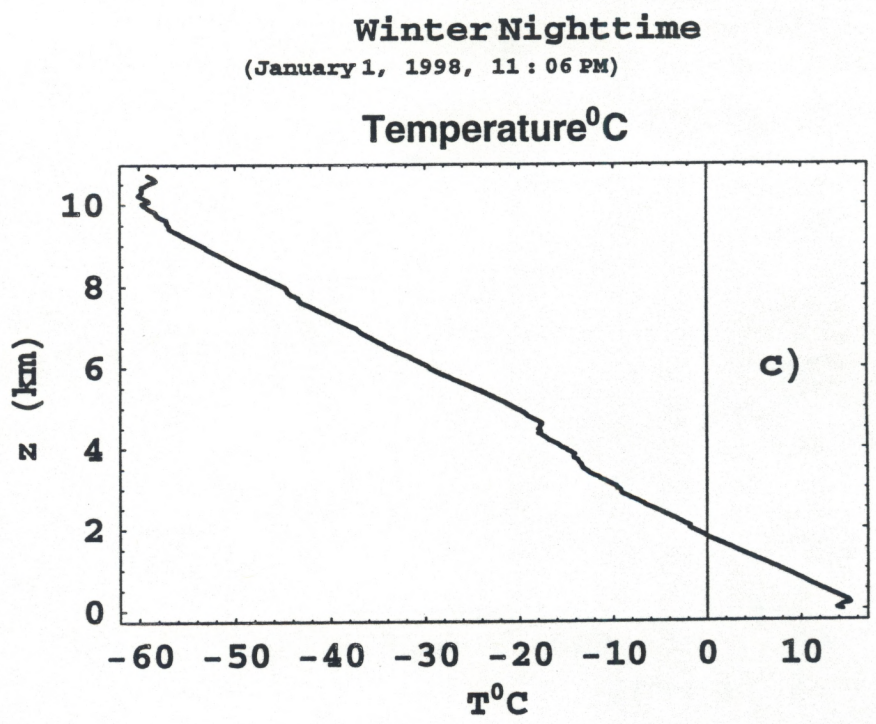
Winter Nighttime
(January 1, 1998, 11 : 06 PM)
Temperature^{0}C
z (km)
10
8
6
4
2
0
-60 -50 -40 -30 -20 -10 0 10
T^{0}C
c)

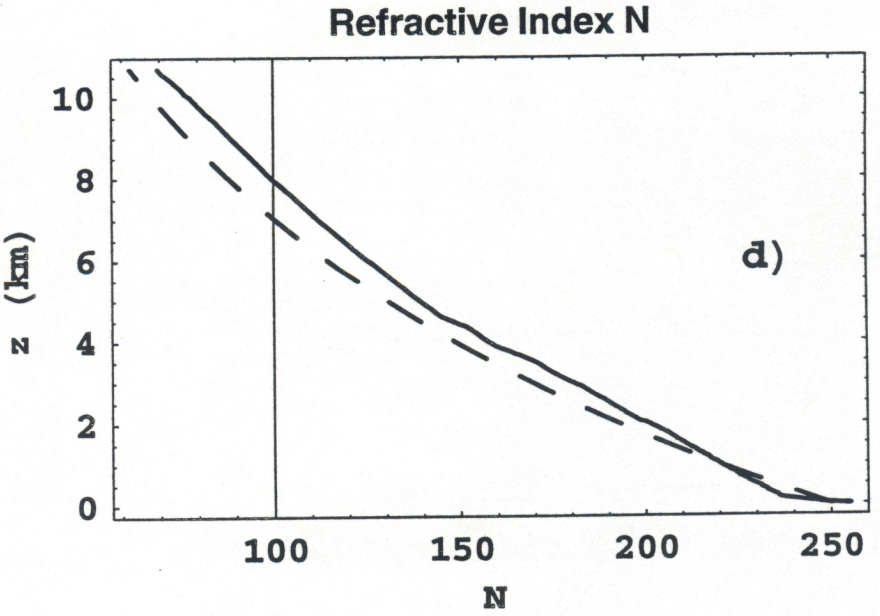
Refractive Index N
z (km)
10
8
6
4
2
0
100 150 200 250
N
d)

Fig. 8 c, d

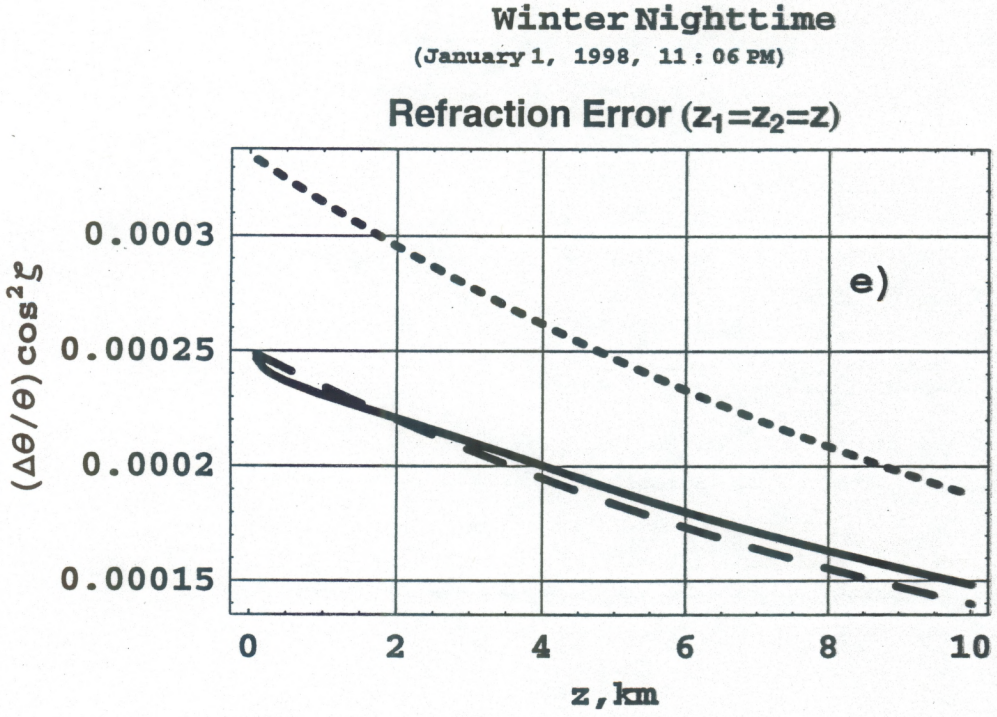
Winter Nighttime
(January 1, 1998, 11 : 06 PM)
Refraction Error ($z_1=z_2=z$)
$(\Delta\theta/\theta)\cos^2\zeta$
0.0003
0.00025
0.0002
0.00015
e)
0
2
4
6
8
10
z, km

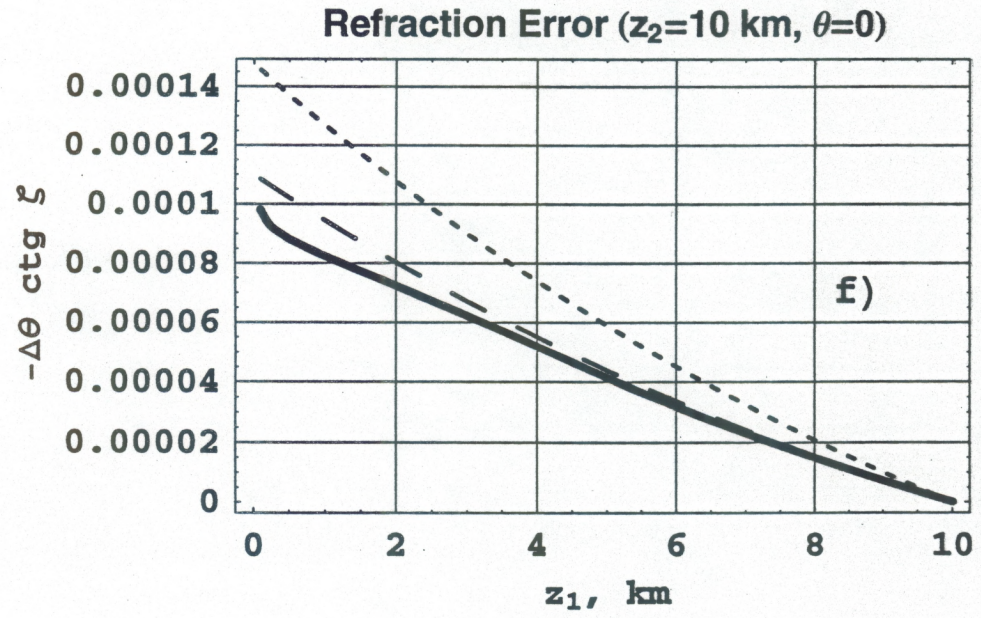
Refraction Error (z_2=10 km, θ=0)
$-\Delta\theta$ ctg ζ
0.00014
0.00012
0.0001
0.00008
0.00006
0.00004
0.00002
0
f)
0
2
4
6
8
10
z_1, km

Fig .8 e, f

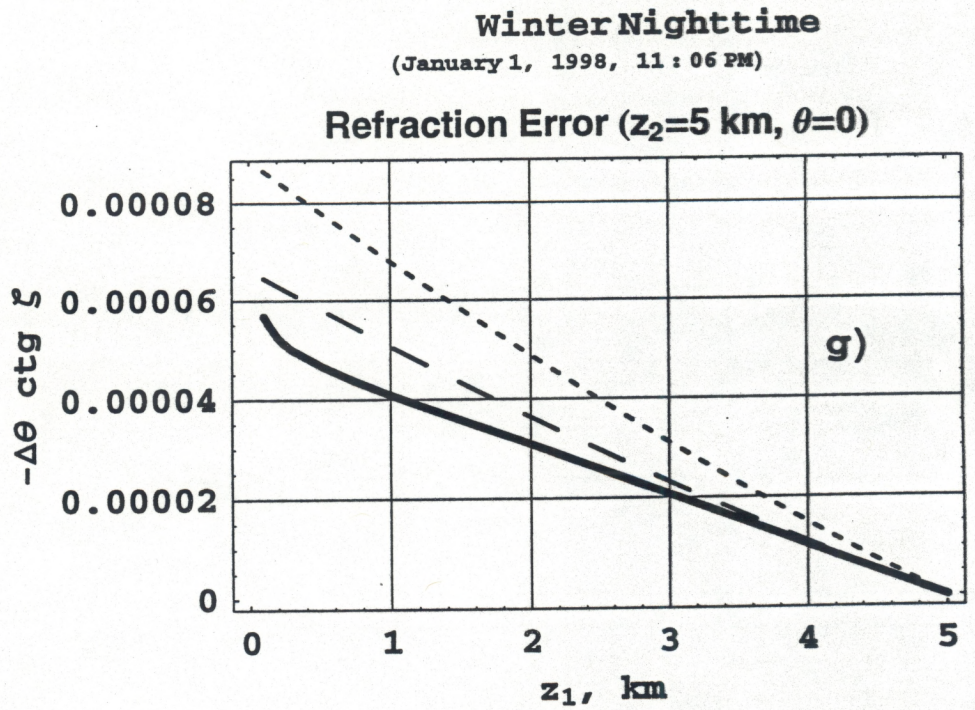
Winter Nighttime
(January 1, 1998, 11 : 06 PM)
Refraction Error (z_2=5 km, θ=0)
0.00008
0.00006
0.00004
0.00002
0
-Δθ ctg ζ
g)
0
1
2
3
4
5
z_1, km

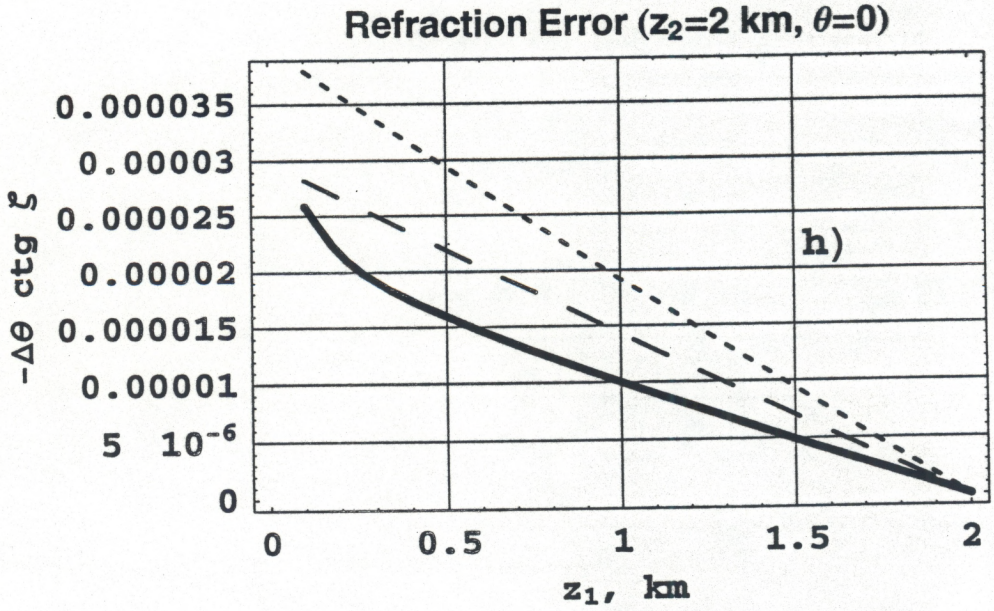
Refraction Error (z_2=2 km, θ=0)
0.000035
0.00003
0.000025
0.00002
0.000015
0.00001
5 10^-6
0
-Δθ ctg ζ
h)
0
0.5
1
1.5
2
z_1, km

Fig. 8 g, h

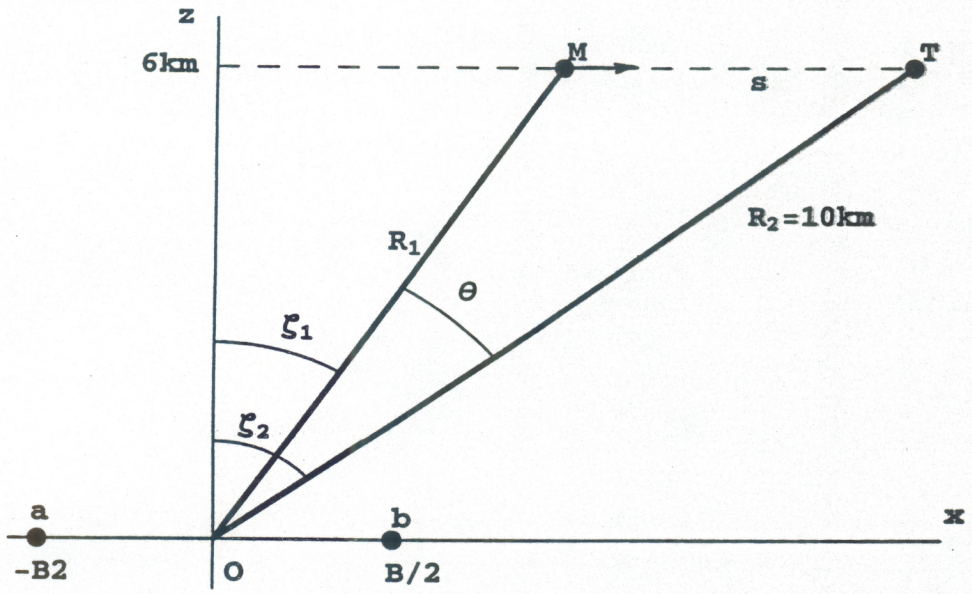

Scenario 1 ($z_1 = z_2 = 6$ km, $\zeta_2 = 53°$)

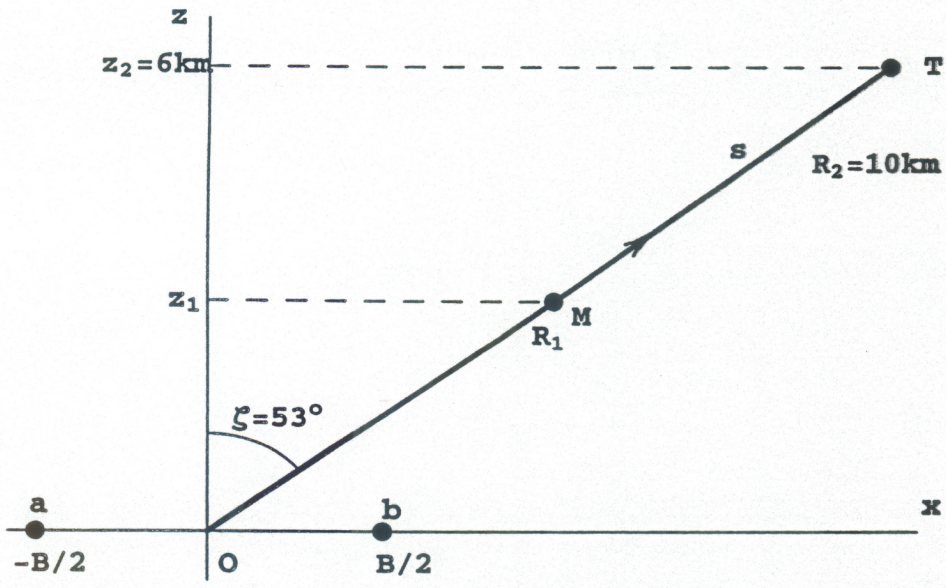

Scenario 2 ($\zeta_1 = \zeta_2 = \zeta = 53^0$)

Fig .9

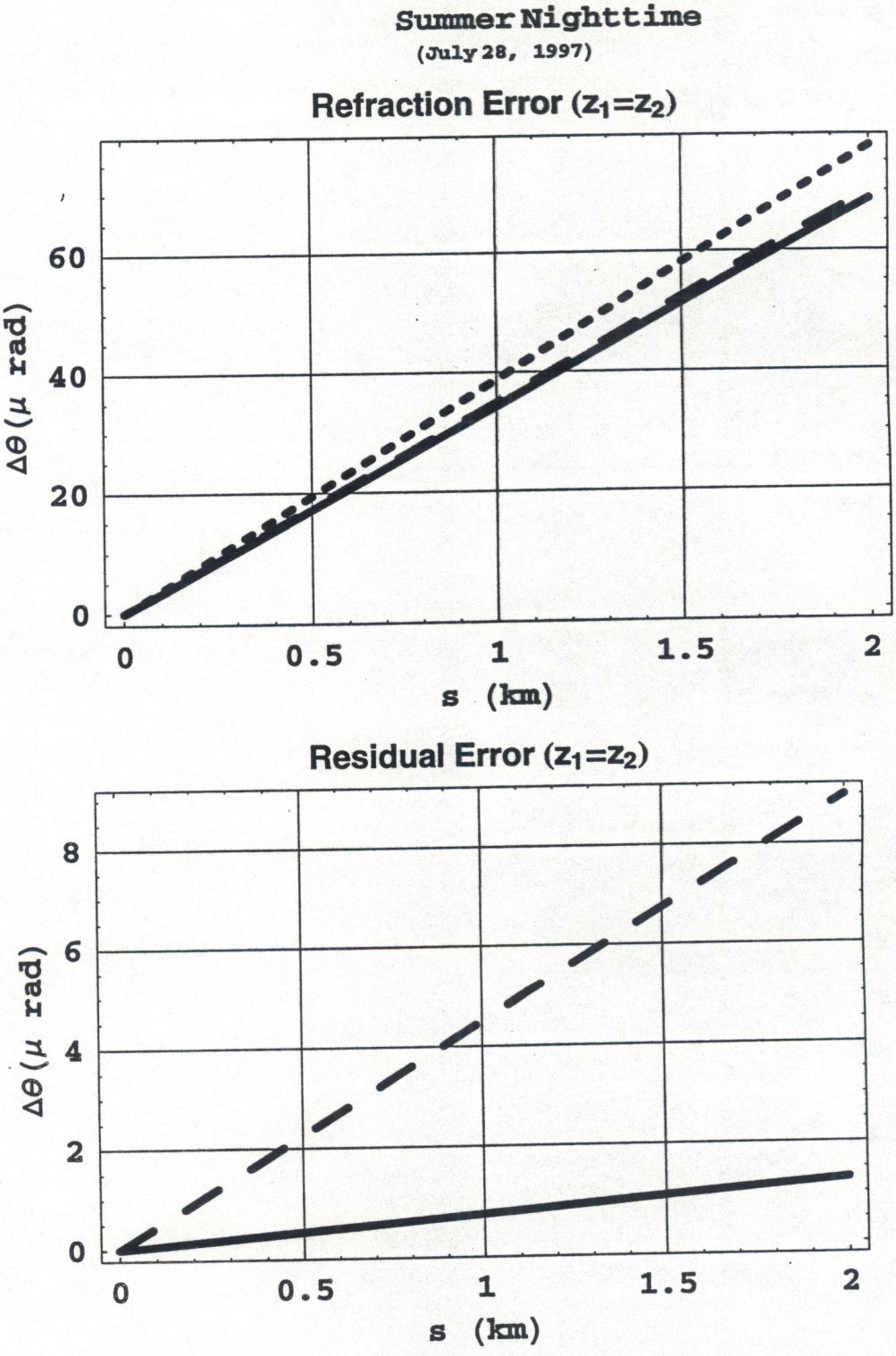
Summer Nighttime
(July 28, 1997)
Refraction Error (z_1=z_2)
Δθ (μ rad)
60
40
20
0
0
0.5
1
1.5
2
s (km)
Residual Error (z_1=z_2)
Δθ (μ rad)
8
6
4
2
0
0
0.5
1
1.5
2
s (km)

Fig .10 a

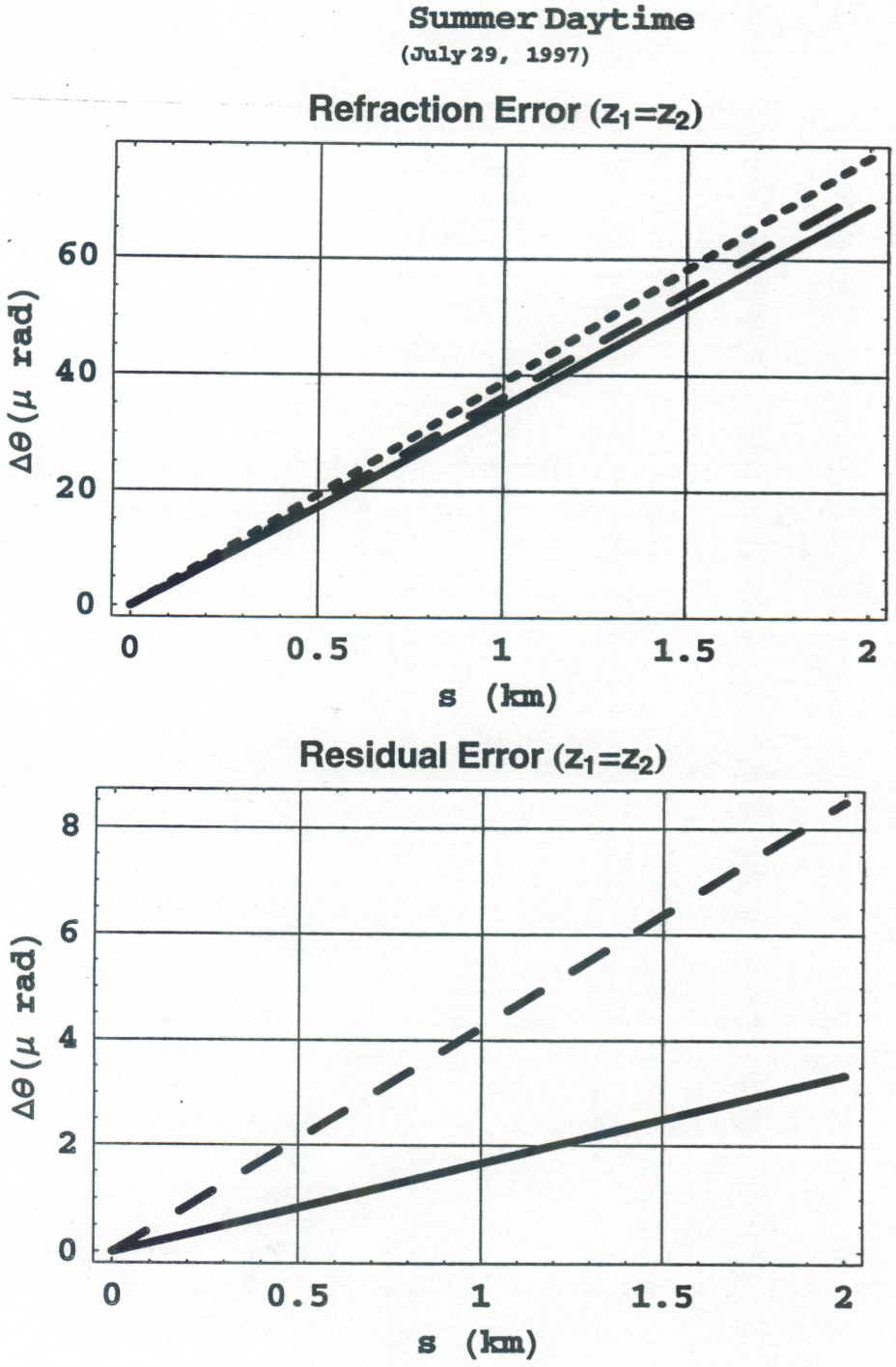
Summer Daytime
(July 29, 1997)
Refraction Error (z_1=z_2)
Δθ(μ rad)
60
40
20
0
0
0.5
1
1.5
2
s (km)
Residual Error (z_1=z_2)
Δθ(μ rad)
8
6
4
2
0
0
0.5
1
1.5
2
s (km)

Fig .10 b

Winter Nighttime
(January 2, 1998)

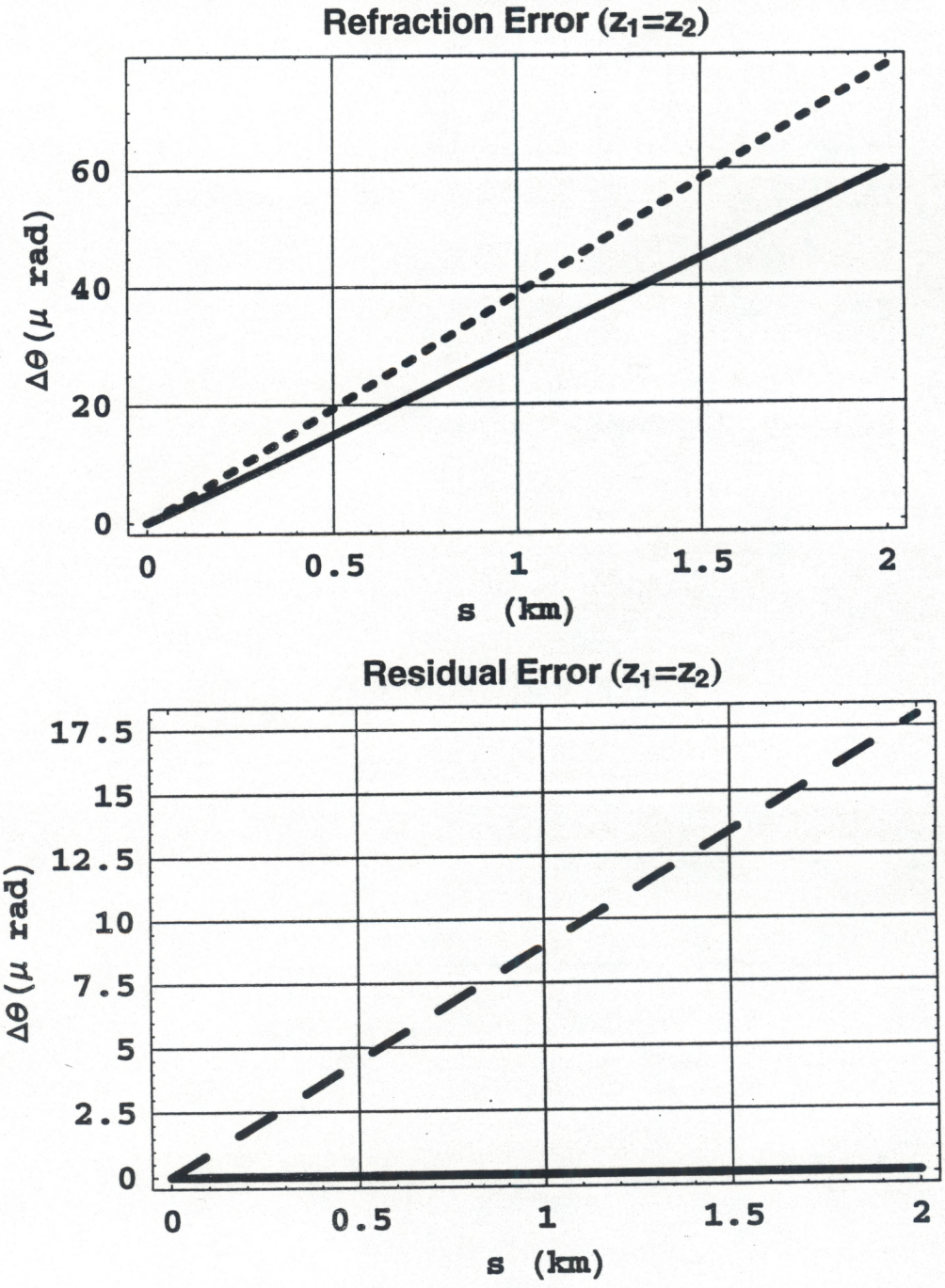

Fig .10 c

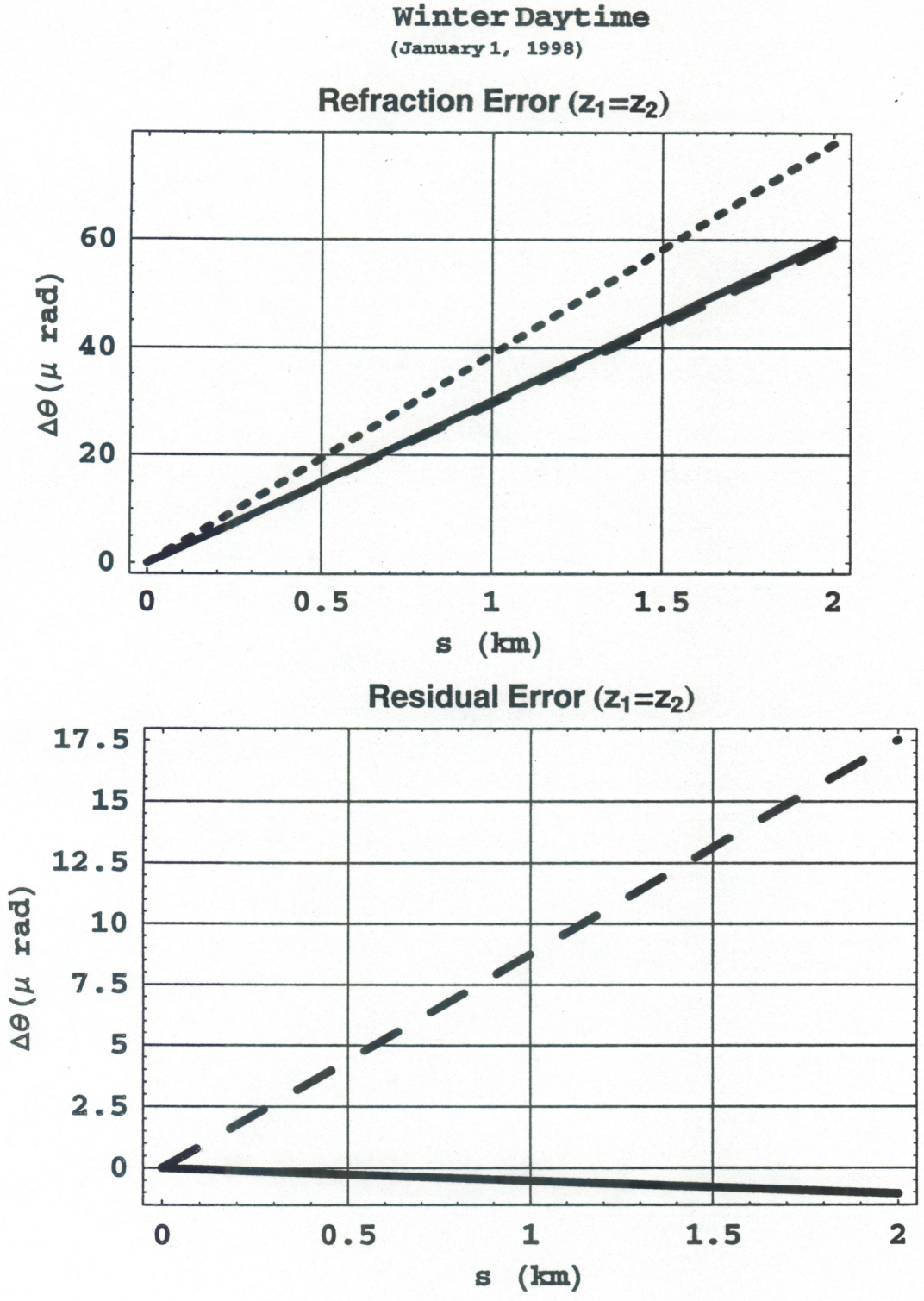
Winter Daytime
(January 1, 1998)
Refraction Error ($z_1=z_2$)
$\Delta\theta$ (μ rad)
60
40
20
0
0
0.5
1
1.5
2
s (km)
Residual Error ($z_1=z_2$)
$\Delta\theta$ (μ rad)
17.5
15
12.5
10
7.5
5
2.5
0
0
0.5
1
1.5
2
s (km)

Fig .10 d

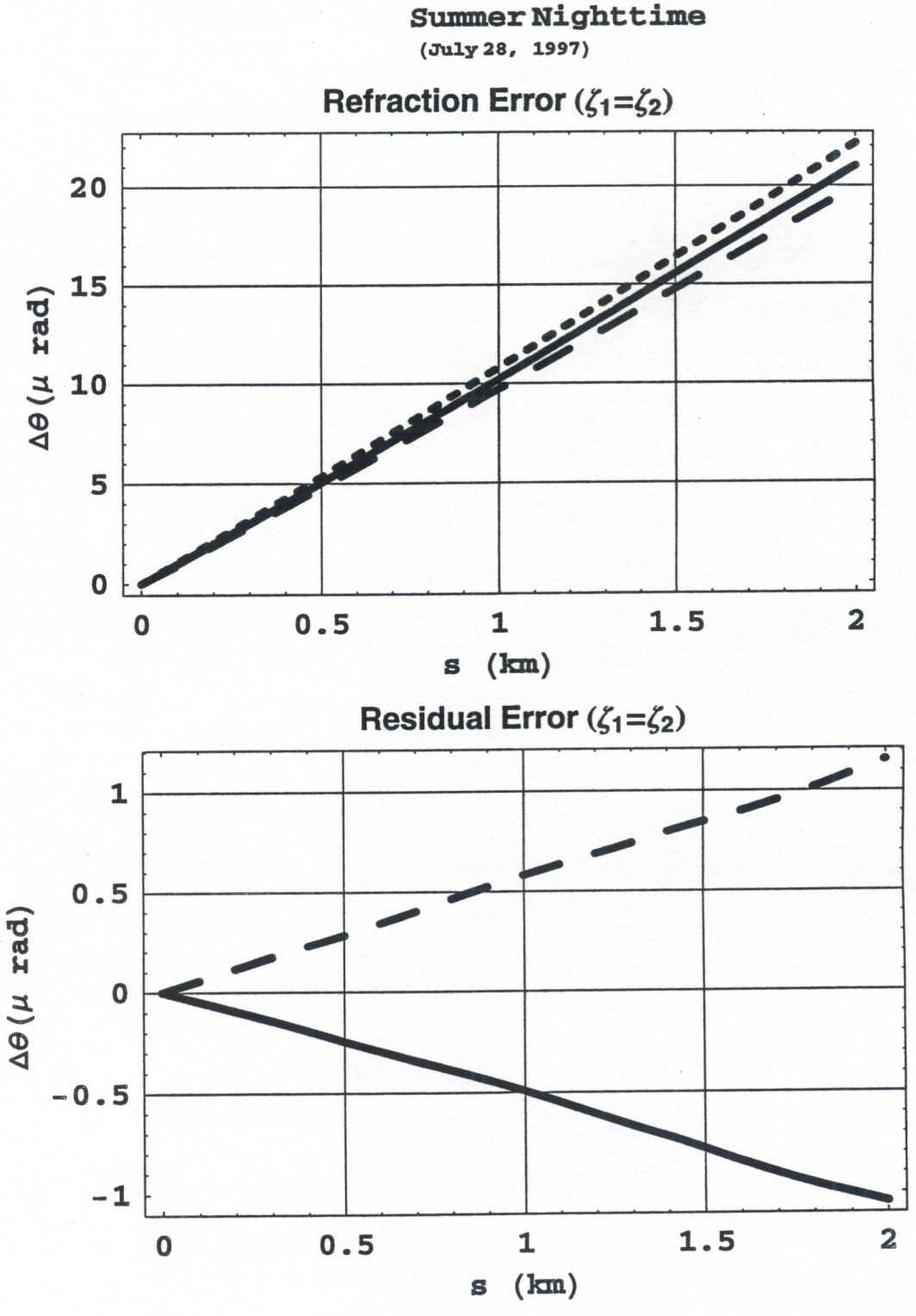
Summer Nighttime
(July 28, 1997)
Refraction Error ($\zeta_1=\zeta_2$)
Δθ (μ rad)
20
15
10
5
0
0
0.5
1
1.5
2
s (km)
Residual Error ($\zeta_1=\zeta_2$)
Δθ (μ rad)
1
0.5
0
-0.5
-1
0
0.5
1
1.5
2
s (km)

Fig .11 a

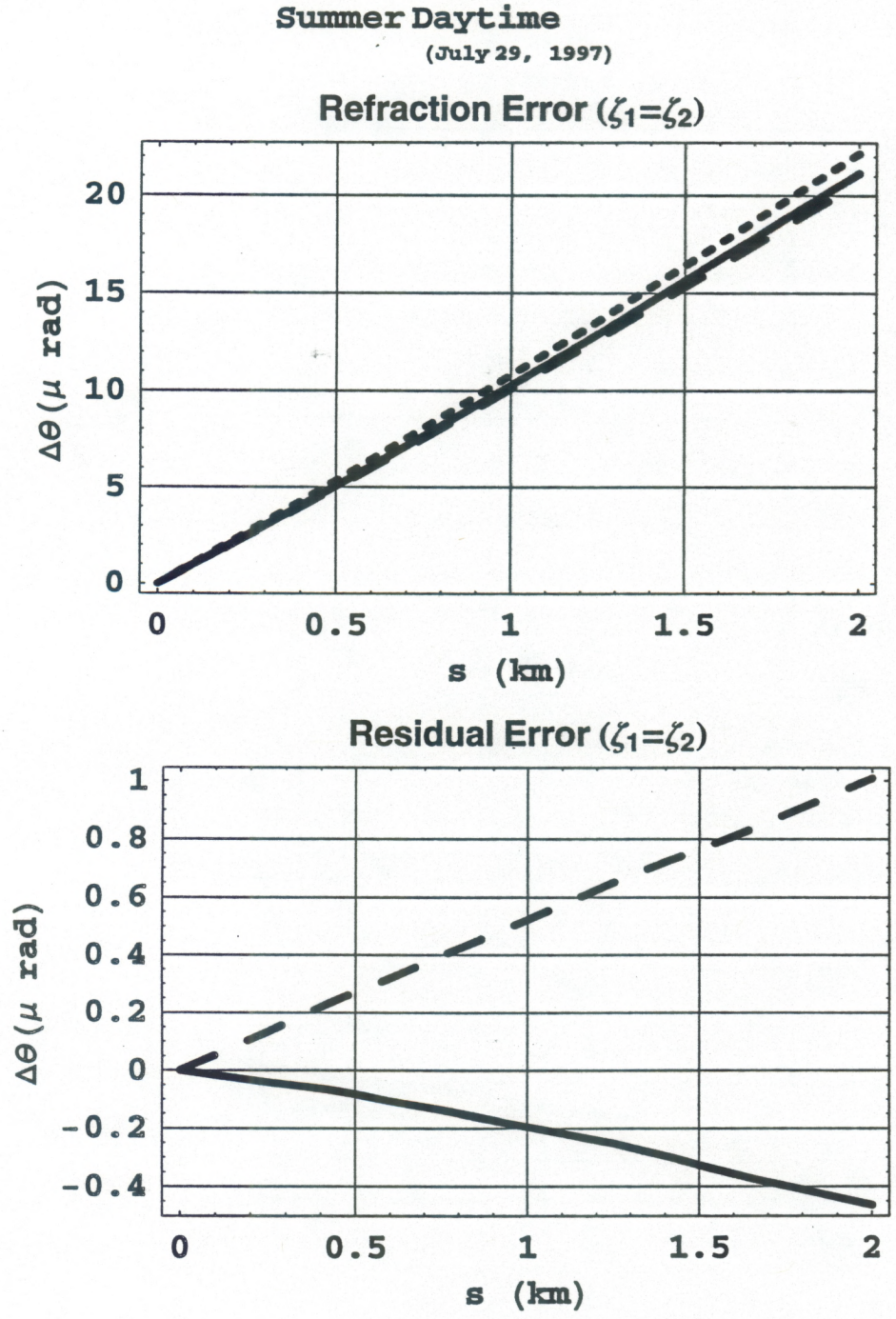
Summer Daytime
(July 29, 1997)
Refraction Error ($\zeta_1=\zeta_2$)
$\Delta\theta$ (μ rad)
20
15
10
5
0
0
0.5
1
1.5
2
s (km)
Residual Error ($\zeta_1=\zeta_2$)
$\Delta\theta$ (μ rad)
1
0.8
0.6
0.4
0.2
0
-0.2
-0.4
0
0.5
1
1.5
2
s (km)

Fig .11 b

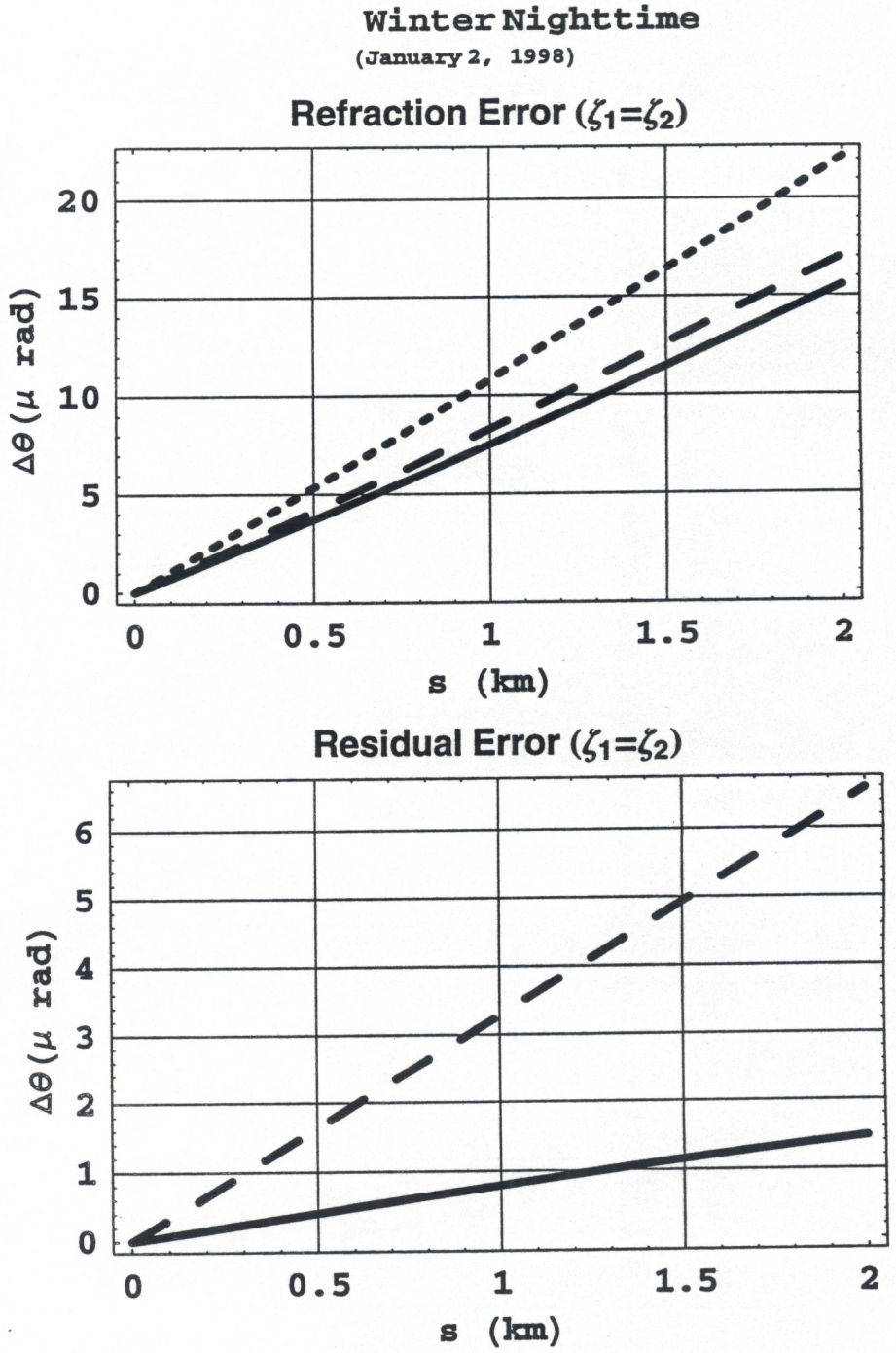
Winter Nighttime
(January 2, 1998)
Refraction Error ($\zeta_1=\zeta_2$)
$\Delta\theta$ (μ rad)
0
5
10
15
20
0
0.5
1
1.5
2
s (km)
Residual Error ($\zeta_1=\zeta_2$)
$\Delta\theta$ (μ rad)
0
1
2
3
4
5
6
0
0.5
1
1.5
2
s (km)

Fig .11 c

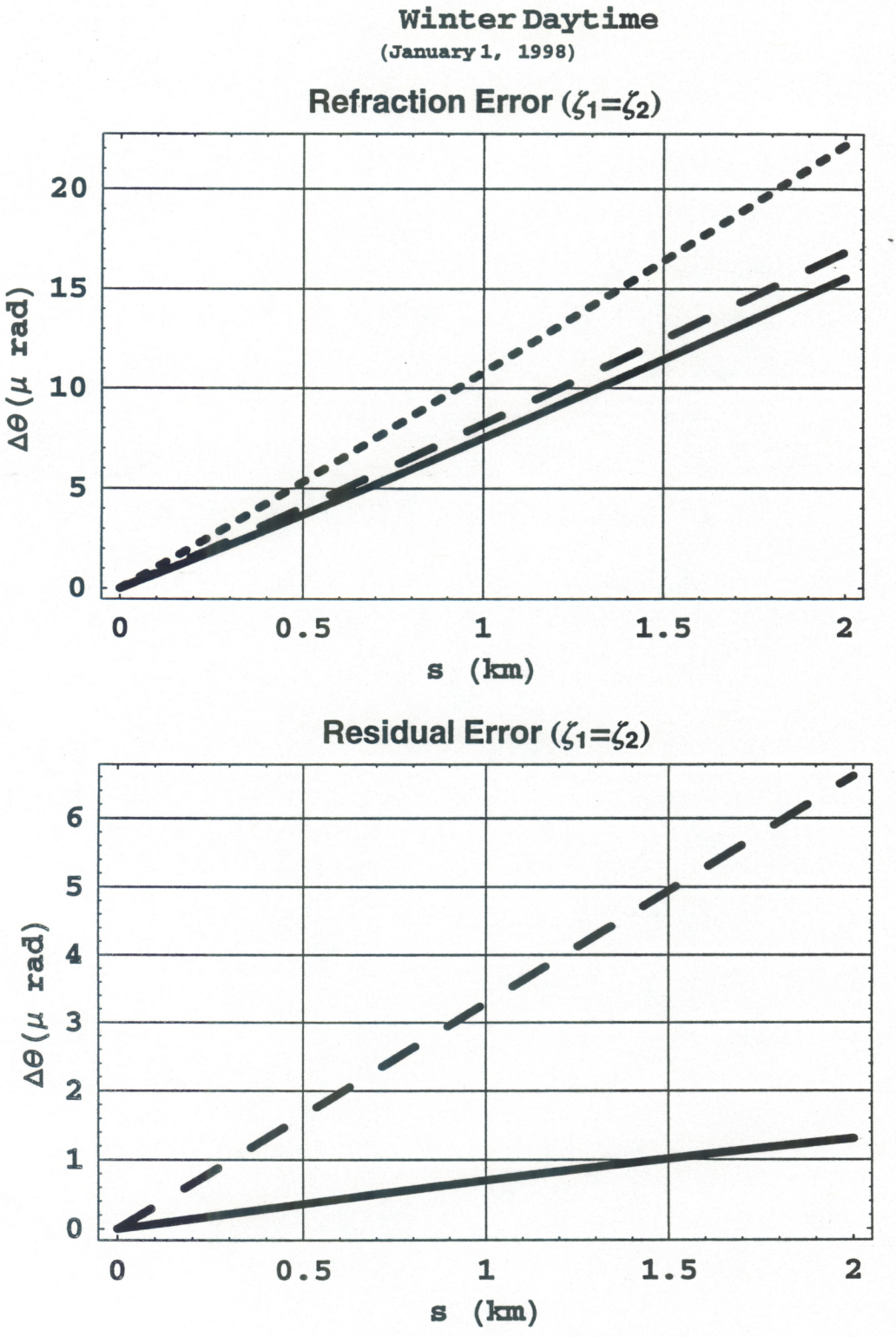
Winter Daytime
(January 1, 1998)
Refraction Error (ζ_1=ζ_2)
$\Delta\theta$ (μ rad)
0
5
10
15
20
0
0.5
1
1.5
2
s (km)
Residual Error (ζ_1=ζ_2)
$\Delta\theta$ (μ rad)
0
1
2
3
4
5
6
0
0.5
1
1.5
2
s (km)

Fig .11 d

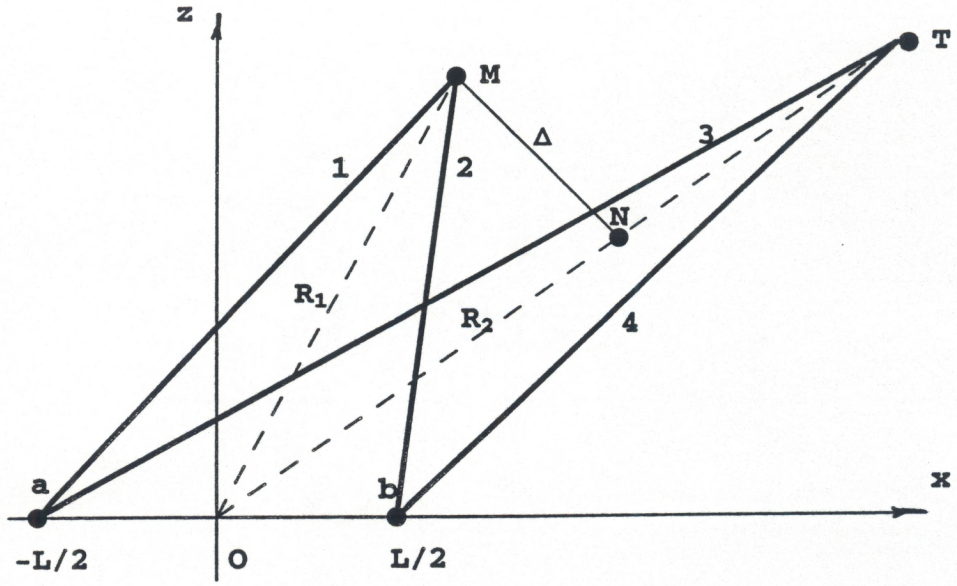

Fig .12

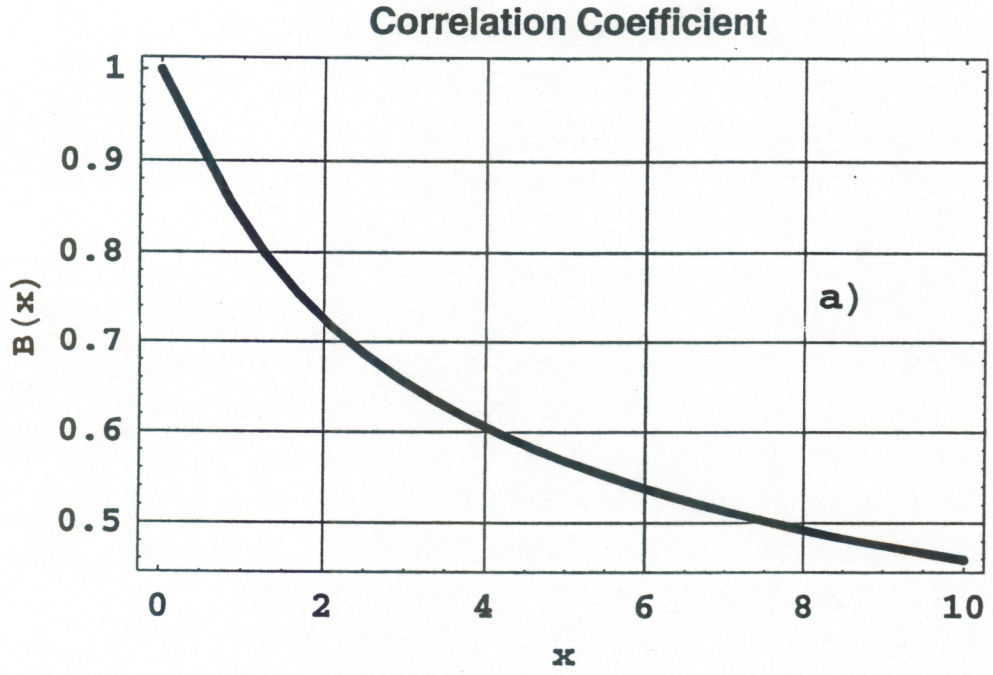
Correlation Coefficient
1
0.9
0.8
0.7
0.6
0.5
B(x)
a)
0
2
4
6
8
10
x

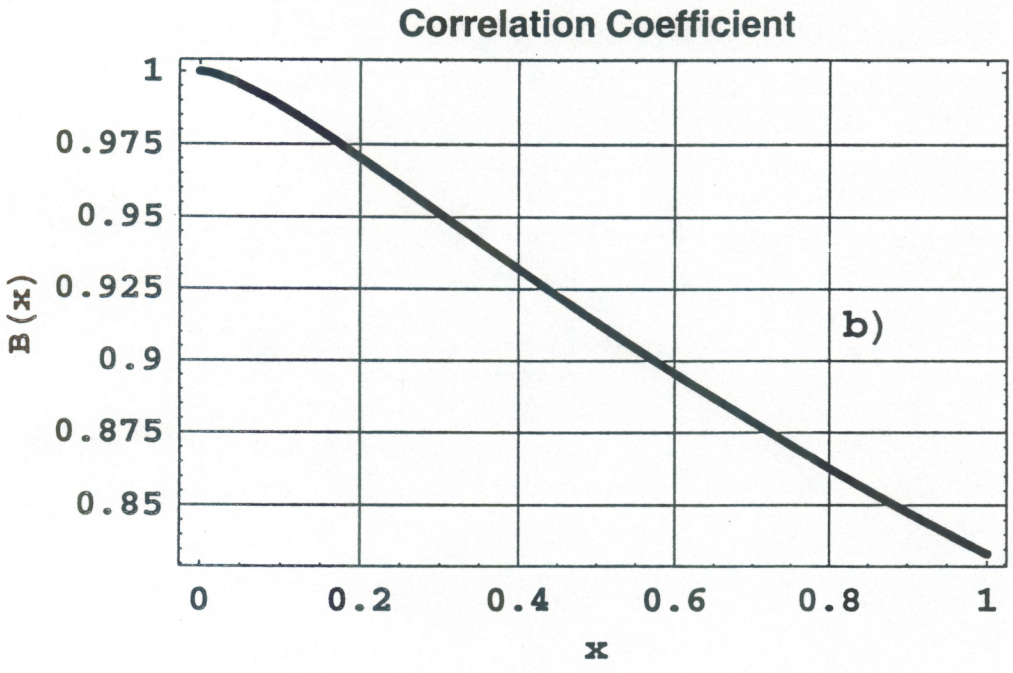
Correlation Coefficient
1
0.975
0.95
0.925
0.9
0.875
0.85
B(x)
b)
0
0.2
0.4
0.6
0.8
1
x

Fig .13 a, b

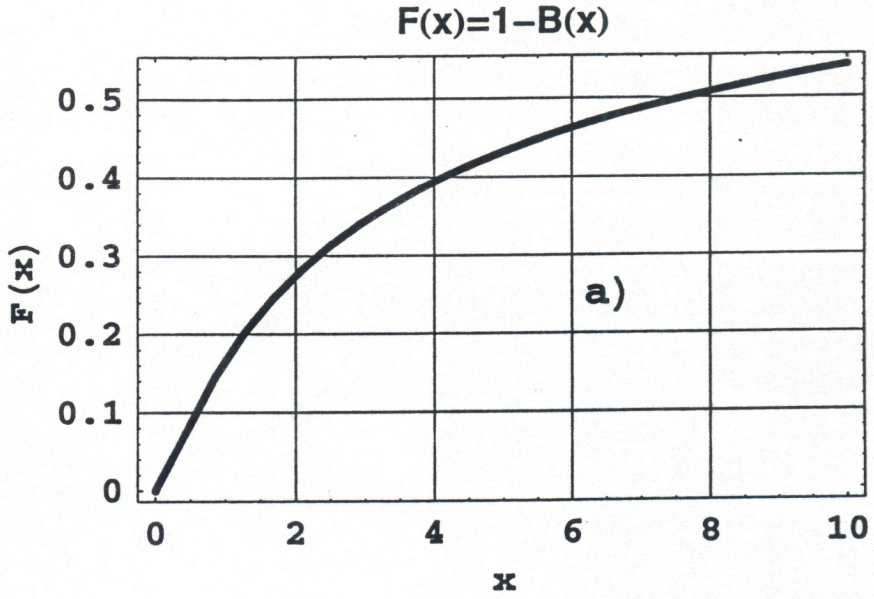
F(x)=1−B(x)
0.5
0.4
0.3
0.2
0.1
0
F(x)
a)
0
2
4
6
8
10
x

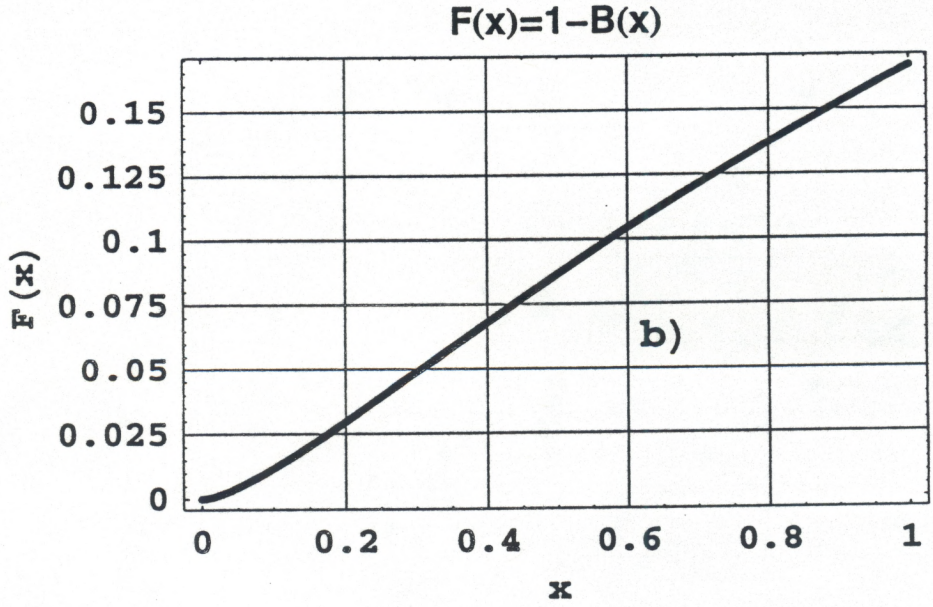
F(x)=1−B(x)
0.15
0.125
0.1
0.075
0.05
0.025
0
F(x)
b)
0
0.2
0.4
0.6
0.8
1
x

Fig .14 a, b

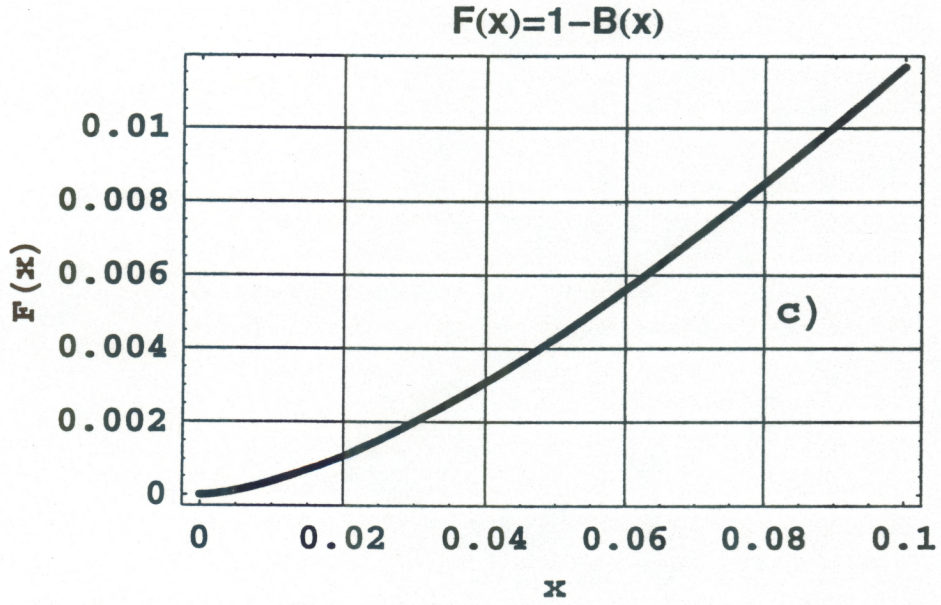

Fig . 14 c

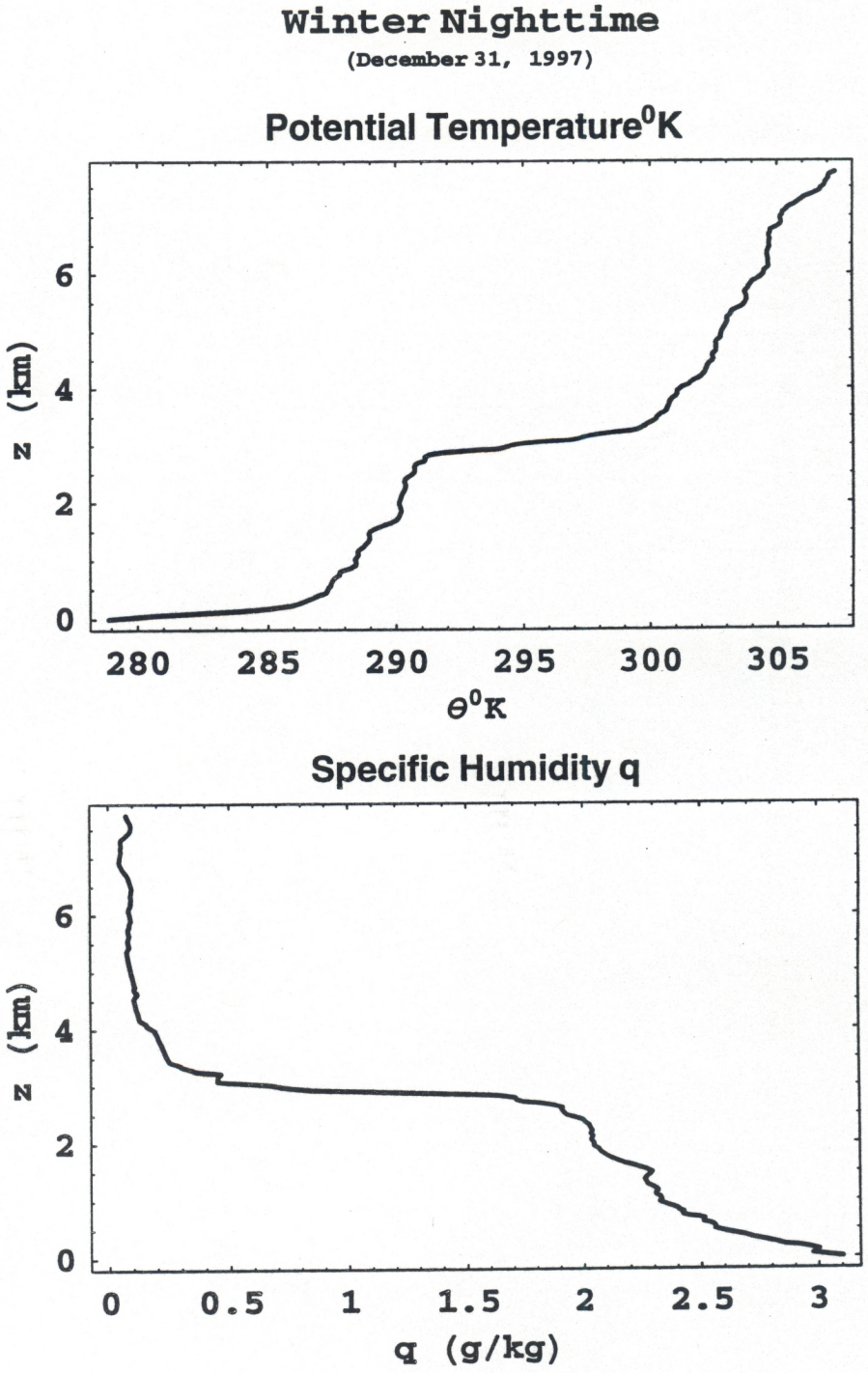
Winter Nighttime
(December 31, 1997)
Potential Temperature⁰K
z (km)
0
2
4
6
280
285
290
295
300
305
θ⁰K
Specific Humidity q
z (km)
0
2
4
6
0
0.5
1
1.5
2
2.5
3
q (g/kg)

Fig .15 a

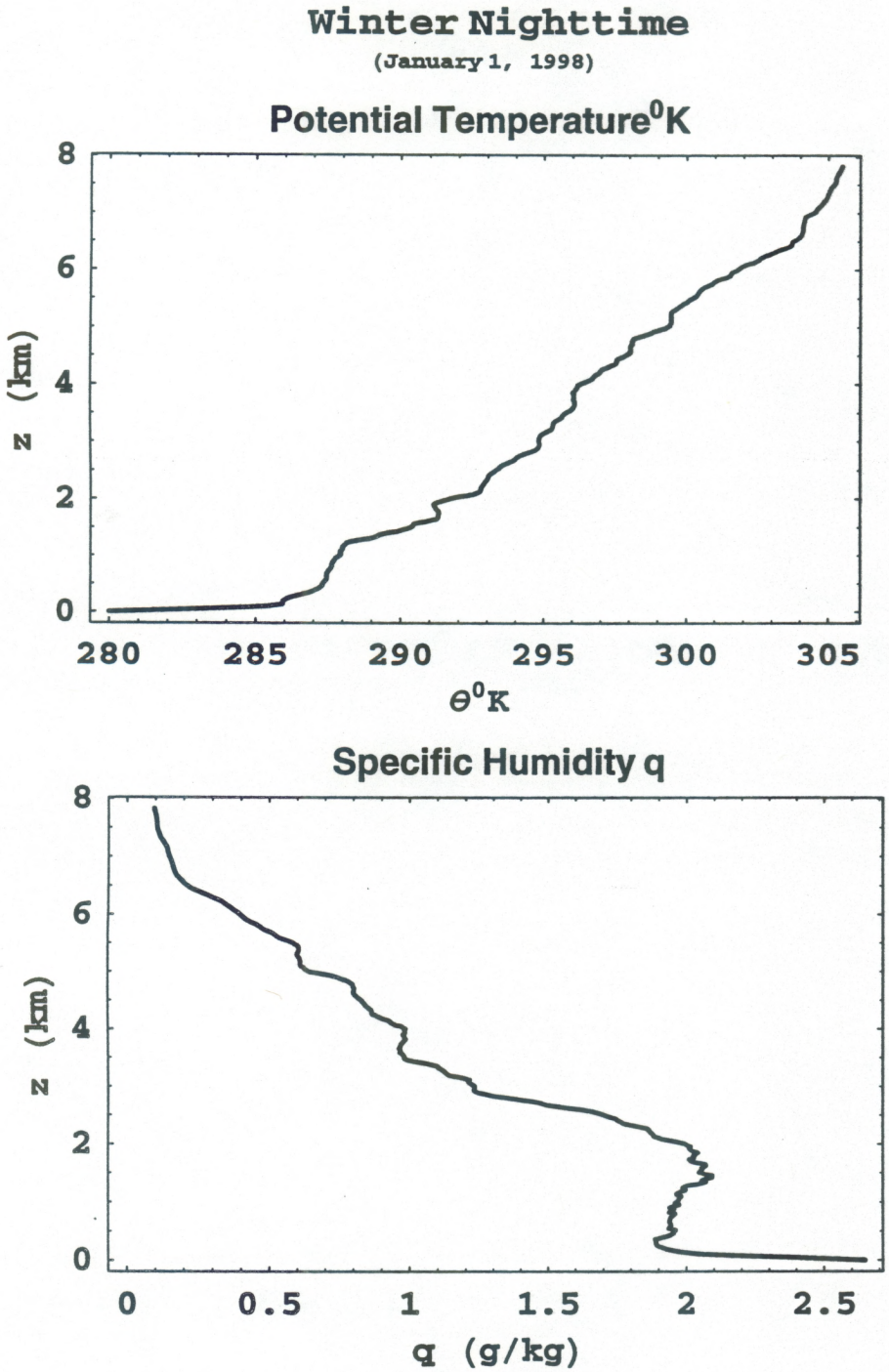
Winter Nighttime
(January 1, 1998)
Potential Temperature⁰K
z (km)
θ⁰K
Specific Humidity q
z (km)
q (g/kg)

Fig .15 b

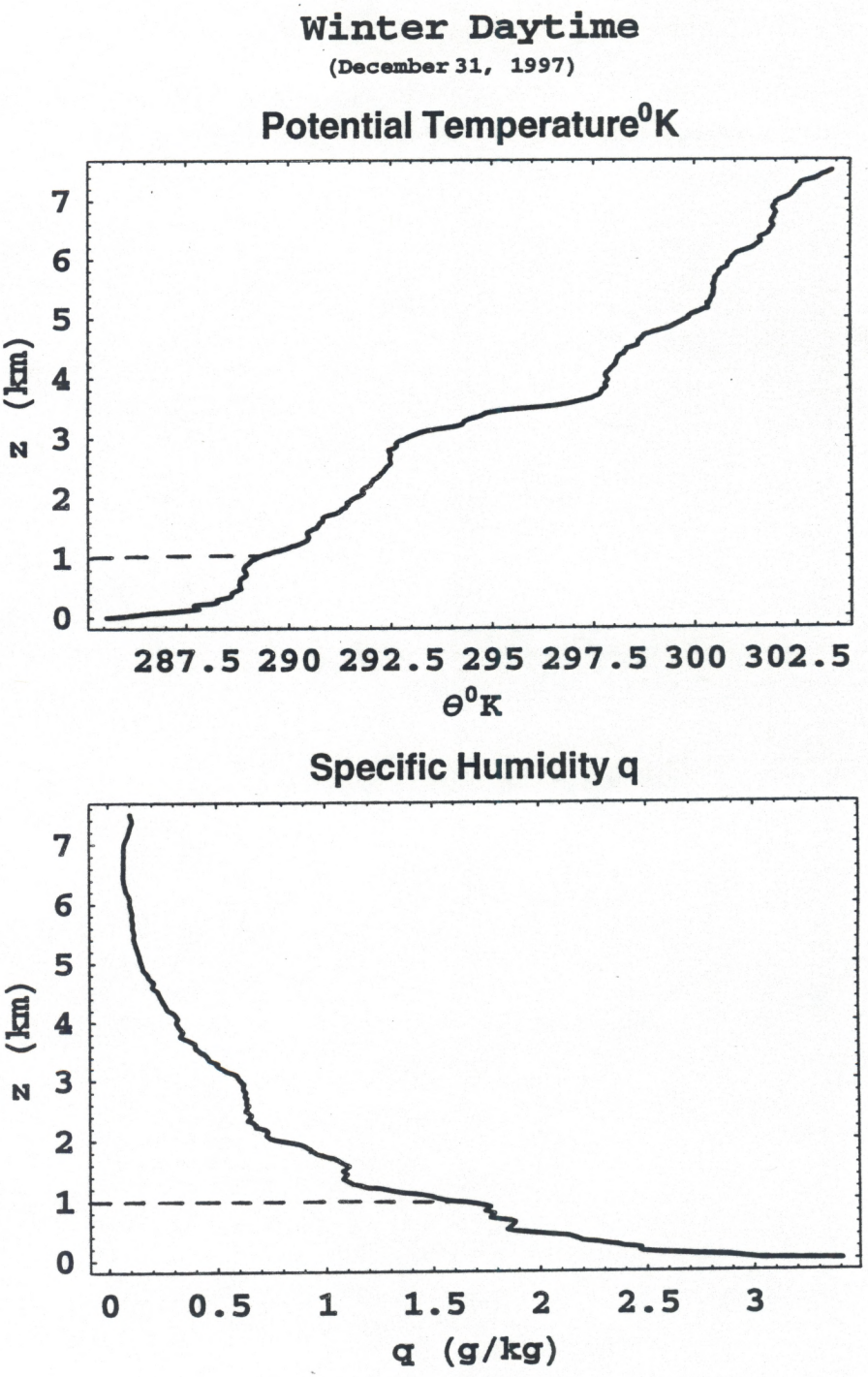
Winter Daytime
(December 31, 1997)
Potential Temperature⁰K
z (km)
0
1
2
3
4
5
6
7
287.5 290 292.5 295 297.5 300 302.5
θ⁰K
Specific Humidity q
z (km)
0
1
2
3
4
5
6
7
0 0.5 1 1.5 2 2.5 3
q (g/kg)

Fig .16 a

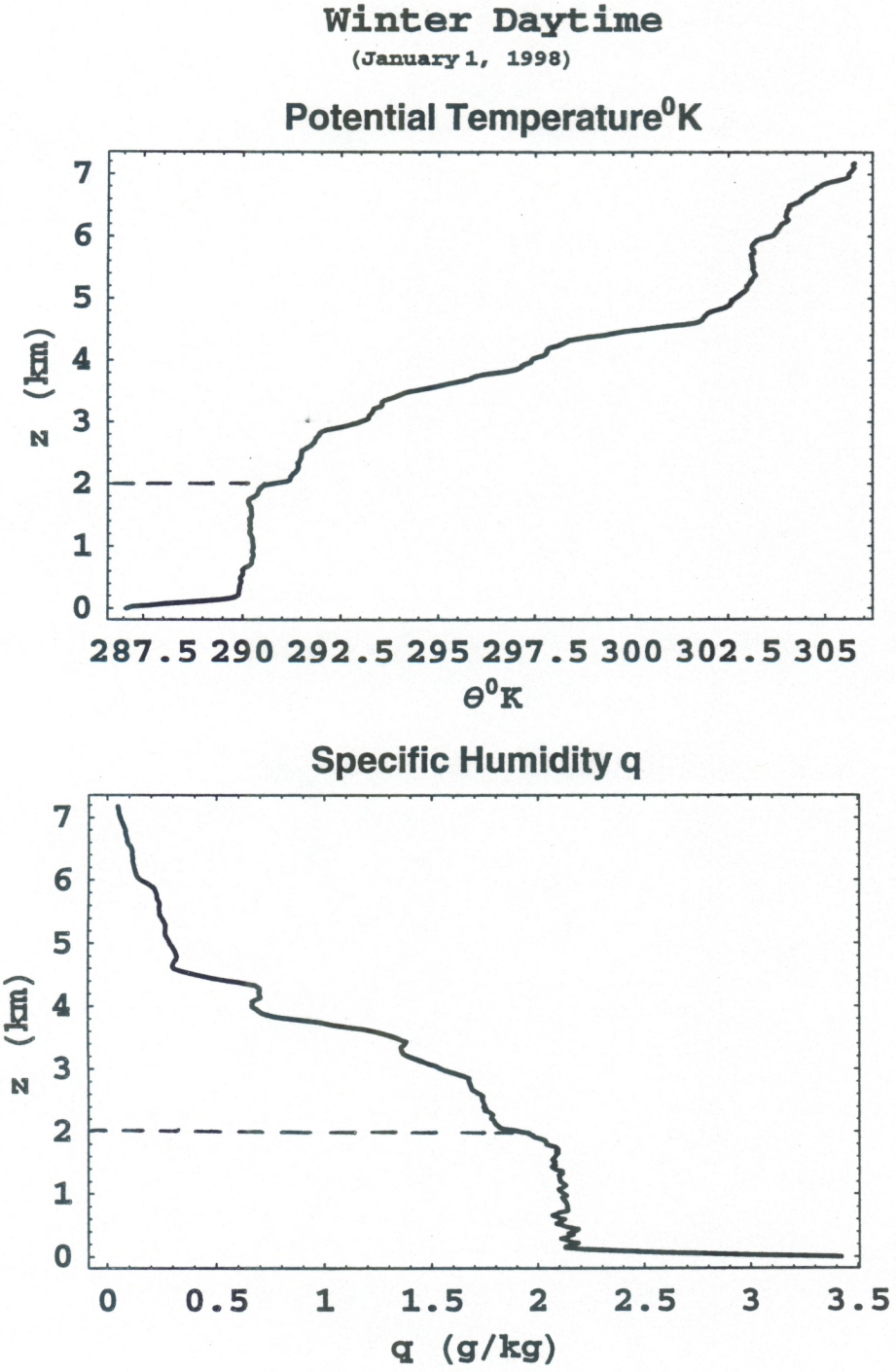
Winter Daytime
(January 1, 1998)
Potential Temperature⁰K
z (km)
0
1
2
3
4
5
6
7
287.5 290 292.5 295 297.5 300 302.5 305
θ⁰K
Specific Humidity q
z (km)
0
1
2
3
4
5
6
7
0 0.5 1 1.5 2 2.5 3 3.5
q (g/kg)

Fig .16 b

Summer Nighttime

(July 28, 1997)

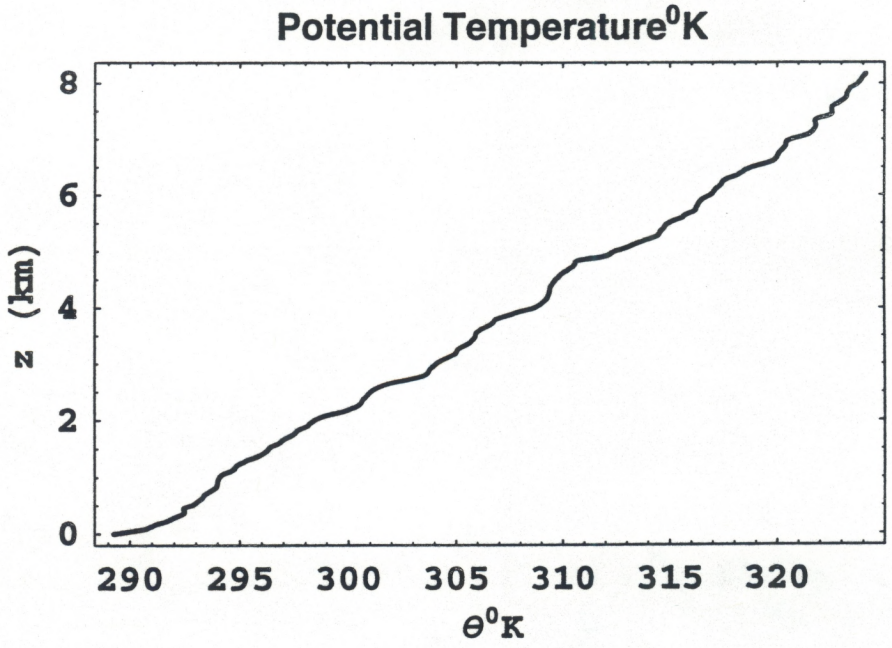

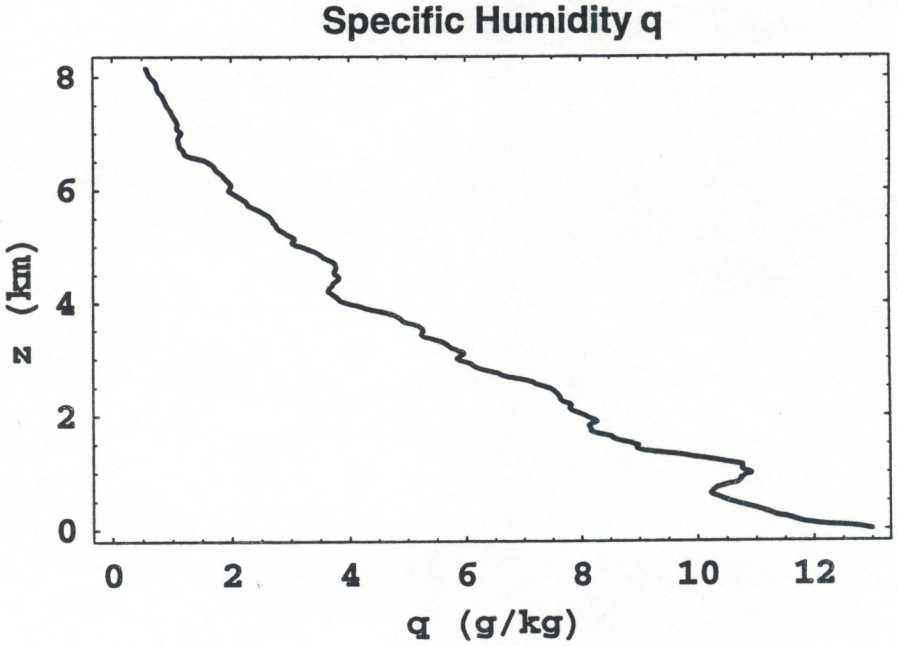

Fig .17 a

Summer Nighttime

(July 29, 1997)

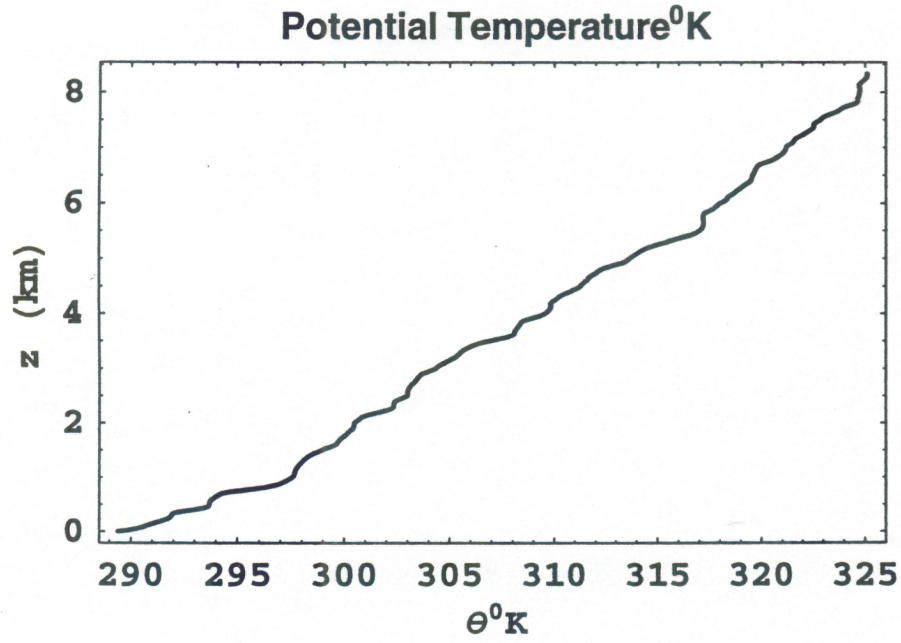

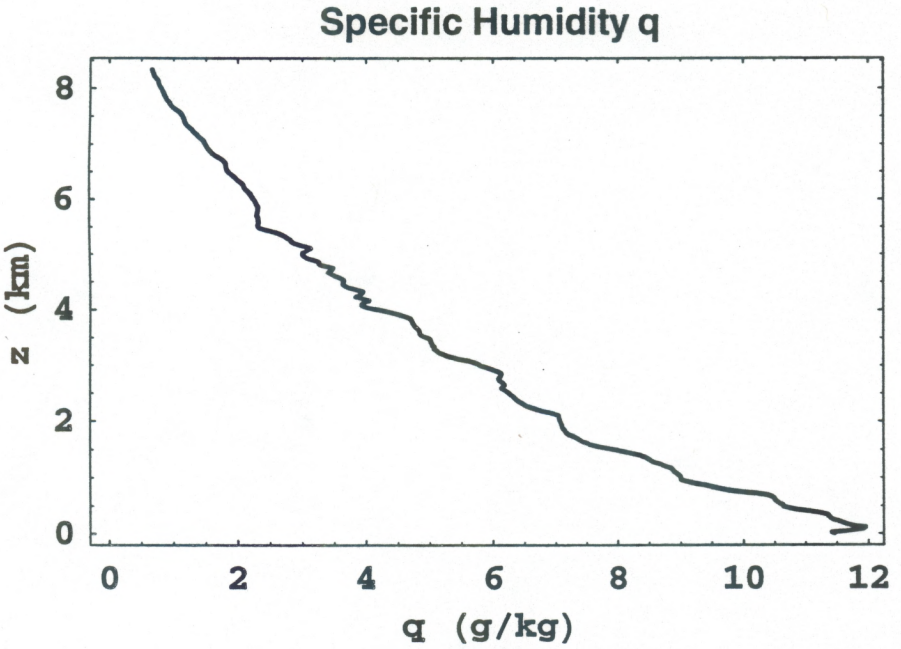

Fig .17 b

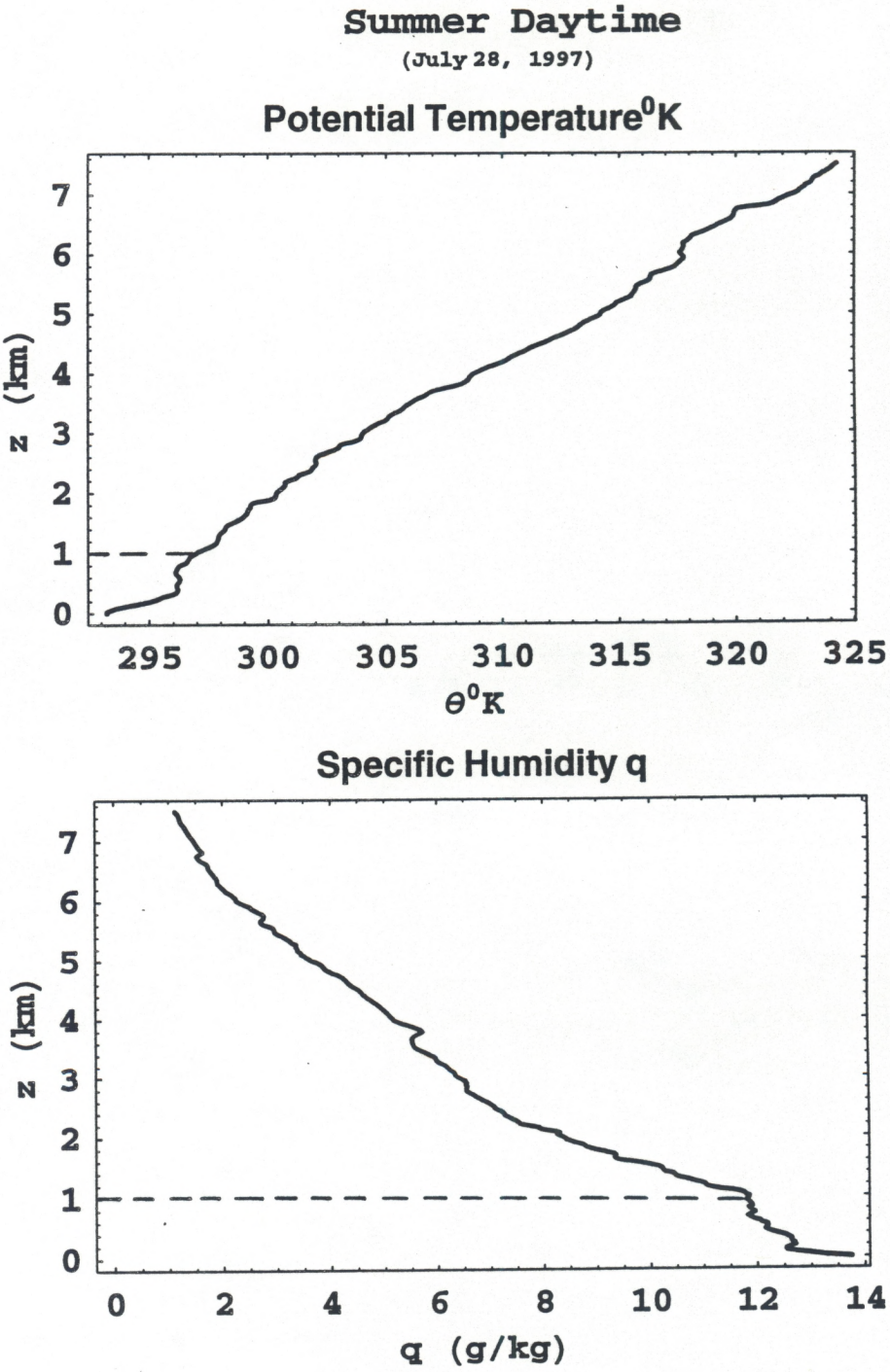
Summer Daytime
(July 28, 1997)
Potential Temperature⁰K
z (km)
0
1
2
3
4
5
6
7
295
300
305
310
315
320
325
θ⁰K
Specific Humidity q
z (km)
0
1
2
3
4
5
6
7
0
2
4
6
8
10
12
14
q (g/kg)

Fig .18 a

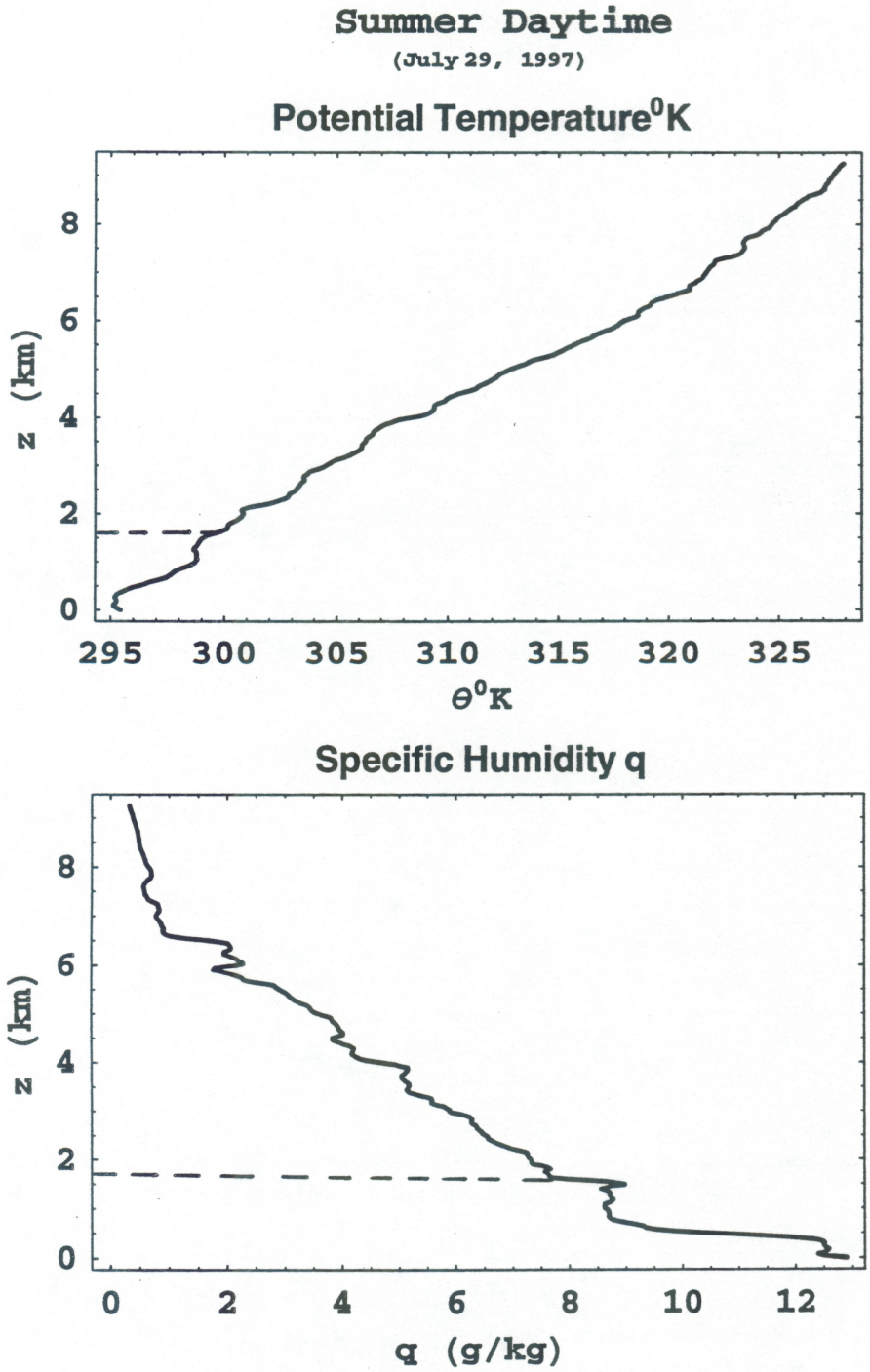
Summer Daytime
(July 29, 1997)
Potential Temperature⁰K
z (km)
0
2
4
6
8
295
300
305
310
315
320
325
θ⁰K
Specific Humidity q
z (km)
0
2
4
6
8
0
2
4
6
8
10
12
q (g/kg)

Fig .18 b

Winter Nighttime

(January 1, 1998)

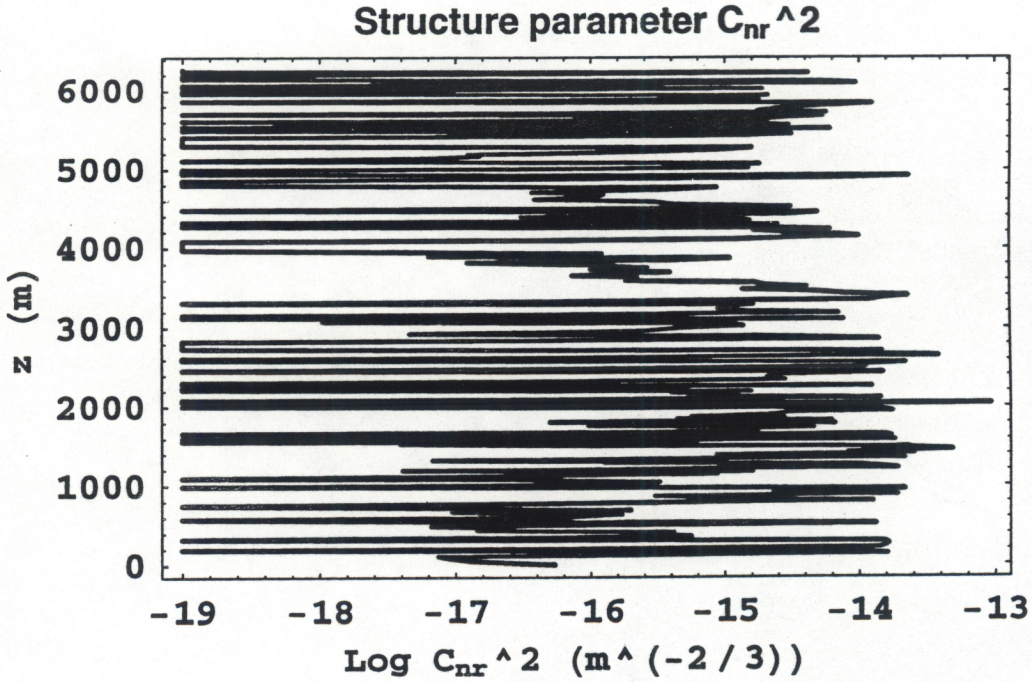

(January 2, 1998)

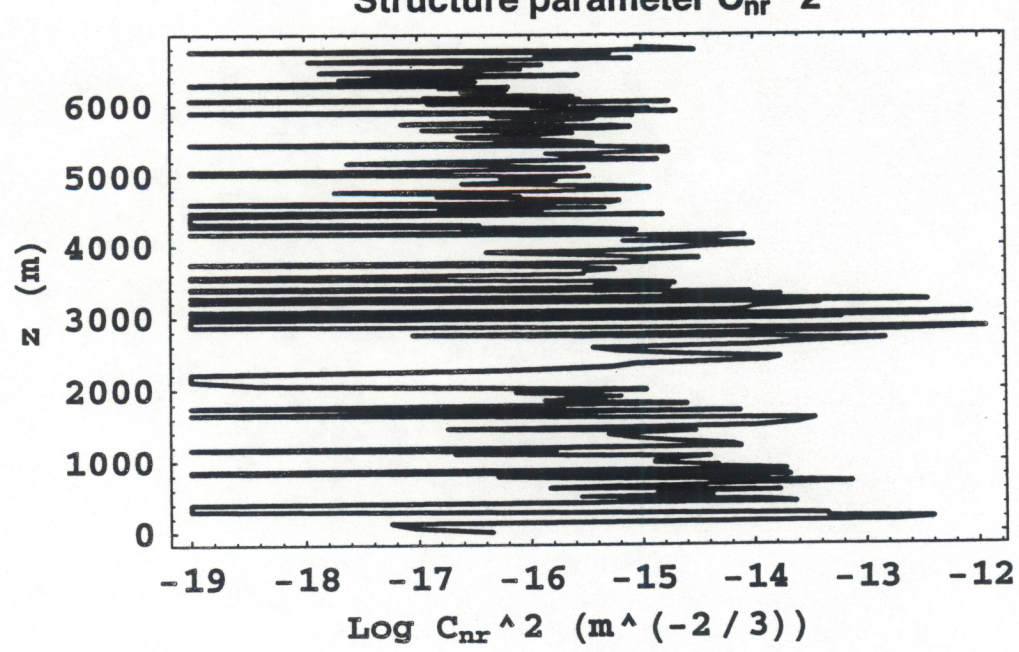

Fig .19

Winter Daytime

(December 31, 1997)

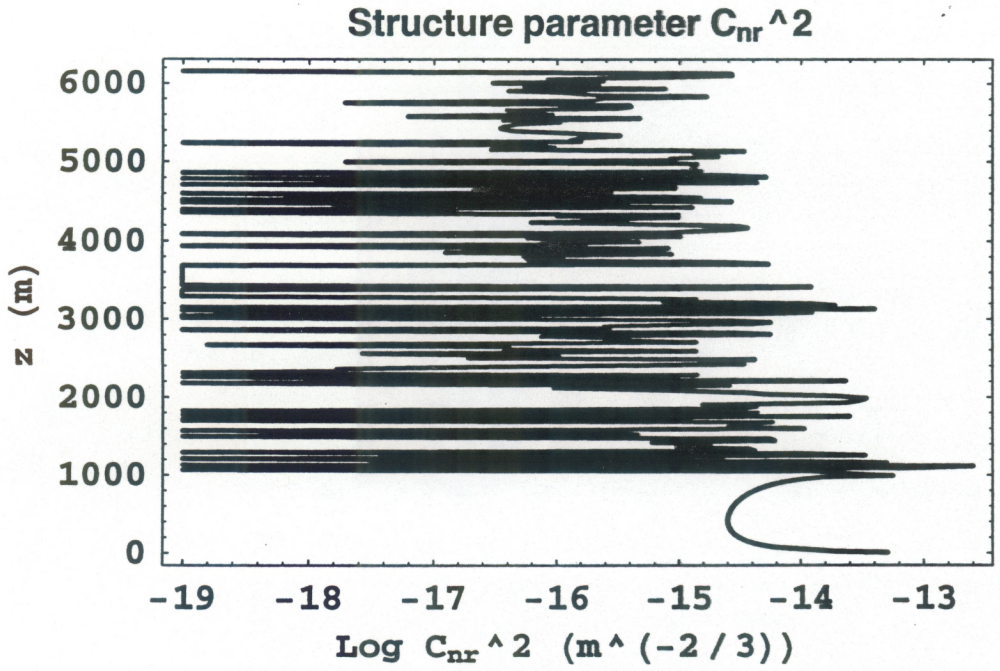

(January 1, 1998)

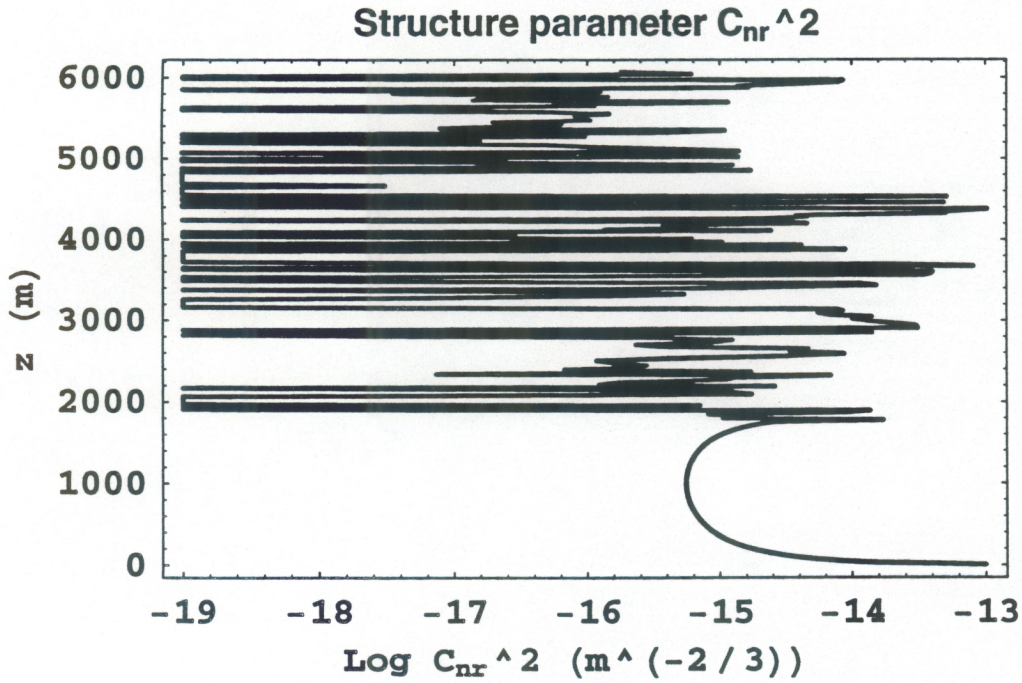

Fig .20

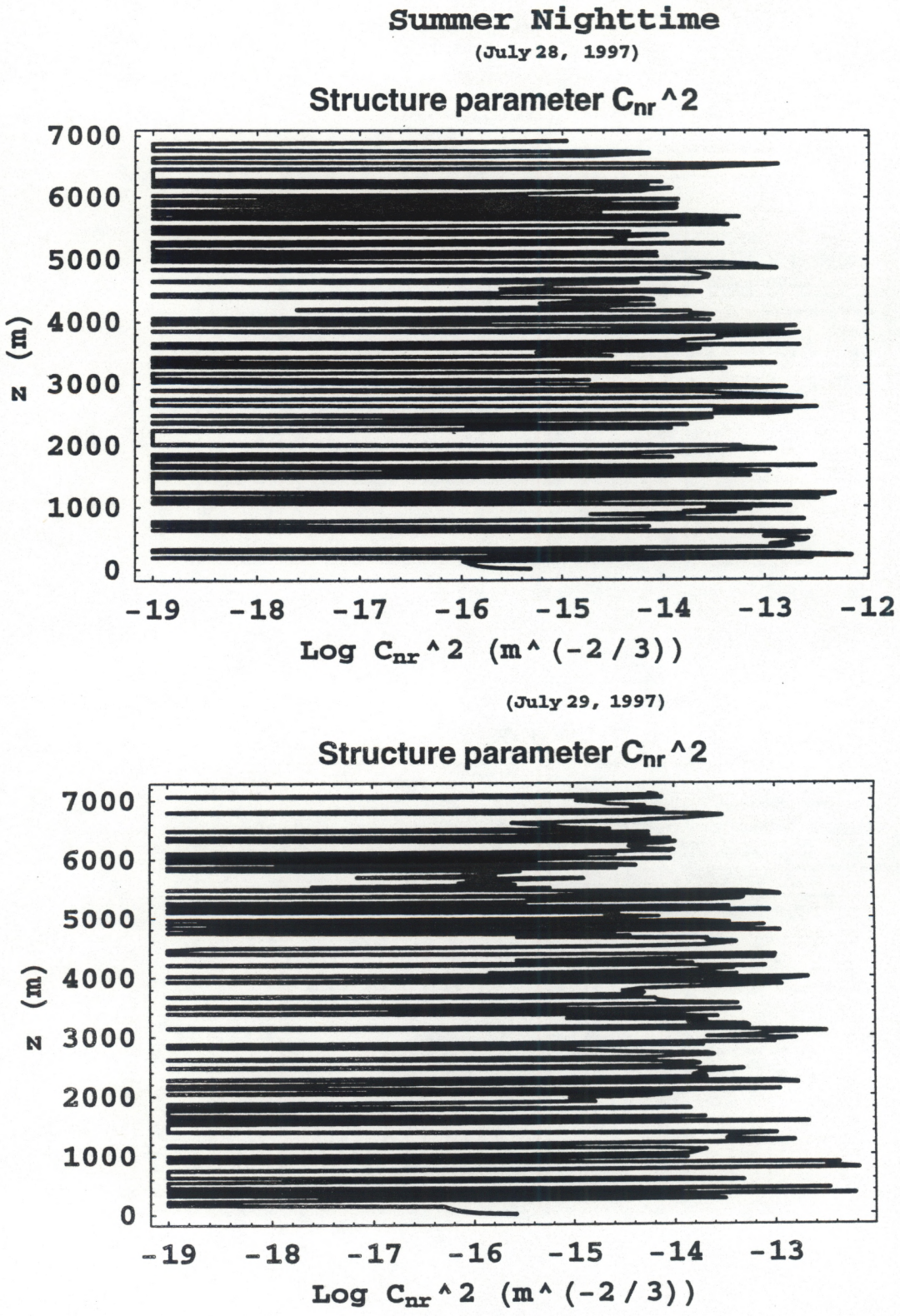
Summer Nighttime
(July 28, 1997)
Structure parameter C_{nr}^2
7000
6000
5000
4000
3000
2000
1000
0
z (m)
-19 -18 -17 -16 -15 -14 -13 -12
Log C_{nr}^2 (m^(-2/3))
(July 29, 1997)
Structure parameter C_{nr}^2
7000
6000
5000
4000
3000
2000
1000
0
z (m)
-19 -18 -17 -16 -15 -14 -13
Log C_{nr}^2 (m^(-2/3))

Fig .21

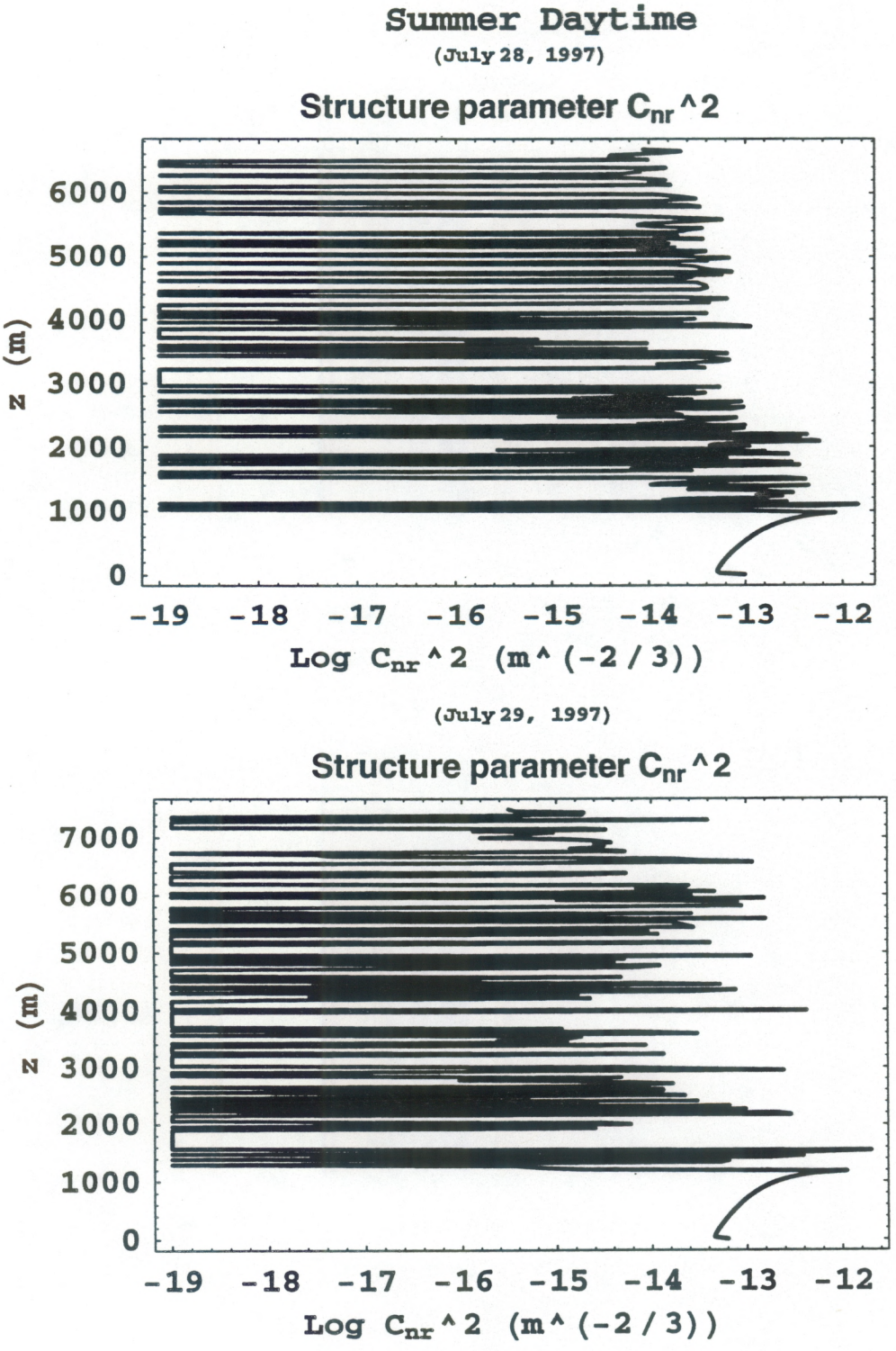
Summer Daytime
(July 28, 1997)
Structure parameter Cnr^2
6000
5000
4000
3000
2000
1000
0
z (m)
-19 -18 -17 -16 -15 -14 -13 -12
Log Cnr^2 (m^(-2/3))
(July 29, 1997)
Structure parameter Cnr^2
7000
6000
5000
4000
3000
2000
1000
0
z (m)
-19 -18 -17 -16 -15 -14 -13 -12
Log Cnr^2 (m^(-2/3))

Fig .22

Appendix

The numerical results concerning the refraction errors in the stratified atmosphere for two scenarios (see Fig. 9) of approaching missile (M) to the target (T) are attached below for three additional sets of geometrical parameters compared with those in Fig. 10(a-d) and Fig. 11(a-d):
A). R_2=5 km, z_2=3 km, ς_2=53° - Fig. A1- Fig. A8;
B).R_2=8 km, z_2=1 km, ς_2=82° - Fig. B1- Fig. B8;
C).R_2=5 km, z_2=0.7 km, ς_2=82° - Fig. C1- Fig. C8.

Scenario 1 corresponds to a horizontal approach (z_1=z_2), and Scenario 2 corresponds to an inclined approach (ς_1=ς_2); s is the distance between the missile and the target.
In the **upper** plots of all of these figures three different refraction errors $\Delta\theta$ (μrad) are shown:

1) - the solid curves correspond to the refraction error $\Delta\theta_{real}$ due to the real refraction-index profile obtained directly from the balloon data;

2) - the short-dashed curves correspond to the refraction error $\Delta\theta_{stand}$ predicted by the exponential standard atmospheric (N_0=335.3) refractive-index profile (25);

3) - the long-dashed curves correspond to the refraction error $\Delta\theta_{adj}$ predicted by the exponential refractive-index profile (25) adjusted to the real value at the surface, i.e. N_0 =N(0).

In the **lower** plots two residual errors are shown:

1) - the long-dashed curves correspond to the residual $\Delta\theta_{stand}$-$\Delta\theta_{real}$;

2) - the solid curves correspond to the residual error Res $\Delta\theta$=$\Delta\theta_{adj}$-$\Delta\theta_{real}$.

Winter Nighttime

(January 2, 1998)

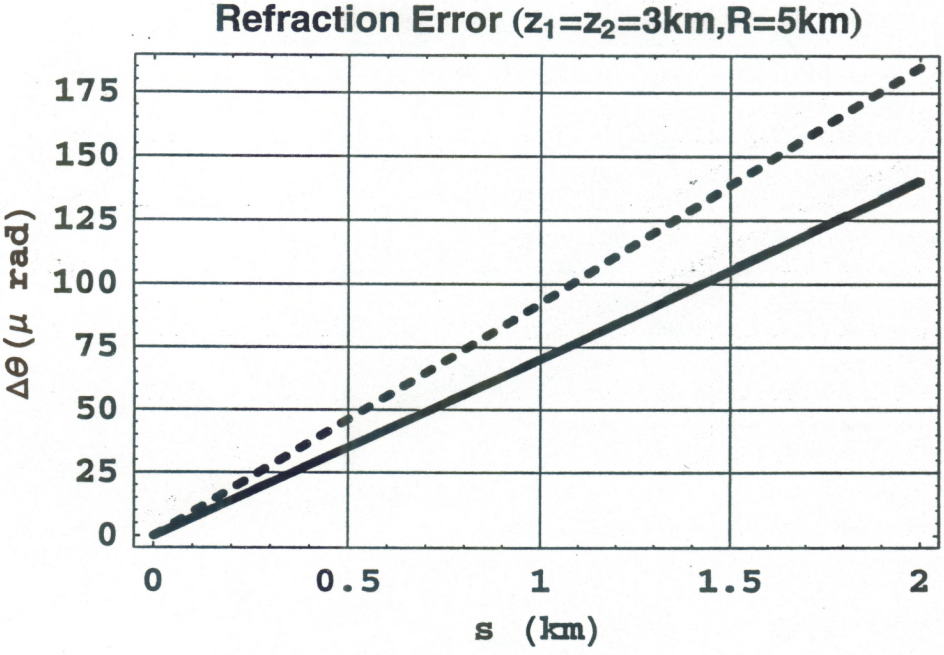

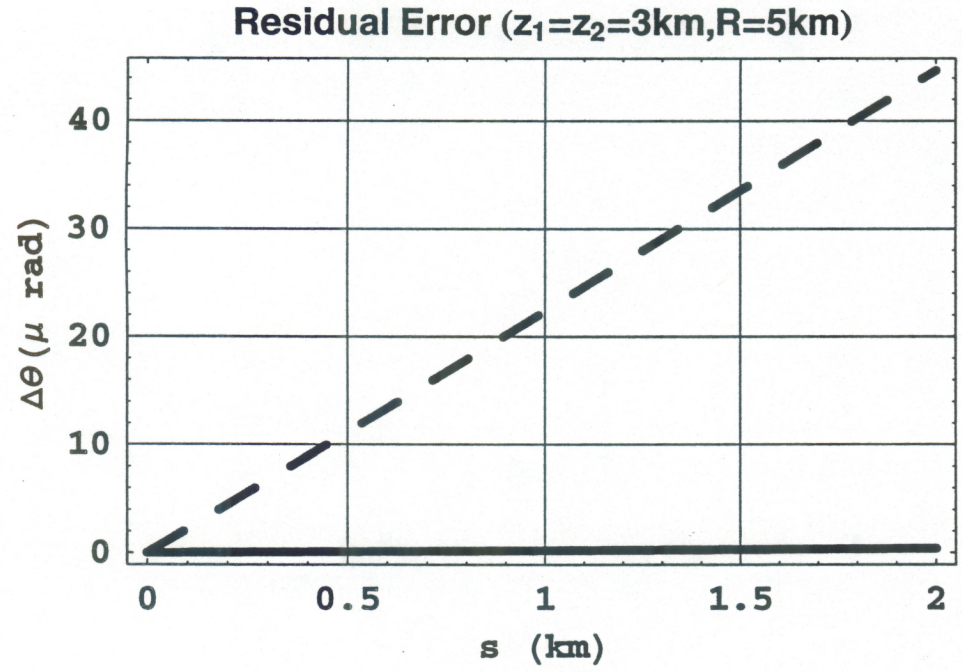

Fig. A1

Summer Nighttime

(July 28, 1997)

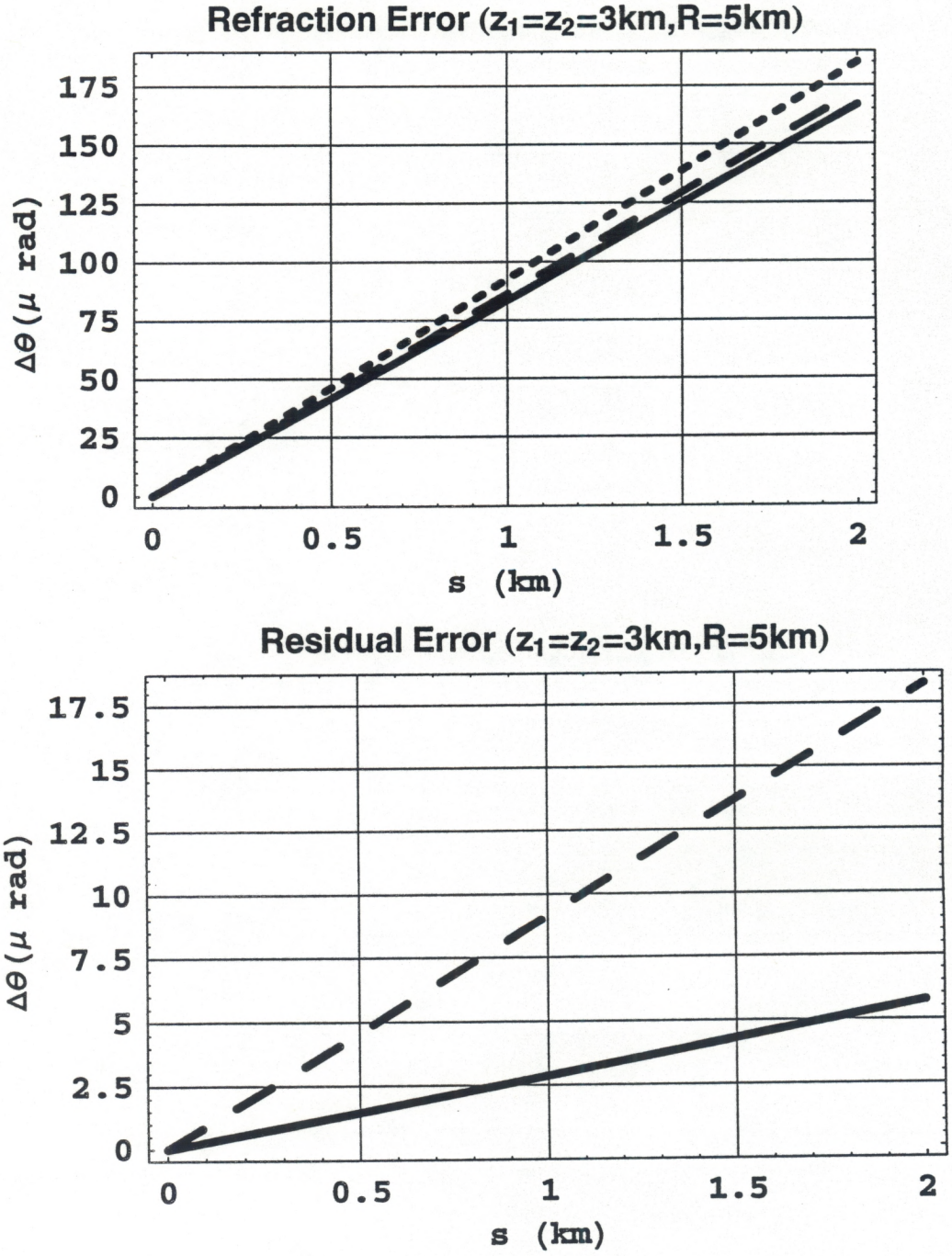

Fig. A3

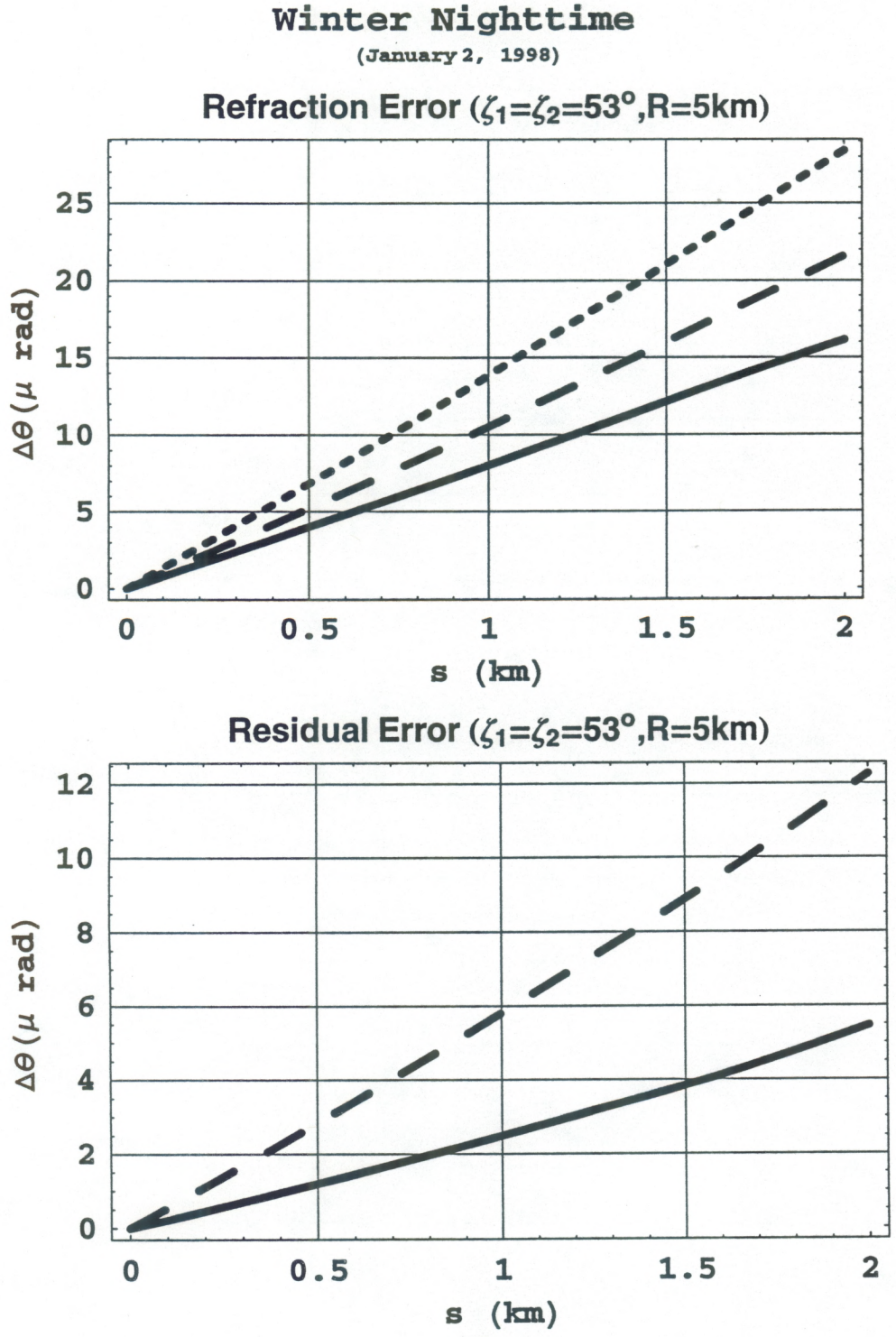
Winter Nighttime
(January 2, 1998)
Refraction Error ($\zeta_1=\zeta_2=53°$,R=5km)
$\Delta\theta$ (μ rad)
25
20
15
10
5
0
0
0.5
1
1.5
2
s (km)
Residual Error ($\zeta_1=\zeta_2=53°$,R=5km)
$\Delta\theta$ (μ rad)
12
10
8
6
4
2
0
0
0.5
1
1.5
2
s (km)

Fig. A4

Winter Daytime

(January 1, 1998)

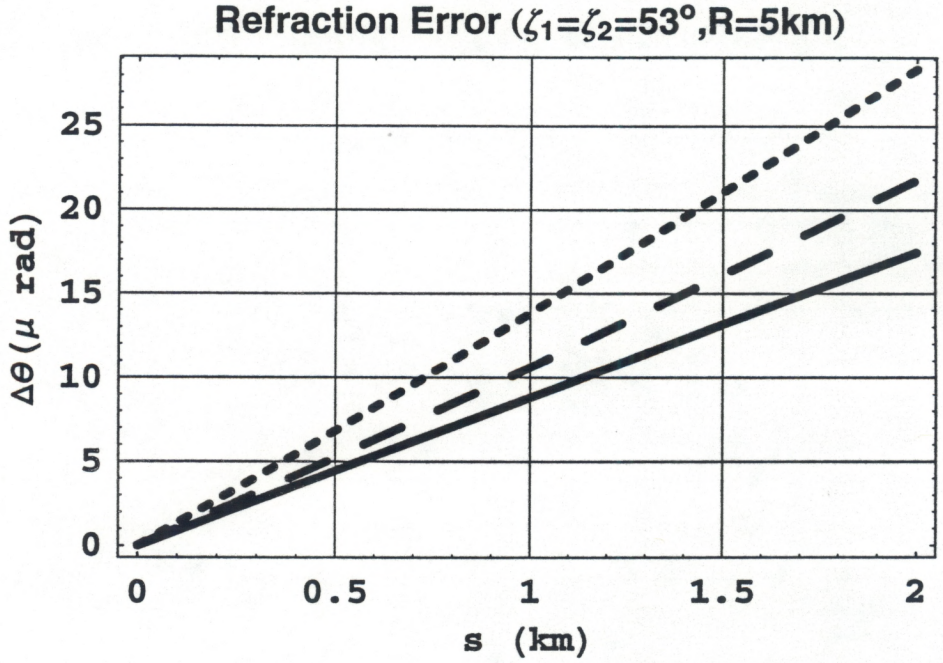

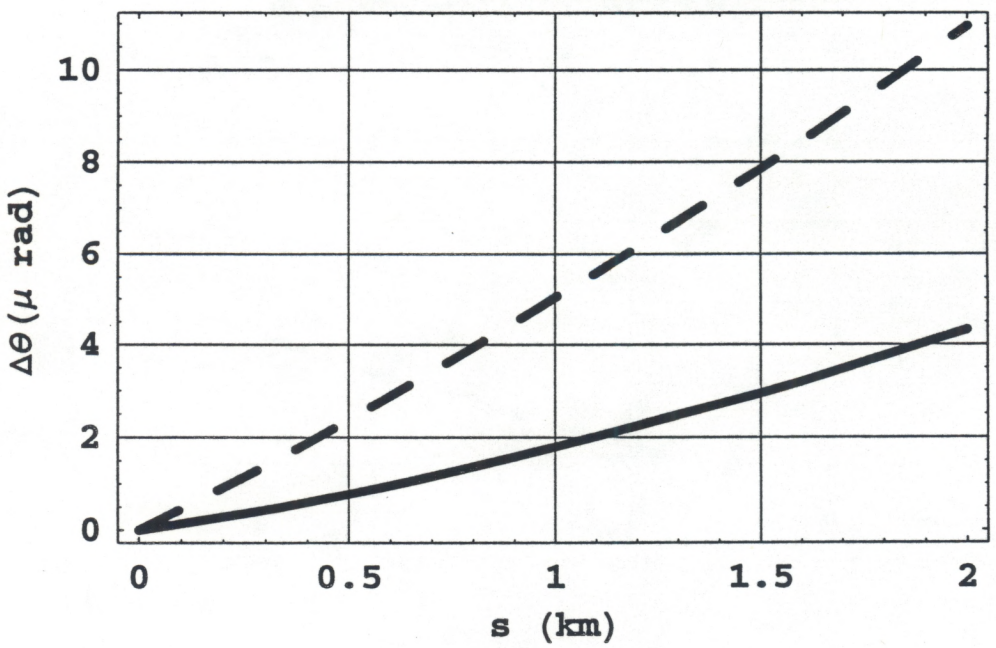

Fig. A5

Summer Nighttime

(July 28, 1997)

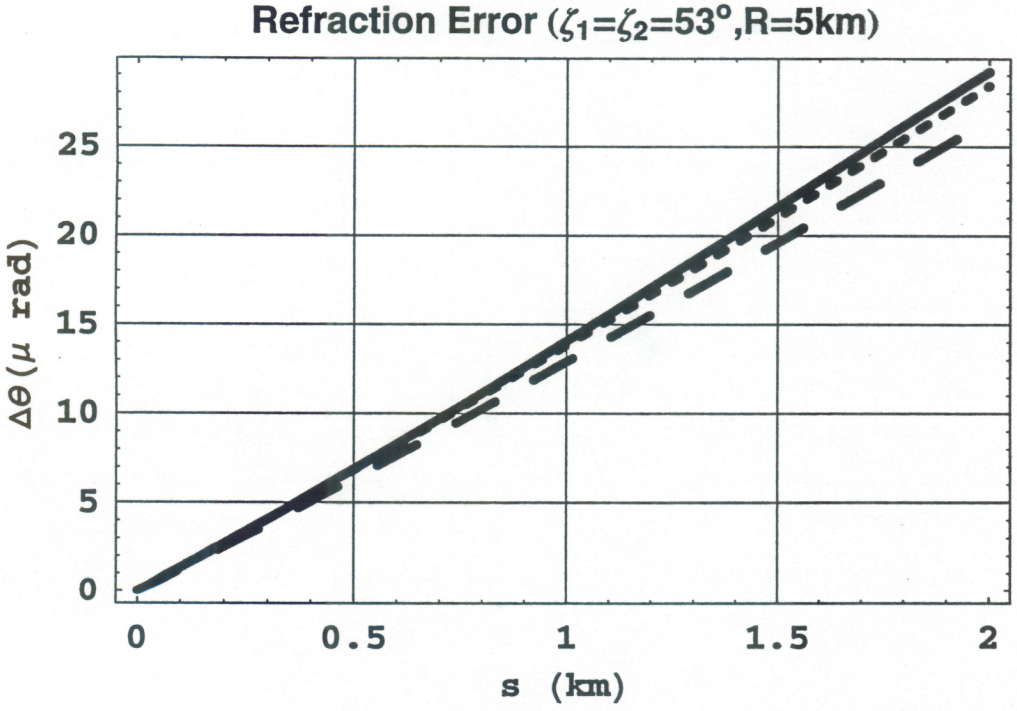

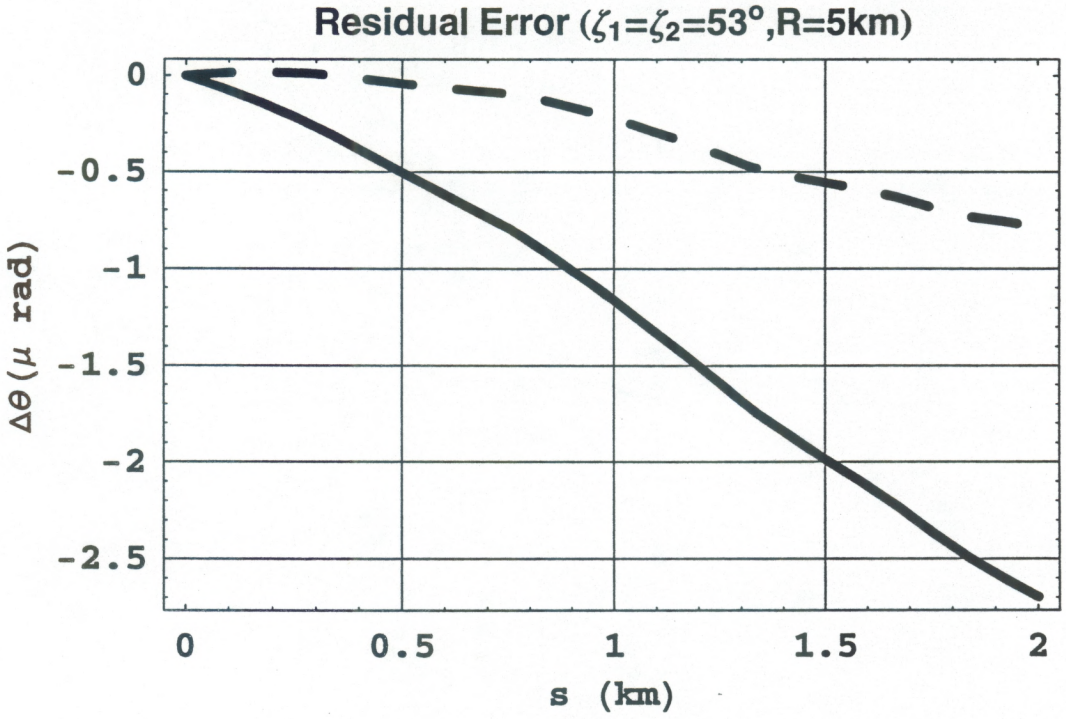

Fig. A6

Summer Daytime

(July 29, 1997)

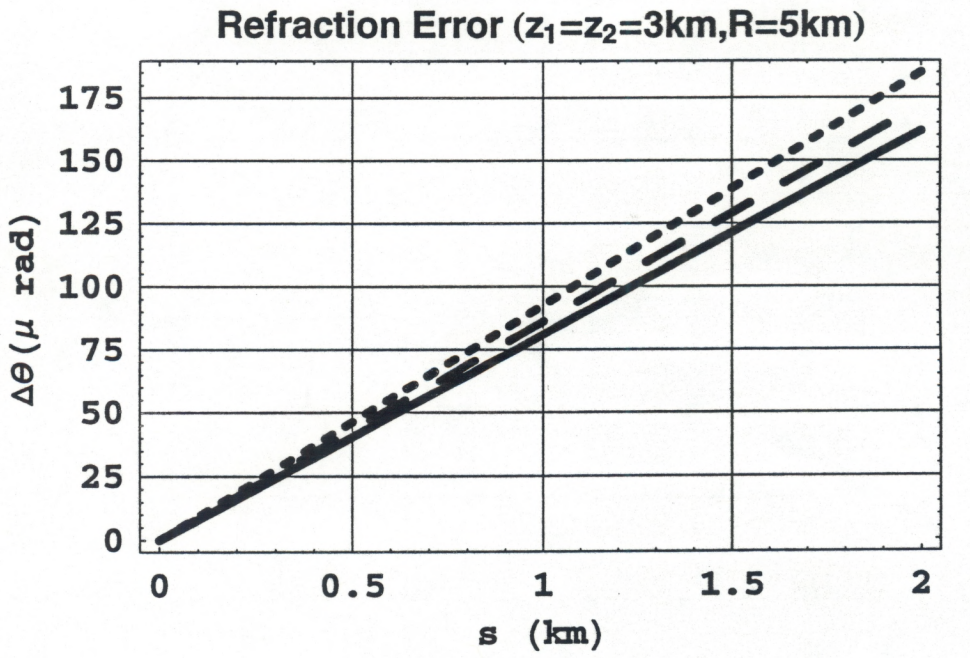

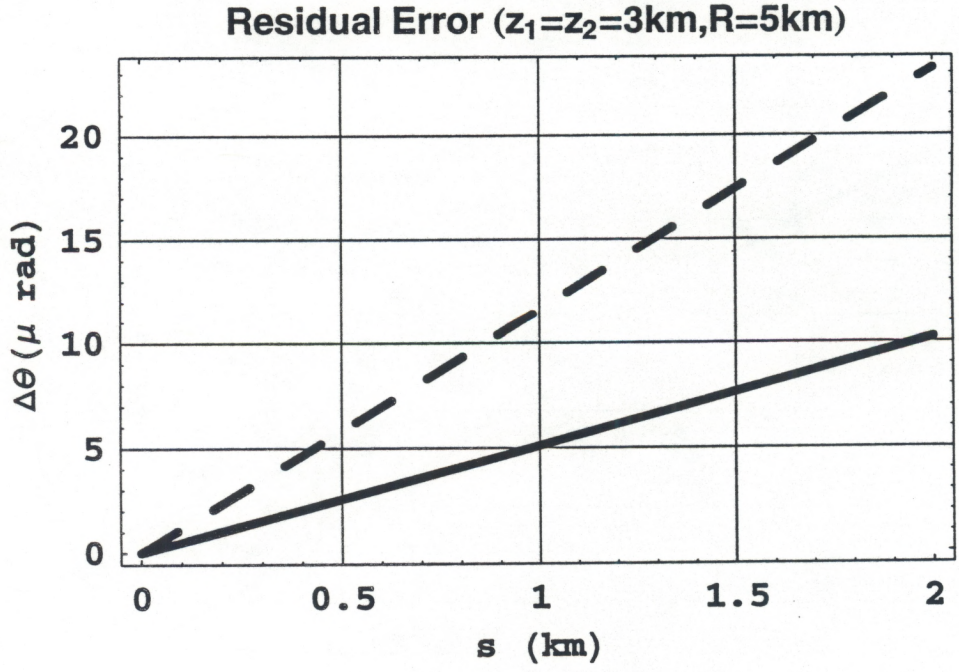

Fig. A7

Summer Daytime

(July 29, 1997)

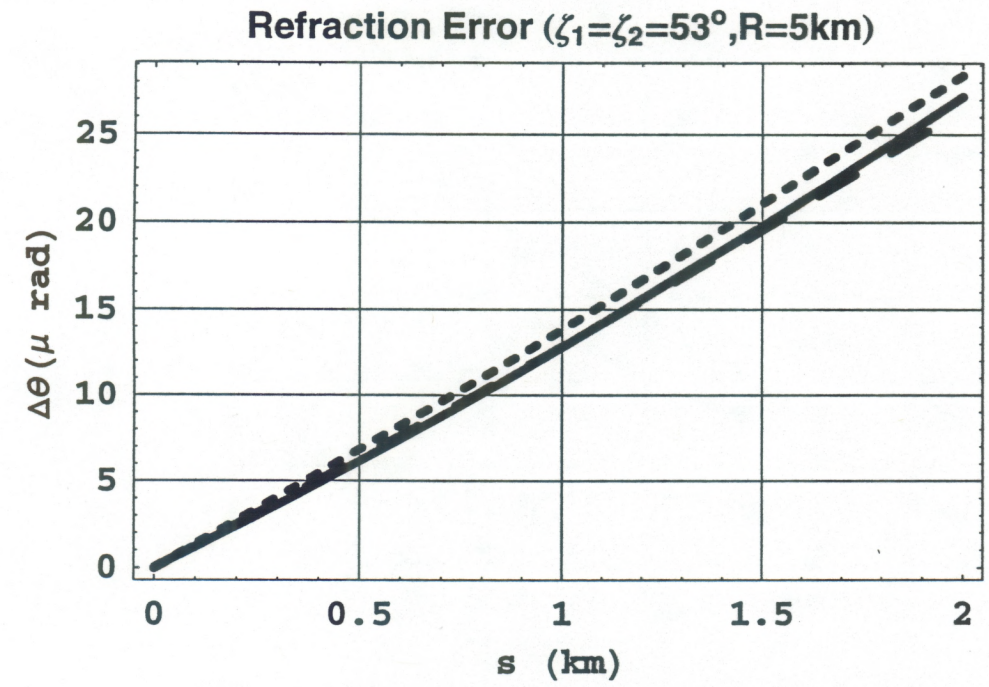

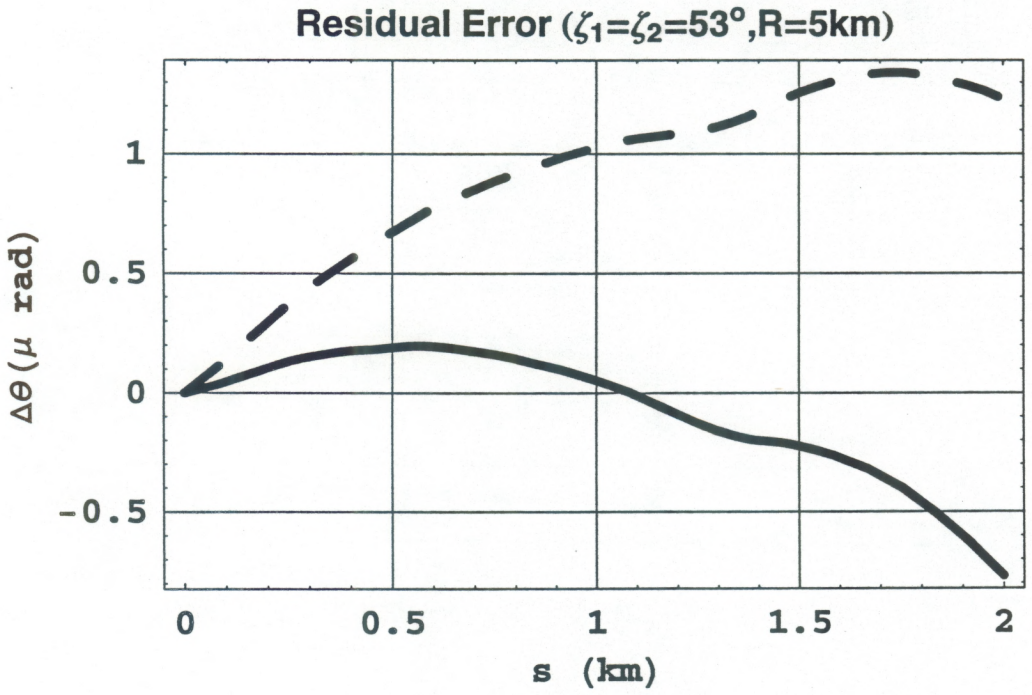

Fig. A8

Winter Nighttime

(January 1, 1998)

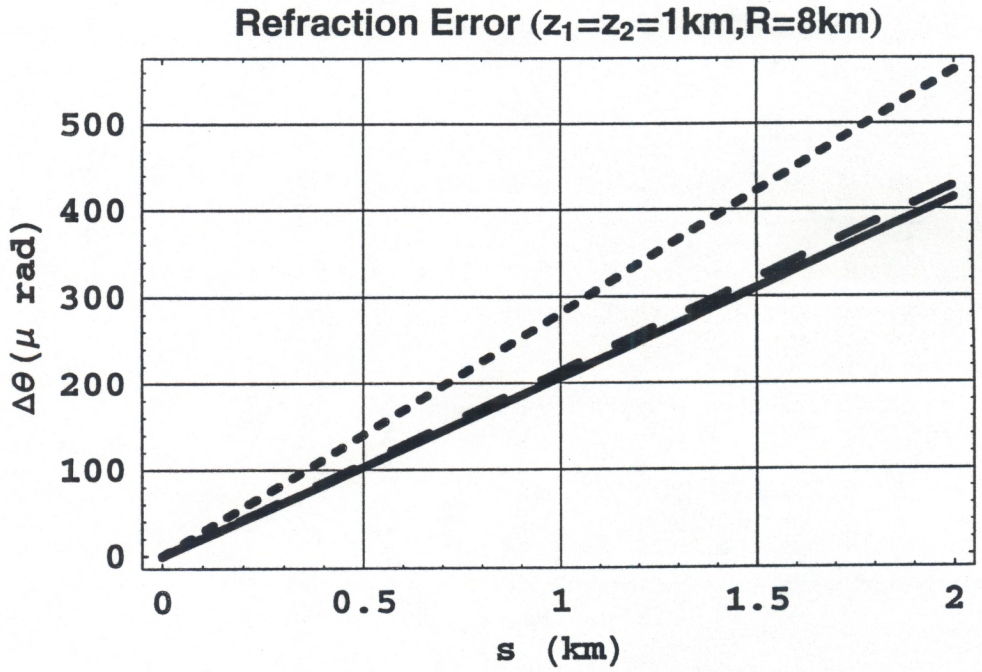

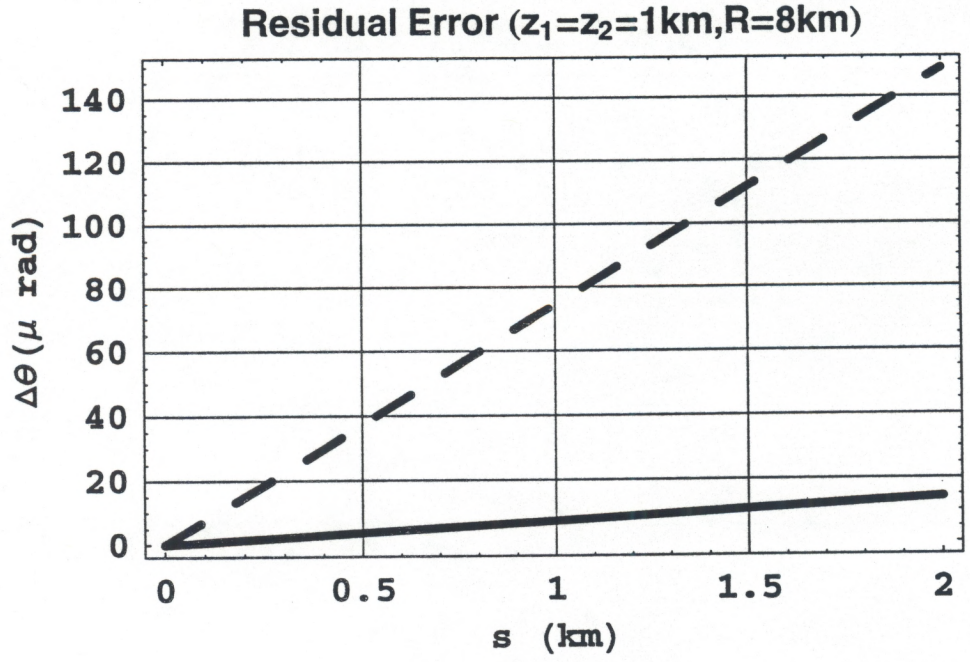

Fig. B1

Winter Nighttime

(January 1, 1998)

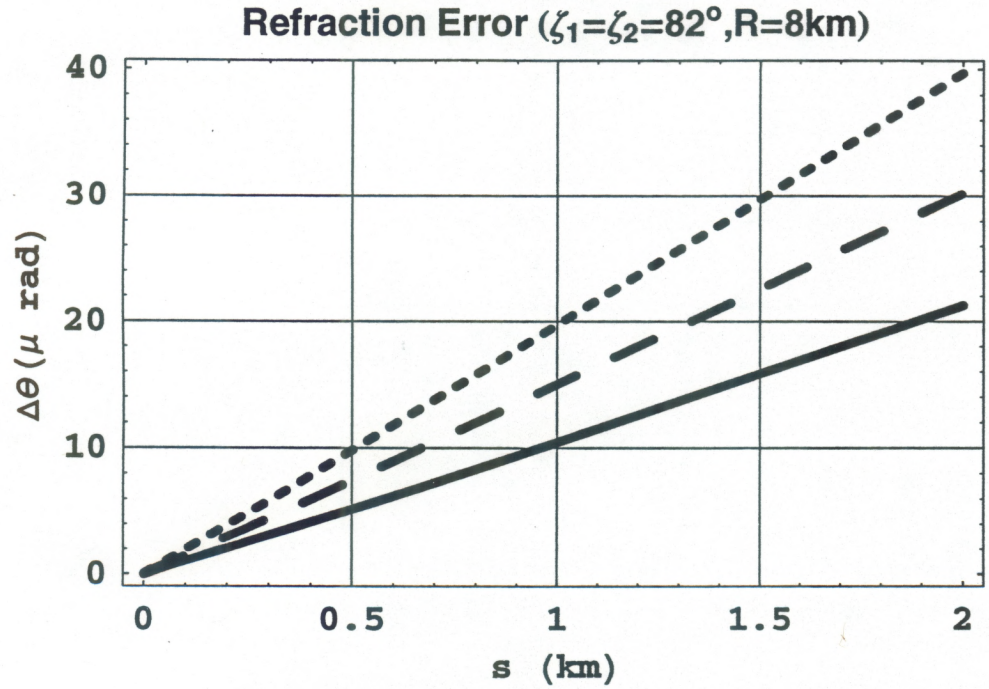

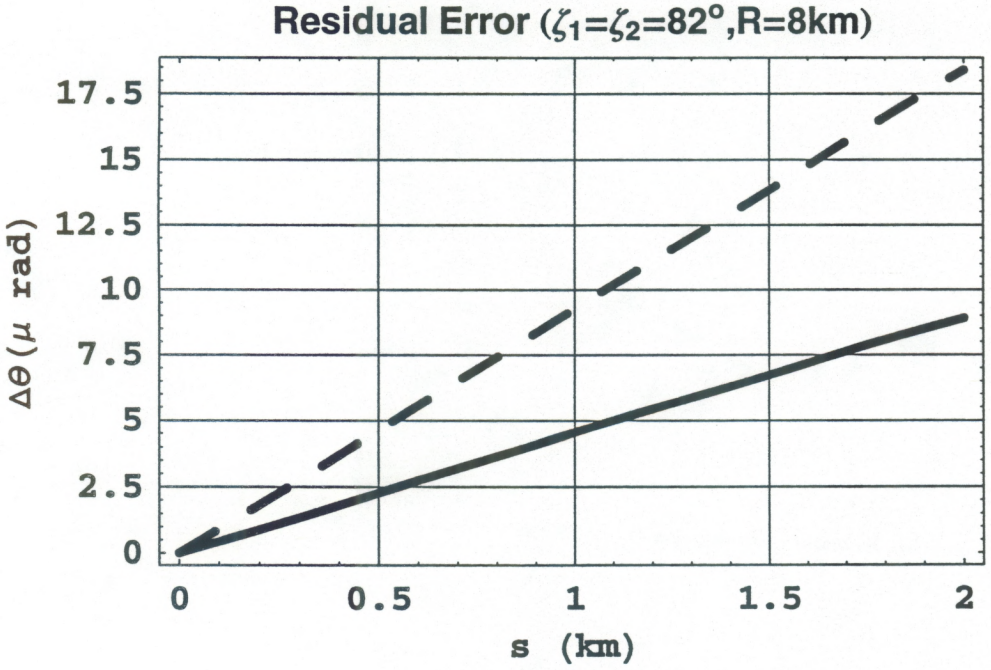

Fig. B2

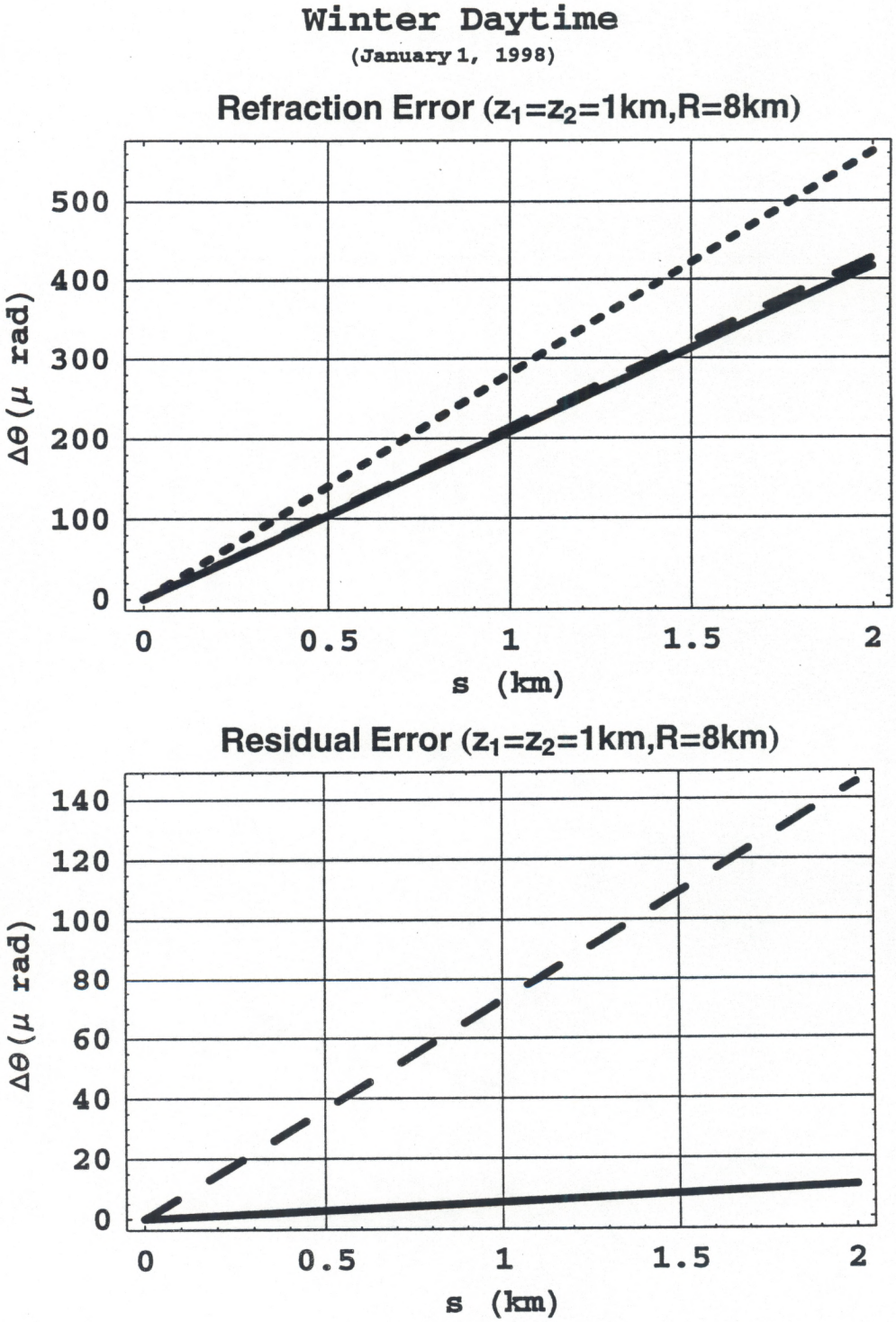
Winter Daytime
(January 1, 1998)
Refraction Error (z_1=z_2=1km,R=8km)
500
400
300
200
100
0
Δθ (μ rad)
0
0.5
1
1.5
2
s (km)
Residual Error (z_1=z_2=1km,R=8km)
140
120
100
80
60
40
20
0
Δθ (μ rad)
0
0.5
1
1.5
2
s (km)

Fig. B3

Winter Daytime

(January 1, 1998)

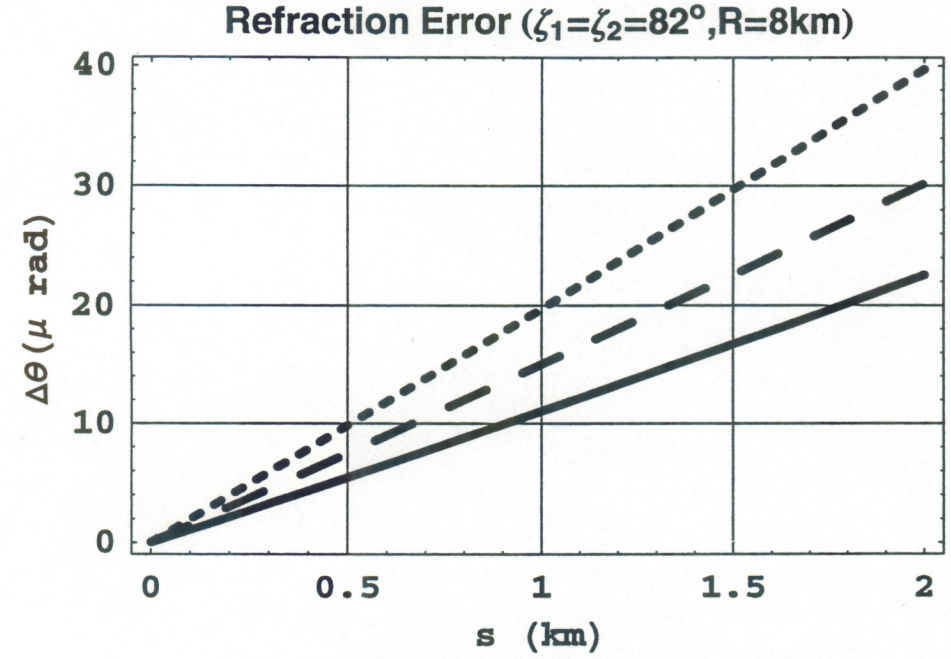

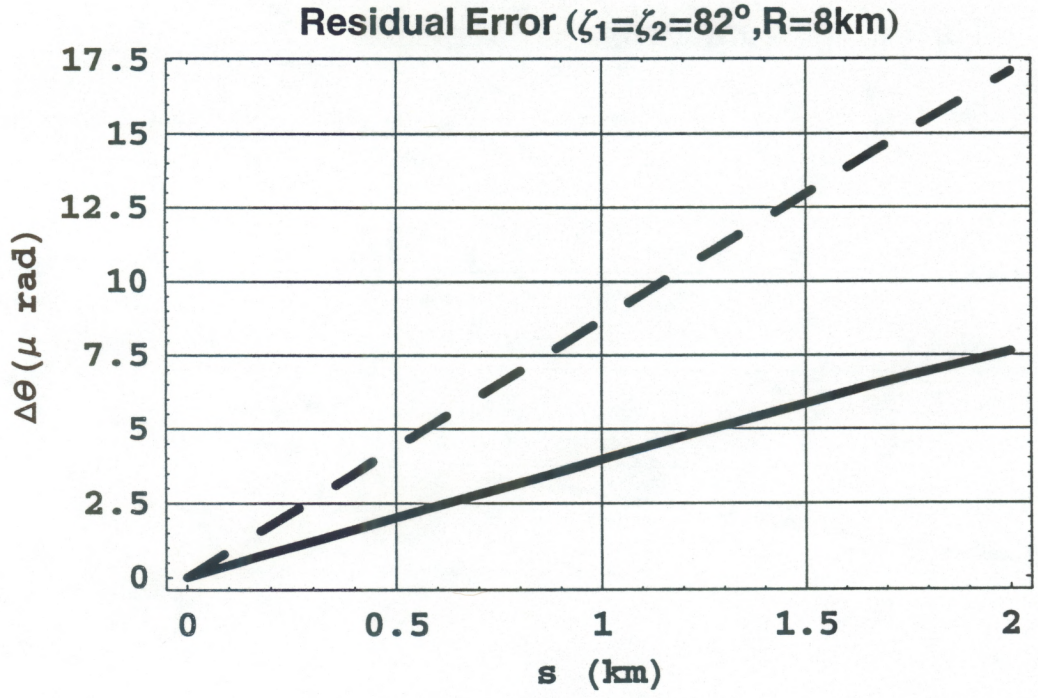

Fig. B4

Summer Nighttime

(July 28, 1997)

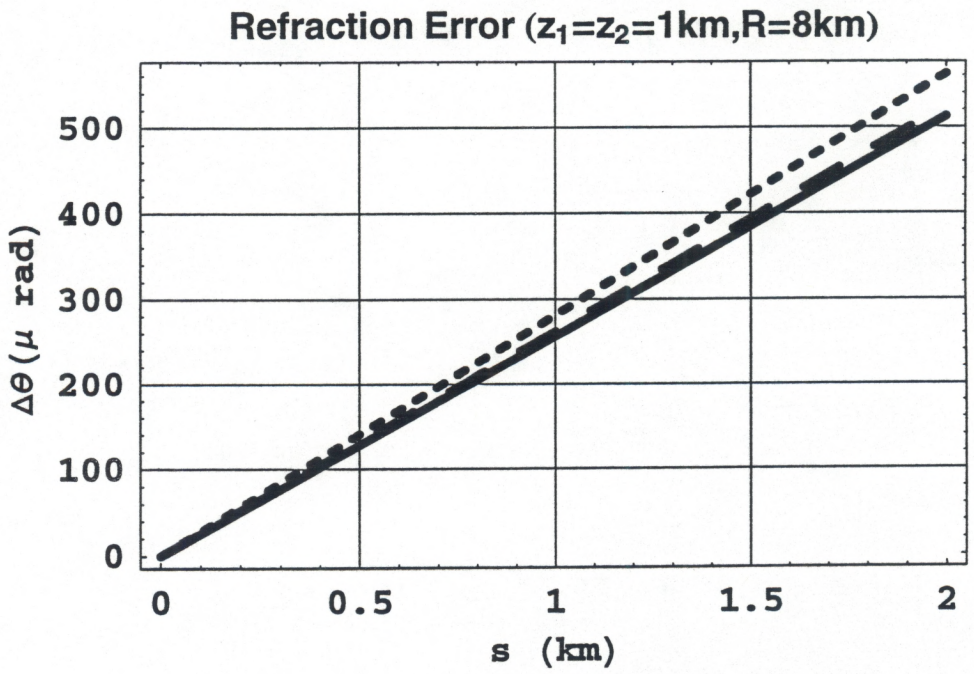

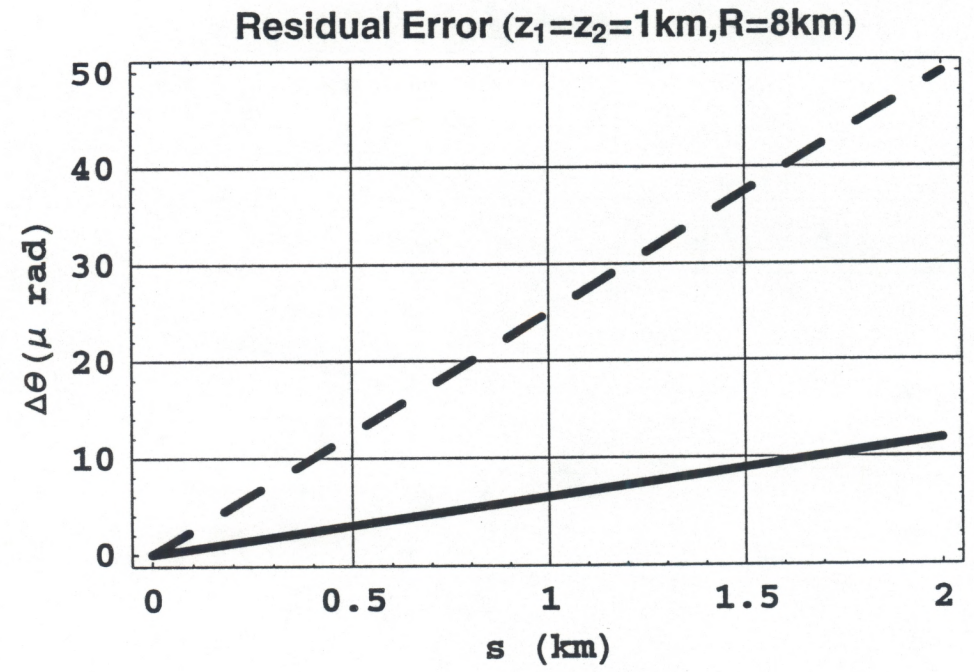

Fig. B5

Summer Nighttime

(July 28, 1997)

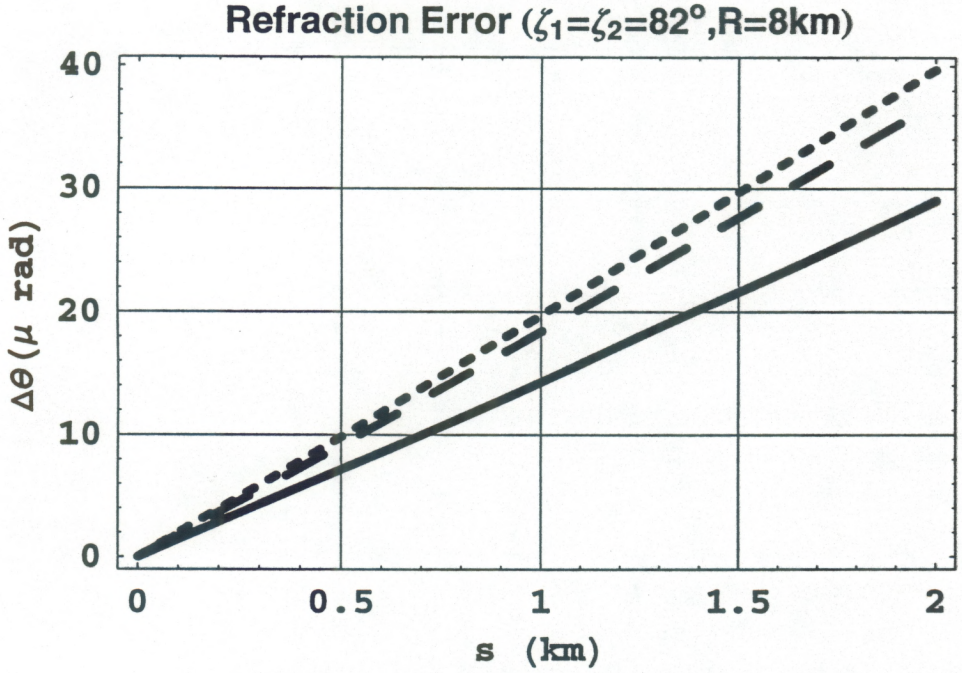

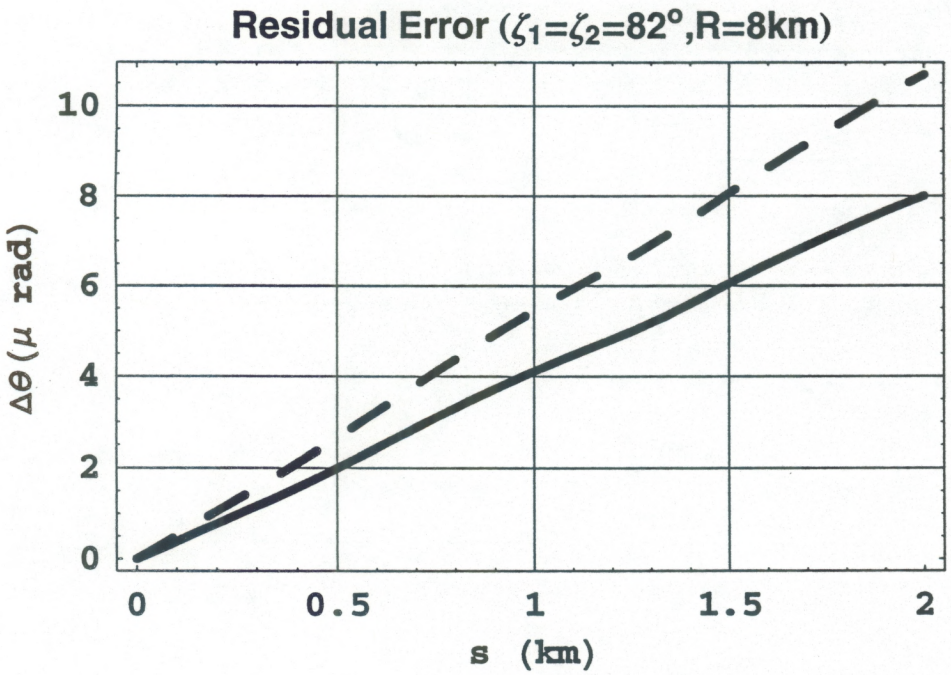

Fig. B6

Summer Daytime

(July 29, 1997)

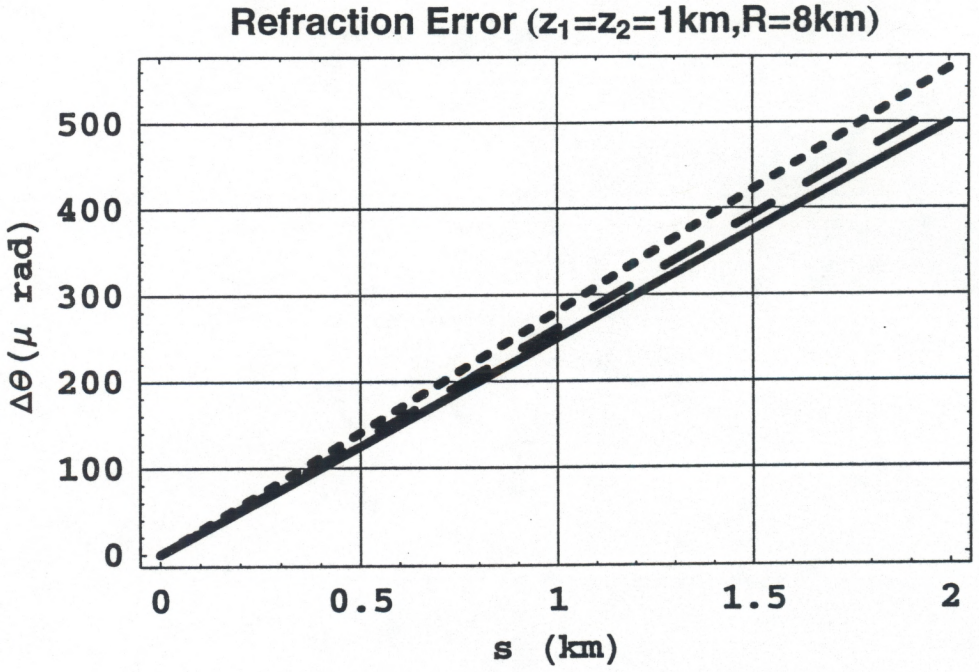

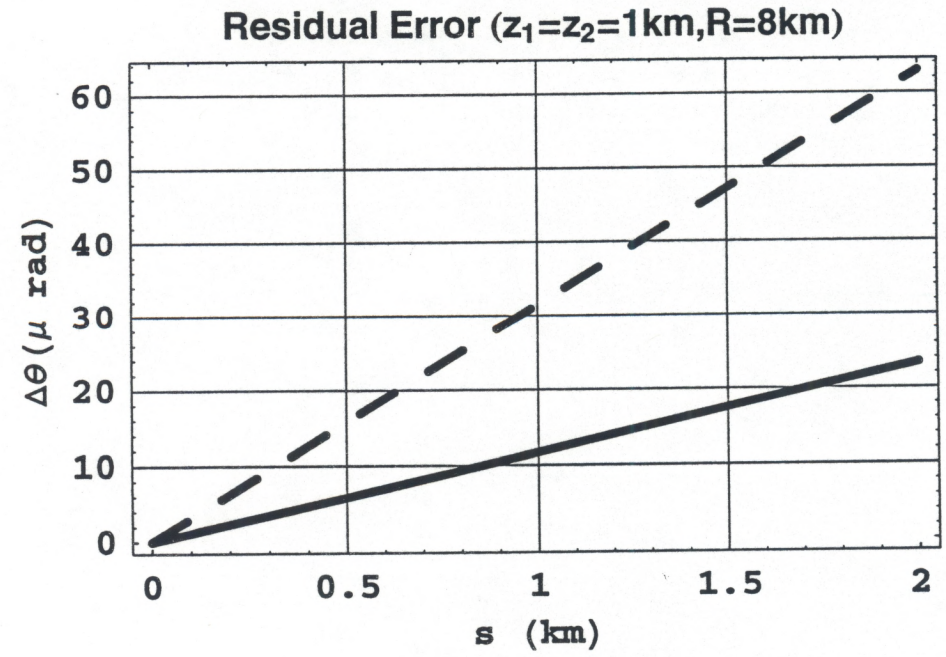

Fig. B7

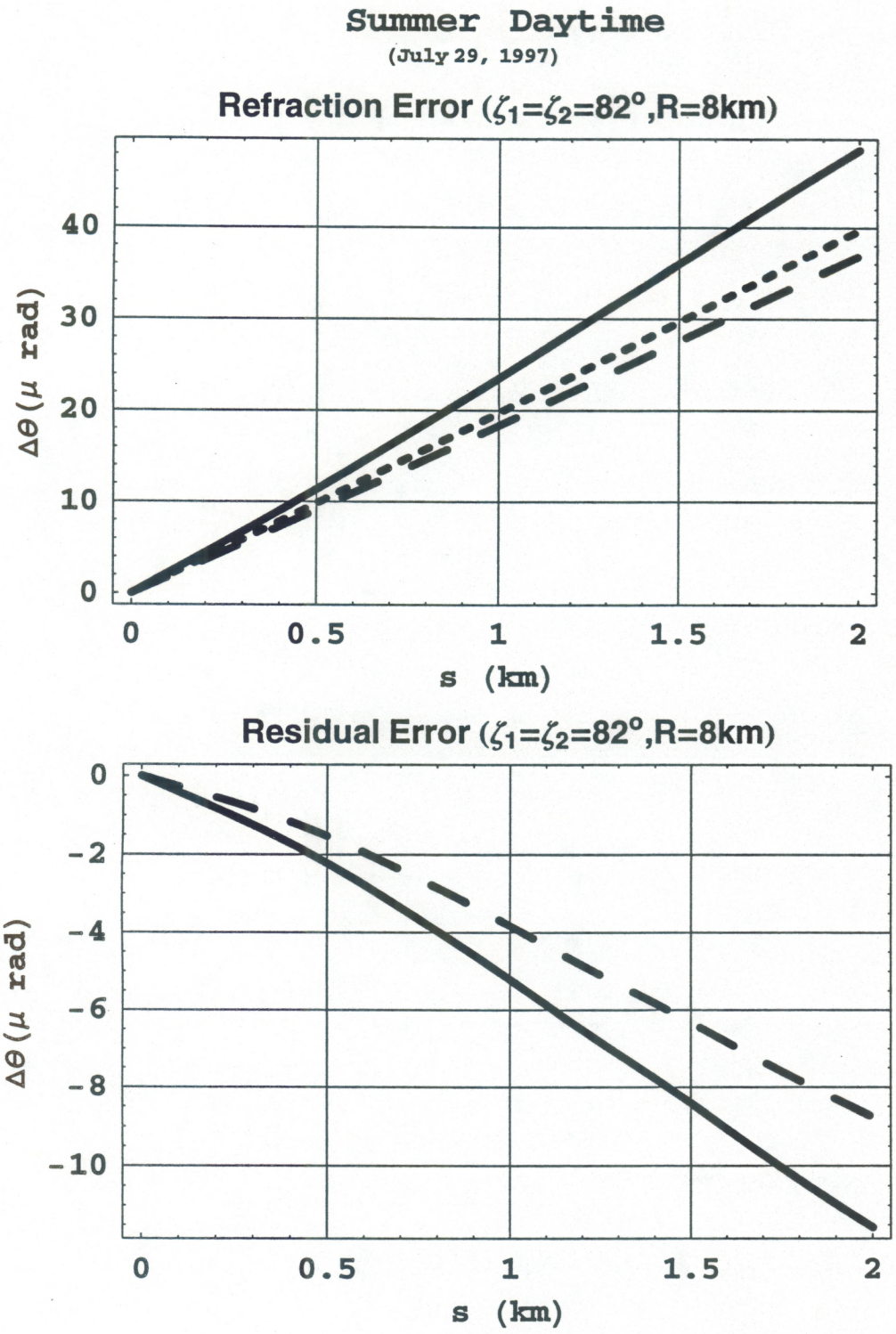
Summer Daytime
(July 29, 1997)
Refraction Error ($\zeta_1=\zeta_2=82^\circ$,R=8km)
40
30
20
10
0
Δθ(μ rad)
0
0.5
1
1.5
2
s (km)
Residual Error ($\zeta_1=\zeta_2=82^\circ$,R=8km)
0
-2
-4
-6
-8
-10
Δθ(μ rad)
0
0.5
1
1.5
2
s (km)

Fig. B8

Winter Nighttime

(January 1, 1998)

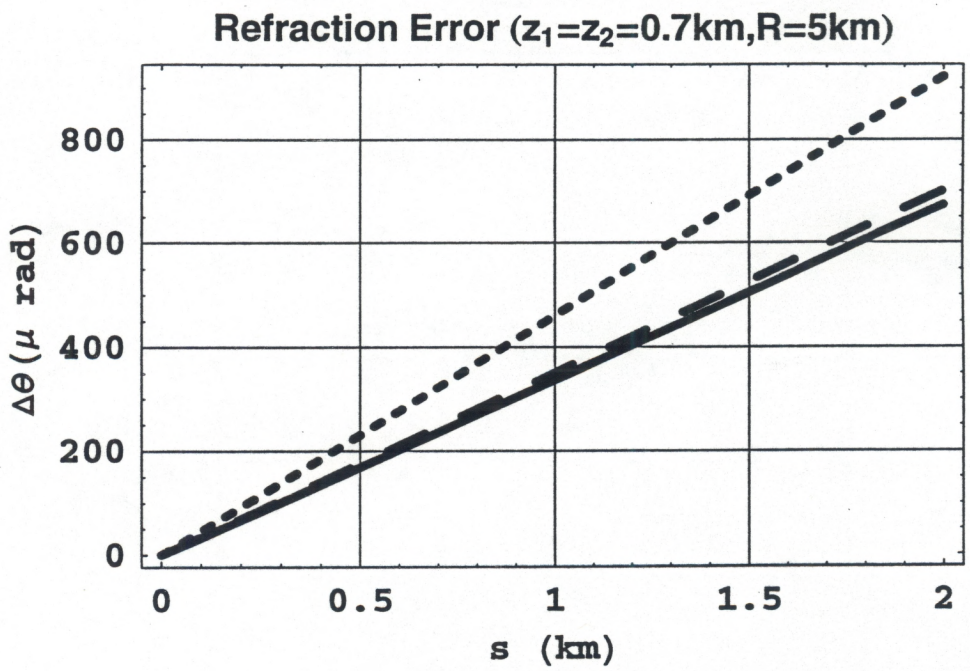

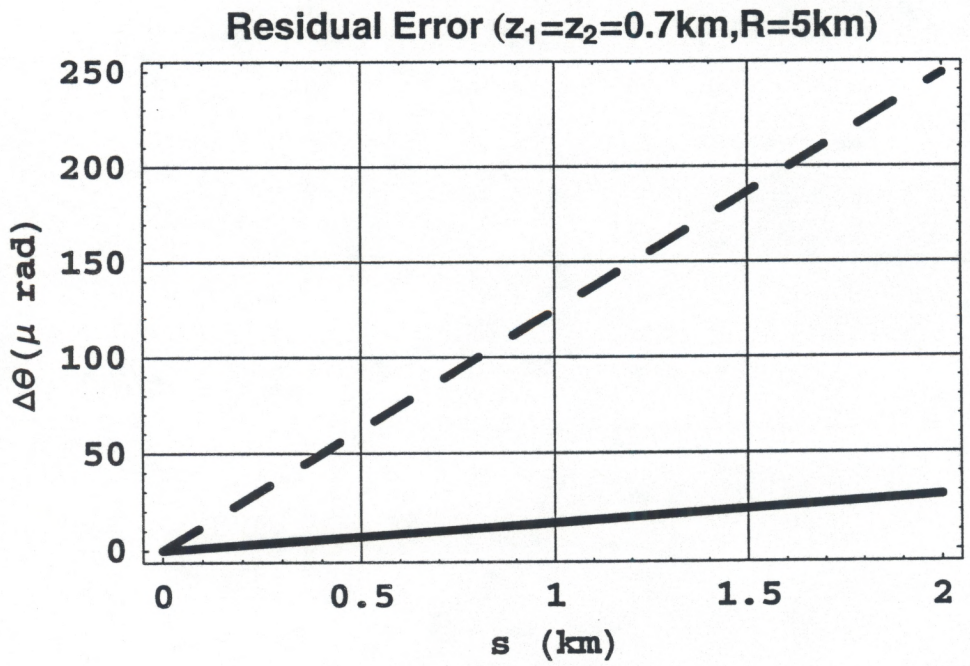

Fig. C1

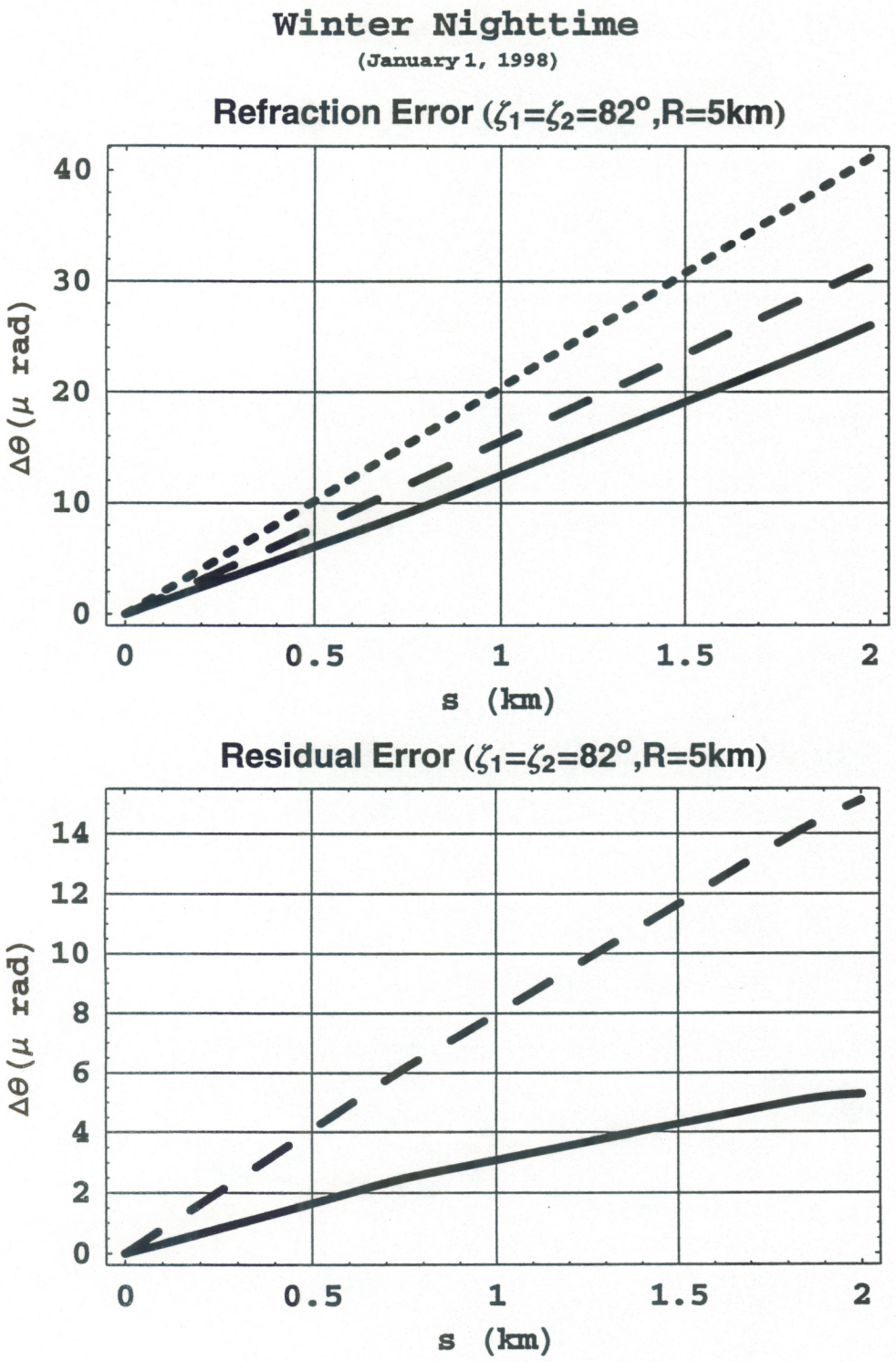
Winter Nighttime
(January 1, 1998)
Refraction Error ($\zeta_1=\zeta_2=82°$,R=5km)
$\Delta\theta$ (μ rad)
40
30
20
10
0
0
0.5
1
1.5
2
s (km)
Residual Error ($\zeta_1=\zeta_2=82°$,R=5km)
$\Delta\theta$ (μ rad)
14
12
10
8
6
4
2
0
0
0.5
1
1.5
2
s (km)

Fig. C2

Winter Daytime

(January 1, 1998)

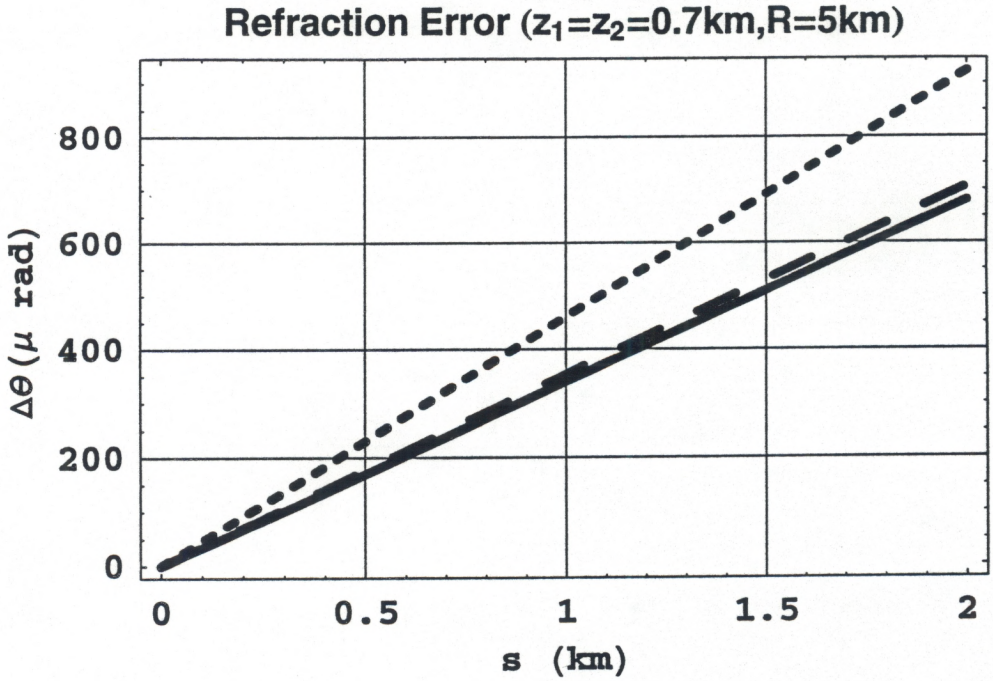

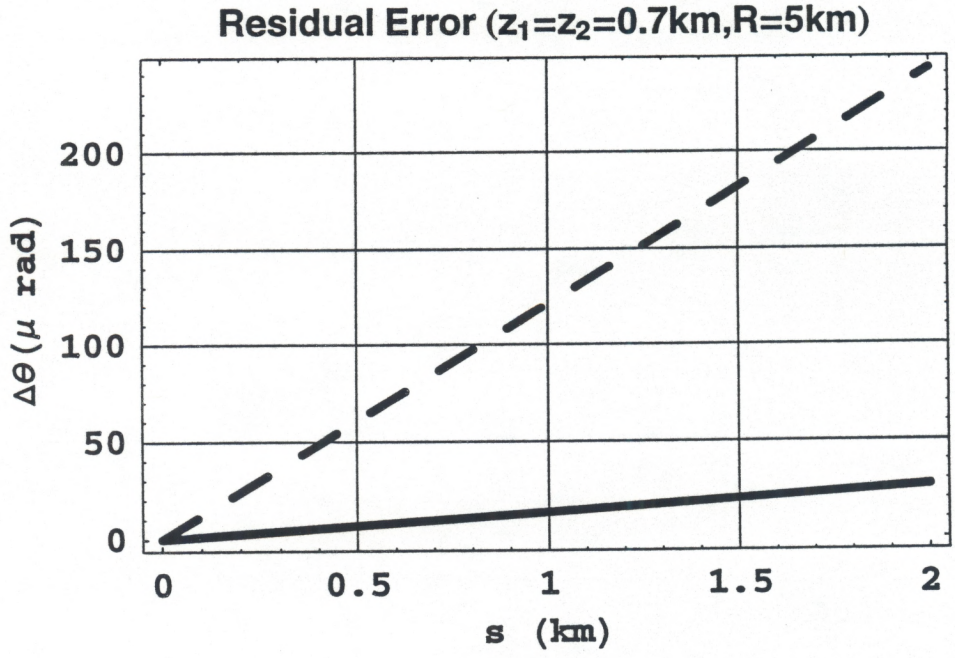

Fig. C3

Winter Daytime

(January 1, 1998)

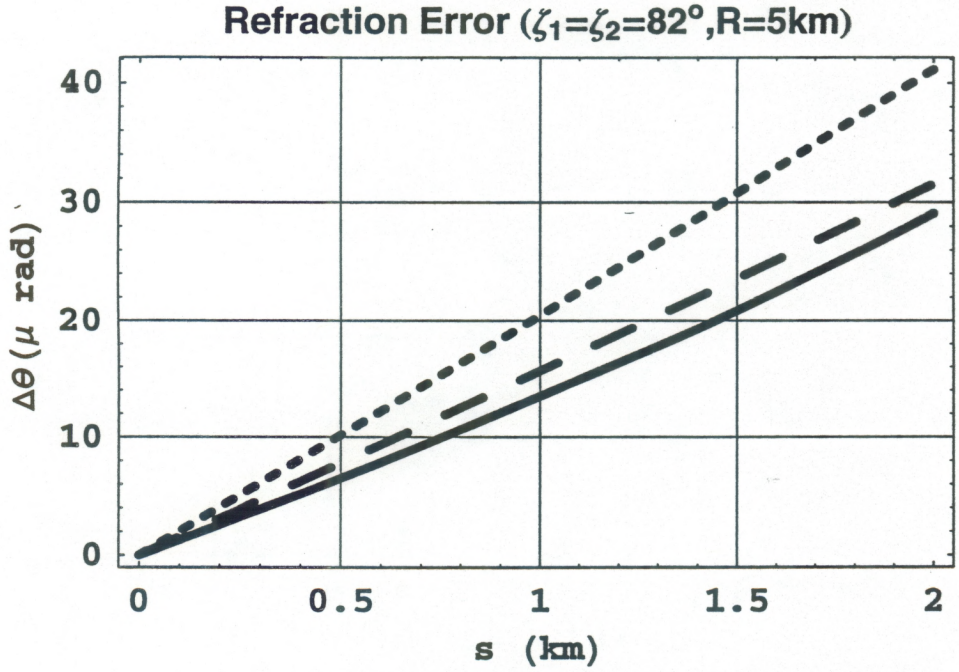

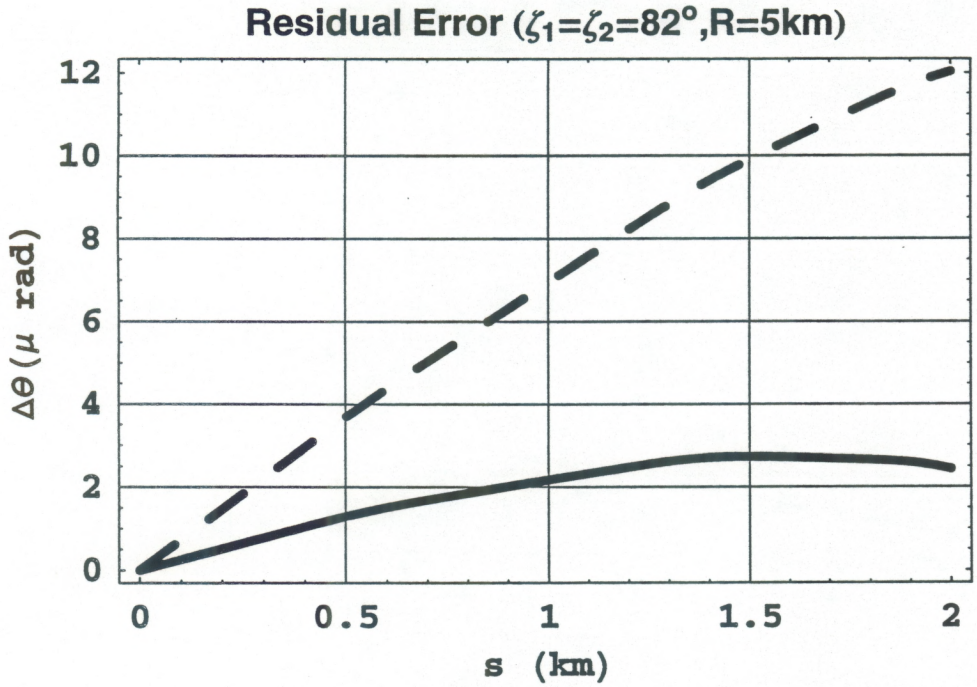

Fig. C4

Summer Nighttime

(July 28, 1997)

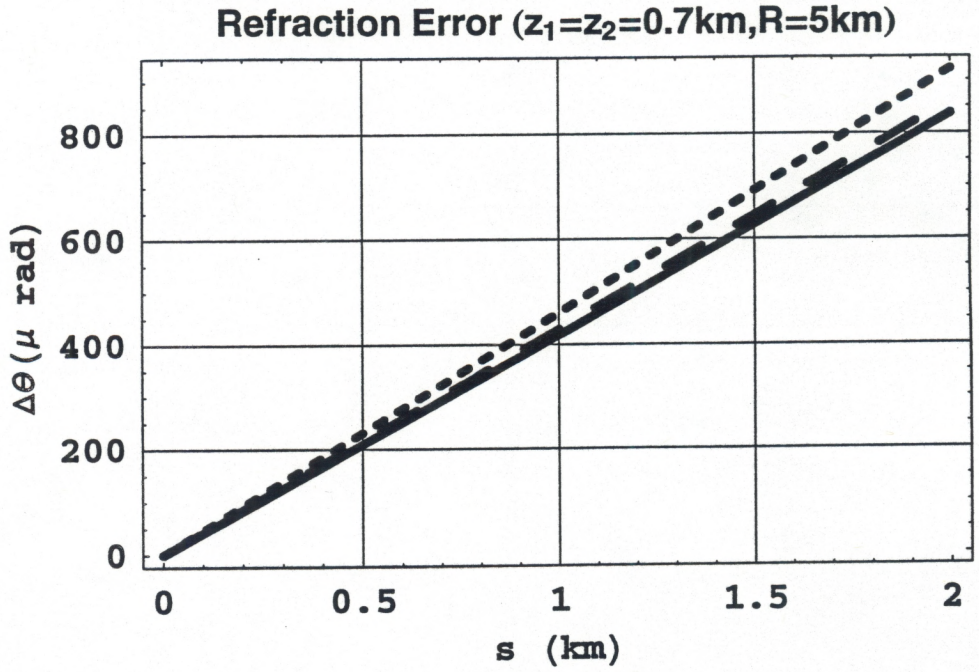

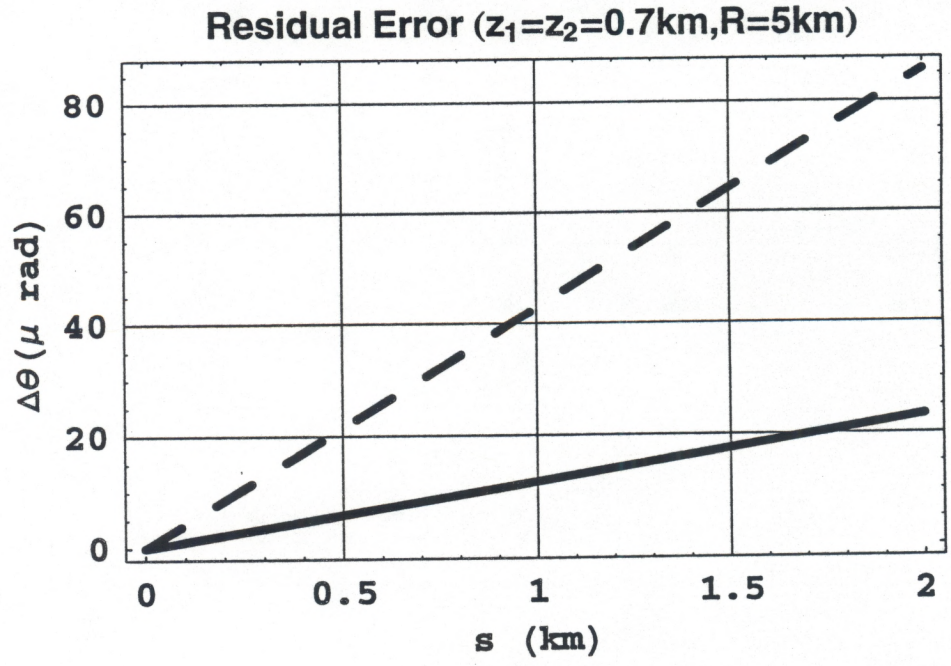

Fig. C5

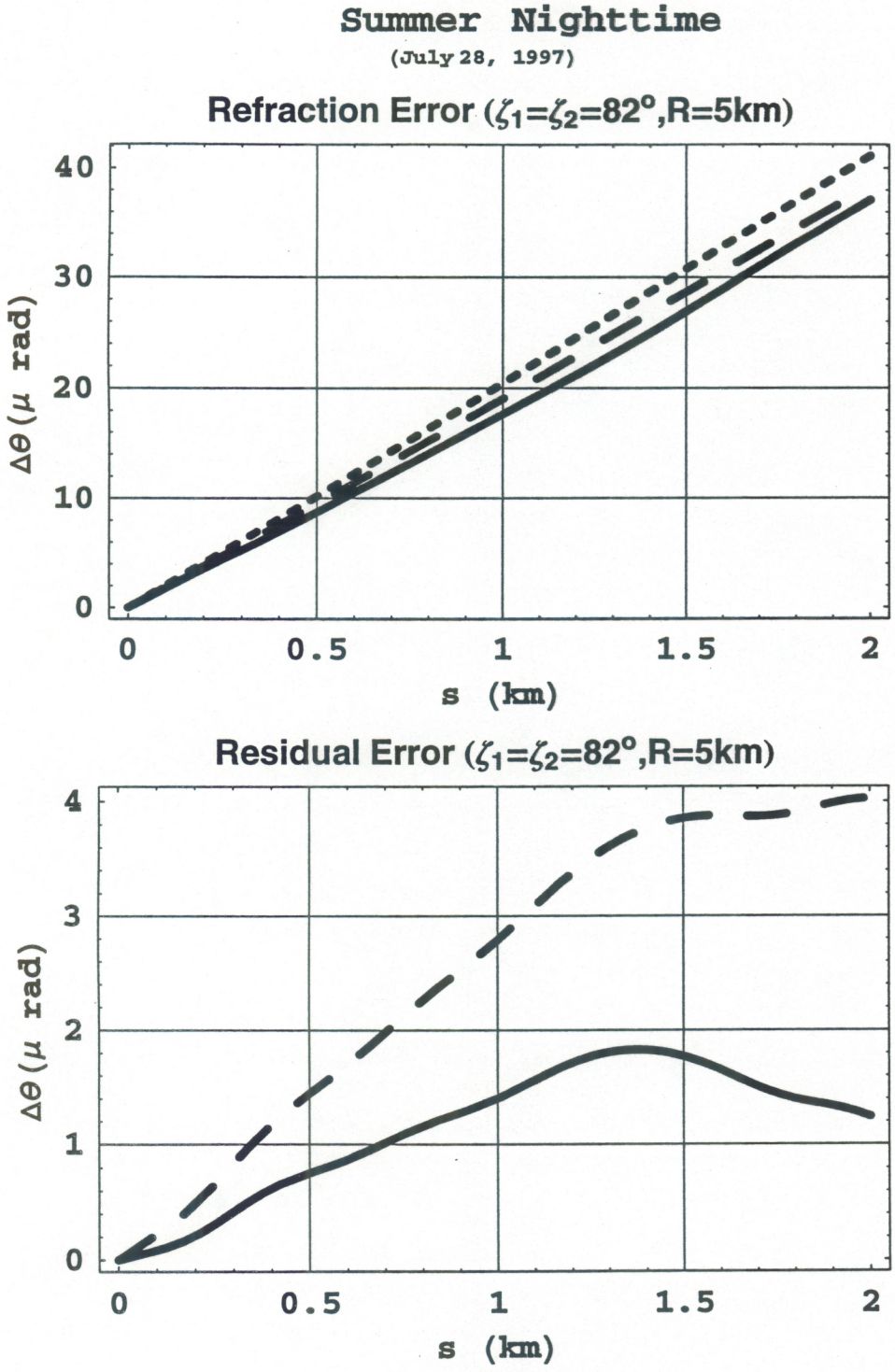
Summer Nighttime
(July 28, 1997)
Refraction Error ($\zeta_1=\zeta_2=82°$,R=5km)
40
30
20
10
0
Δθ (μ rad)
0
0.5
1
1.5
2
s (km)
Residual Error ($\zeta_1=\zeta_2=82°$,R=5km)
4
3
2
1
0
Δθ (μ rad)
0
0.5
1
1.5
2
s (km)

Fig. C6

Summer Daytime

(July 29, 1997)

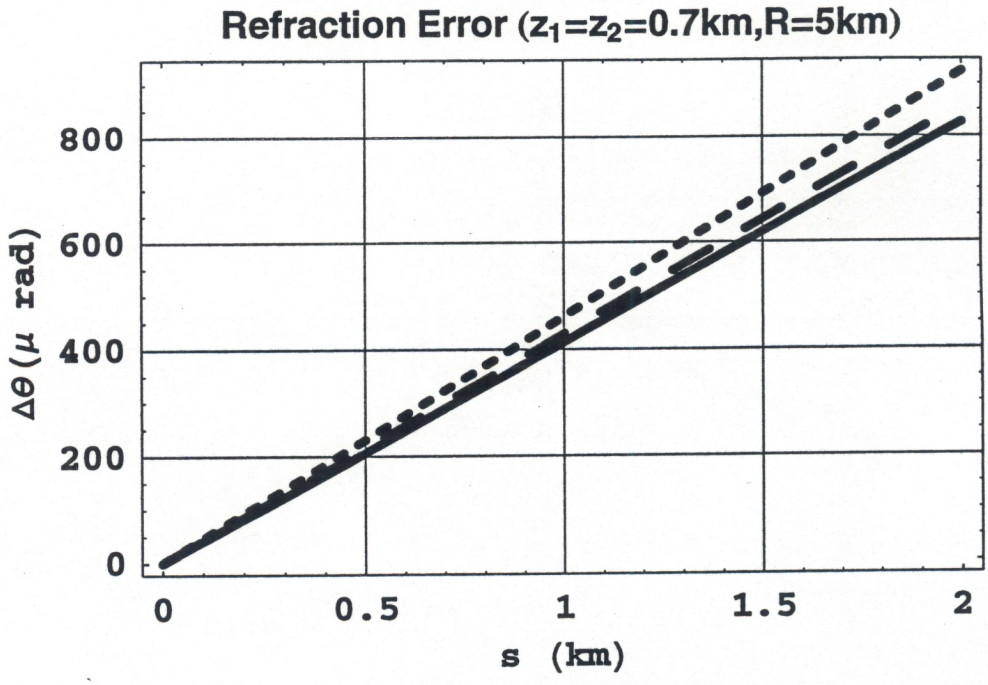

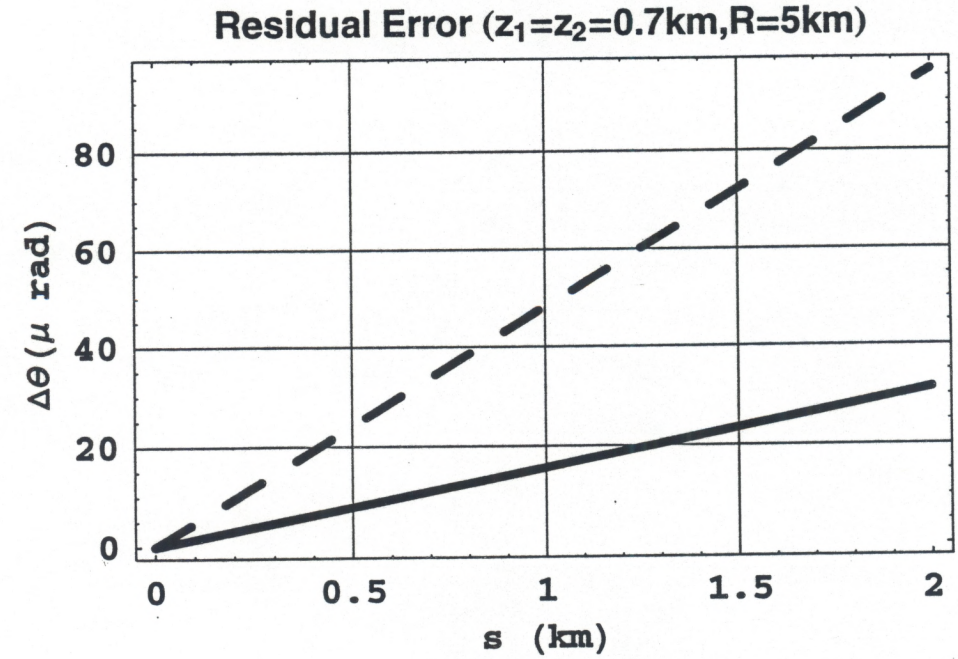

Fig. C7

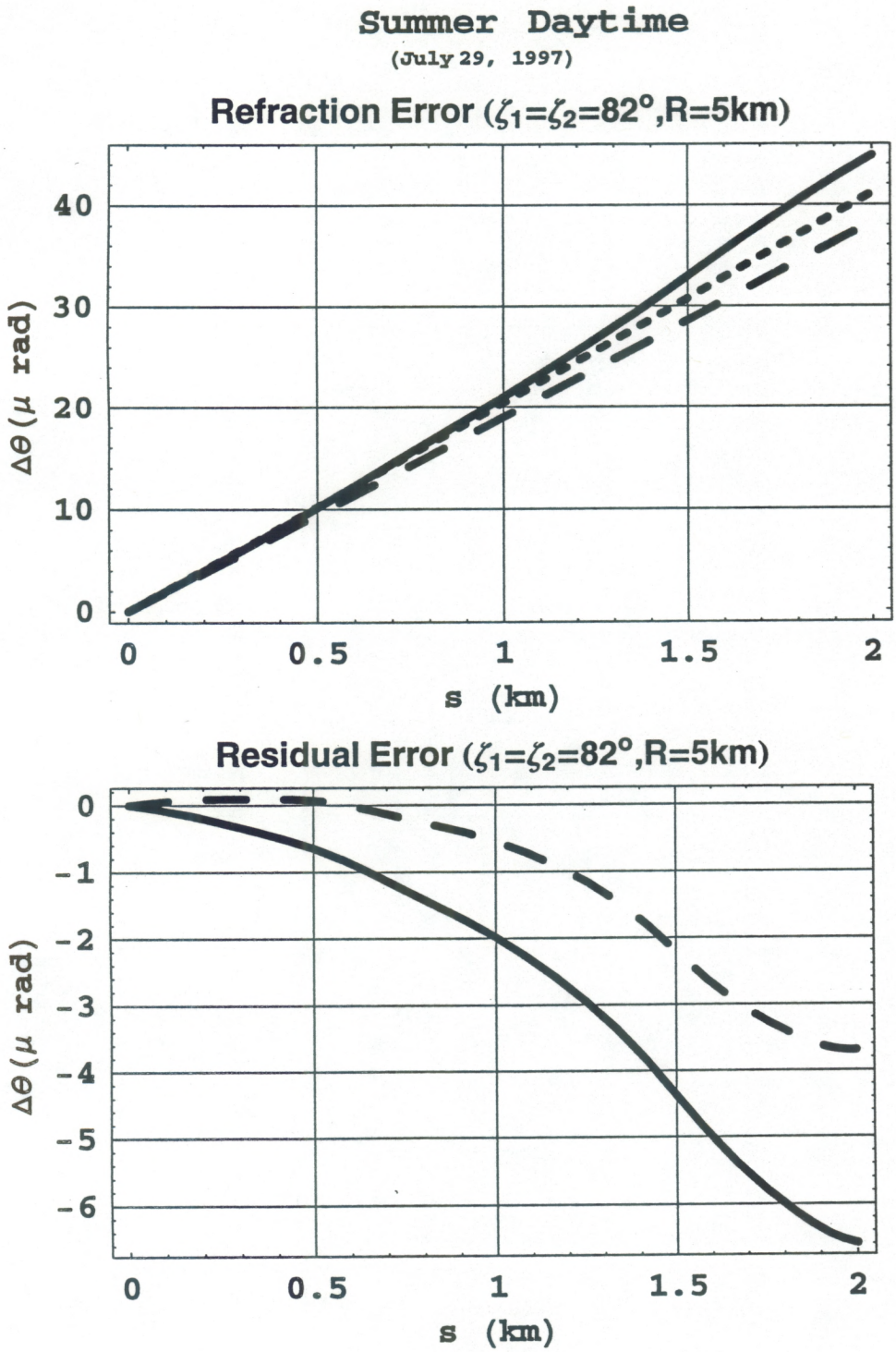
Summer Daytime
(July 29, 1997)
Refraction Error ($\zeta_1=\zeta_2=82°$,R=5km)
40
30
20
10
0
Δθ (μ rad)
0
0.5
1
1.5
2
s (km)
Residual Error ($\zeta_1=\zeta_2=82°$,R=5km)
0
-1
-2
-3
-4
-5
-6
Δθ (μ rad)
0
0.5
1
1.5
2
s (km)

Fig. C8

Table 1.

No.	Altit(m)	Press(mb)	Temp(C)	Humid(%)	Ux (m/s)	Wind (m/s)
1	1611.	842.5	23.	65.	0.	10.
2	1650.	838.7	22.4	63.	6.5	13.1
3	1684.	835.5	21.9	62.	5.1	6.8
4	1710.	833.	21.6	64.	-1.1	3.5
5	1727.	831.4	21.3	65.	-4.1	7.6
6	1756.	828.6	21.1	66.	-4.5	9.
7	1783.	826.	20.9	67.	-1.1	8.7
8	1822.	822.3	20.6	68.	1.6	8.
9	1851.	819.5	20.3	69.	-0.1	4.4
10	1875.	817.3	20.	69.	1.5	4.1
11	1902.	814.7	19.7	71.	1.6	6.2
12	1938.	811.3	19.4	72.	-0.9	4.4
13	1968.	808.5	19.2	72.	0.2	2.4
14	1991.	806.4	19.	73.	0.4	4.4
15	2023.	803.4	18.9	72.	0.1	5.9
16	2058.	800.1	18.7	70.	0.4	6.4
17	2087.	797.4	18.5	69.	-0.2	5.
18	2121.	794.3	18.4	64.	0.9	3.2
19	2150.	791.6	18.3	63.	0.9	6.2
20	2192.	787.7	18.3	58.	1.6	6.5
21	2222.	785.	18.1	57.	1.7	4.8
22	2255.	782.	17.9	57.	2.6	6.1
23	2291.	778.7	18.1	56.	2.8	4.6
24	2319.	776.1	17.9	56.	-0.7	3.4
25	2357.	772.7	17.6	55.	-0.4	4.1
26	2390.	769.7	17.4	55.	0.5	4.5
27	2424.	766.7	17.2	55.	-1.3	4.4
28	2457.	763.7	16.9	55.	0.	4.5
29	2493.	760.5	16.7	56.	-0.5	5.
30	2529.	757.3	16.6	56.	-1.8	4.8
31	2559.	754.6	16.5	56.	-1.5	3.7
32	2591.	751.8	16.4	56.	-1.	3.8
33	2616.	749.6	16.1	57.	-1.7	6.9
34	2670.	744.9	15.8	57.	-2.1	5.4
35	2700.	742.2	15.5	58.	0.	2.5
36	2723.	740.2	15.3	59.	1.3	4.4
37	2753.	737.6	14.9	60.	0.6	4.9
38	2792.	734.2	14.6	62.	0.4	6.6
39	2827.	731.2	14.3	63.	0.3	5.9
40	2856.	728.7	13.9	64.	0.6	3.7